Experiments on Structural Formation in Plasmas

Habilitationsschrift

zur Erlangung der venia legendi
für das Fach Experimentalphysik

vorgelegt der
Mathematisch-Naturwissenschaftlichen Fakultät der
Christian-Albrechts-Universität
zu Kiel

von
Dr. rer. nat. Dietmar Block

Oktober 2007

1. PREFACE

Since the early days of plasma physics, it is known that plasma is more than a hot gaseous state of matter. The electric charge of the plasma constituents (usually electrons and ions) allows for collective behavior and the time scales of electron and ion dynamics are well separated. Thus, plasmas exhibit a rich variety of phenomena which are unknown to ordinary gases and contribute to the compelling properties of this state of matter. The wealth of phenomena, their relevance for astrophysical and technological applications, and their impact on other fields have driven plasma research for almost a century now and have provided much insight into the formation of static structures, oscillatory instabilities, waves, and turbulence.

With respect to structural formation, the coupling parameter Γ is an important quantity. It is defined as the ratio of electrostatic interaction energy of nearest neighbors and the thermal energy of the particles. For most plasmas the coupling parameter is small, and the combination of collective behavior and gradients in density, temperature, or flow velocity, gives rise to large scale modes which themself modify the plasma. This mutual interaction of charged particles and large scale electromagnetic fields determines the dynamical nature of plasmas. Thus, structural formation in the regime of weak coupling is dominated by instabilities and waves, which are frequently in a turbulent state. On the example of drift waves, the first part of this thesis deals with structural formation in the regime of weak coupling. Here, the recent advances are driven by numerical and theoretical approaches while an experimental verification of many predicted processes is missing. Thus, this thesis pays special attention to the diagnostic challenges related to structural formation in plasma turbulence.

In a strongly coupled system ($\Gamma > 1$) the coupling energy exceeds the thermal energy and the spatial configuration of the particles is of importance. In this regime the systems are in a liquid, solid, or even crystalline state due to the strong interaction of nearest neighbors. To study the structural and dynamical properties of strongly coupled systems, the second part of this thesis focuses on complex plasmas. Here, special attention is paid to the formation of crystalline structures in finite dust clouds and their dynamical properties.

Although the processes in the regime of weak and strong coupling differ fundamentally, diagnostic challenges are common to both fields. In both cases, novel diagnostic methods with high spatio-temporal resolution are required to achieve further progress. Therefore, this thesis stresses especially the diagnostic advances in both fields. The thesis ends with concluding remarks and an outlook on future experiments. The author's publications in peer-reviewed journals and the main contributions to international conferences are listed and compiled at the end. The author's journal publications are marked and cited consecutively as "J-1", "J-2" etc. and, in an analogous manner, the conference articles are referenced as "C-1", "C-2" etc.

The work presented here was mainly conducted at the Christian-Albrechts-Universität zu Kiel with contributions from O. Arp, B. Brede, F. Greiner, S. Harms, M. Hirt, M. Kroll, A. Piel, I. Teliban, and T. Trottenberg. The early synchronization experiments of drift waves were a close cooperation with T. Klinger and coworkers. The drift wave simulations have been provided by V. Naulin. MD-simulations were performed in close cooperation with the group of M. Bonitz. They further provided theoretical support for the analysis of Yukawa balls. The stereoscopic investigations of Yukawa balls were a joint activity with the group of A. Melzer in Greifswald.

2. WEAKLY COUPLED PLASMAS

Most plasmas are weakly coupled. In this regime the formation of large-scale structures and their dynamics are governed by linear, nonlinear and frequently turbulent wave phenomena. As a consequence, the investigation of plasma instabilities has a long tradition in plasma physics. Today, the basic instability mechanisms are quite well understood and are subject of many handbooks and introductions to plasma physics, e.g. [46, 140, 181]. Even for the nonlinear dynamics considerable progress has been achieved [34, 53, 97, 108, 255, 302]. However, nonlinear processes and plasma turbulence are still subject of intensive research. This chapter will give a brief introduction to plasma turbulence research with a focus on large-scale structures in drift wave turbulence and related diagnostic problems.

2.1 Status of Research

To give a comprehensive overview of the current understanding of waves and turbulence in plasmas is certainly beyond the scope of this thesis. However, the progress for many instabilities is closely linked to methodical progress, e.g. the development of new diagnostics, new concepts, or advances in numerical modeling. Hence, the development in the field of a certain instability mirrors the general progress to some extent. Among the most prominent instabilities in magnetized plasmas are drift waves. They belong to the class of universal instabilities, because they are driven by gradients in plasma pressure which are common for bounded laboratory plasmas and especially for fusion plasmas. For a fusion reactor, i.e. the quest to produce and confine a hot and dense plasma, transport processes caused by instabilities turned out to be a major problem [96, 97]. Thus, considerable effort has been spent to investigate the linear, nonlinear and turbulent dynamics of drift waves. The following paragraphs will give a brief overview of the current status of research on drift waves, their transport properties and ways to control them.

2.1.1 Drift Wave Instability

The first experimental observations of drift waves were made by D'ANGELO et al. [52, 49, 51] whereas the theoretical basis was founded independently by MOISEEV and SAGDEEV [184] as well as JUKES [118]. Shortly after that, LASHINSKY [148] and CHEN [41, 42, 43, 44] identified the universal character of the instability and linked the observations with microscopic physical processes. They proposed a local and linear drift wave model, which gave an acceptable description of the observations. Improved nonlocal models with arbitrary density profile were developed [45, 47, 59, 60] and the role of the radial electric field and the resulting $E \times B$ rotation of the plasma was first described by MARDEN-MARSHALL et al. [164].

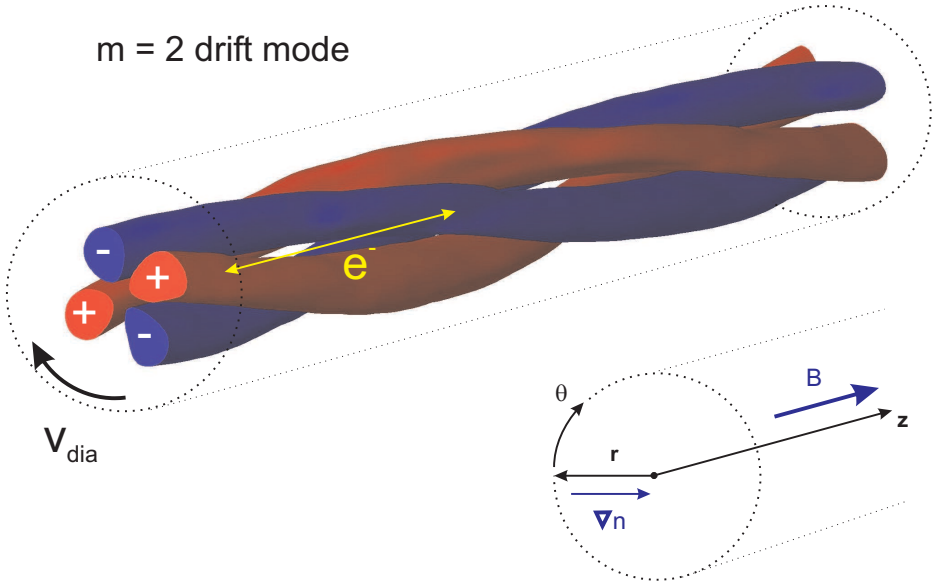

Fig. 2.1: Topology of a $m = 2$ drift mode in a cylindrical plasma column. The cylindrical plasma column is sketched with dotted lines. The magnetic field B is oriented along the z-axis and the density gradient is pointing radially inwards (see subplot). Regions of positive (negative) density perturbation are colored blue (red). The associated potential perturbations are marked with $+$ and $-$. Note that drift waves have a finite wavelength along the magnetic field causing an adiabatic electron response (arrows). Additionally, the whole structure rotates around the center of the plasma column with diamagnetic velocity.

The basic ingredients of these models are shown in Fig. 2.1. If a density gradient in radial direction, an axial magnetic field B, and a density perturbation with a finite wavelength parallel to B are combined, the electron response along B causes a potential perturbation. The resulting azimuthal electric fields and the related $E \times B$ drifts yield to a propagation of the density perturbation with diamagnetic velocity in the azimuthal plane. The typical eigenmodes of drift waves in cylindrical geometry have an integer azimuthal modenumber, e.g. $m = 2$ in Fig. 2.1. The destabilization of drift waves is related to a phase shift of density and potential perturbations which arises due to a finite resistivity along the magnetic field. In general, any perturbation of the parallel electron response, e.g. by collisions or Landau damping, is destabilizing. This stresses that drift waves are three-dimensional objects, although the parallel wavelength is typically much longer than the perpendicular wavelength.

To describe saturation processes, mode coupling, and drift wave turbulence, nonlinear models are mandatory. Quite simple but nevertheless powerful nonlinear models rely on the HASEGAWA-MIMA [81] and HASEGAWA-WAKATANI equations [82]. The

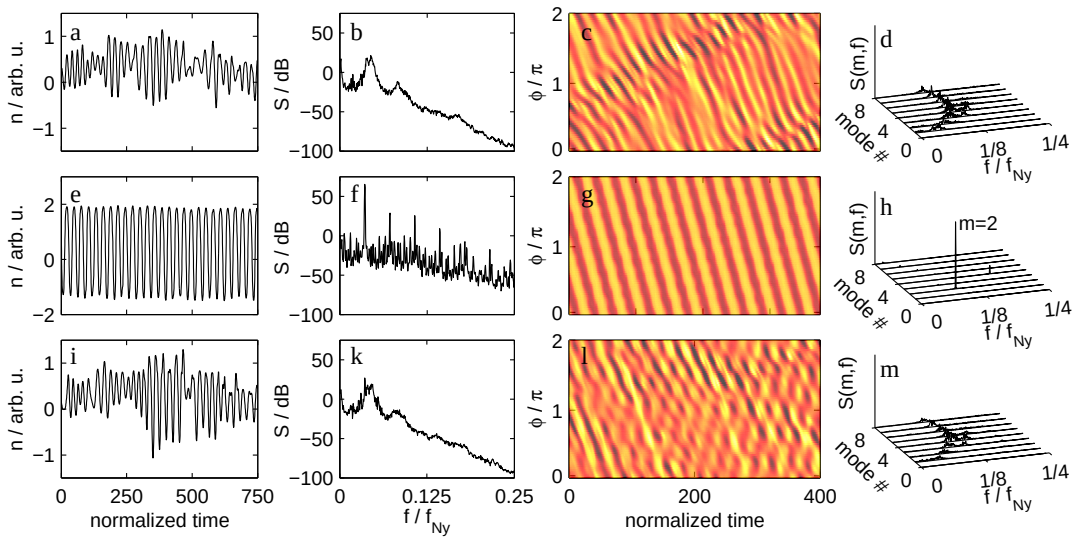

Fig. 2.2: Spatio-temporal drift wave dynamics of a driven Hasegawa-Wakatani model. The three rows correspond to the unperturbed case, active exciter with a co-rotating field, and active exciter with counter-rotating field, respectively. The four columns show the density fluctuations, their frequency power spectrum, and the spatio-temporal density fluctuations measured with an artificial azimuthal probe array. The corresponding frequency-modenumber power spectra are plotted in the right column. From Ref. [J-1].

latter are two coupled nonlinear partial differential equations for density n and vorticity $\nabla_\perp^2\phi$:

$$\frac{\partial}{\partial t}\nabla_\perp^2\phi + \mathbf{V}_{E\times B}\cdot\nabla\nabla_\perp^2\phi = \nabla_\parallel J_\parallel + \mu_w\nabla_\perp^4\phi \tag{2.1}$$

$$\frac{\partial}{\partial t}n + \mathbf{V}_{E\times B}\cdot\nabla\left(N_0+n\right) = \nabla_\parallel J_\parallel + \mu_n\nabla_\perp^2 n \tag{2.2}$$

with $J_\parallel = -\sigma_\parallel\nabla_\parallel\left(\phi - n\right)$. Note that the coupling of the equations is realized by the parallel current, i.e. the dynamics parallel to B. The nonlinearity results from the advection term $\mathbf{V}\cdot\nabla$. Although these models cannot explain the observed anomalous transport in fusion experiments, they already allow to study analytically and numerically a number of nonlinear processes. Especially the formation of large-scale structures can be studied in the framework of these models [96].

With increasing computational power sophisticated nonlinear models were developed, and the modeling of drift wave turbulence is still subject of intense research [53, 97, 255]. Many mechanisms are discussed to cause or at least to be related to the observed transport, e.g. coherent structures [98, 137], streamers and zonal flows [53, 119]. However, the experimental verification of these concepts is difficult because measurements with high spatio-temporal resolution are required [53].

Parallel to the investigation of drift wave dynamics and the related transport, there have been various attempts to control transport, e.g. with feedback experiments which were only partly successful [12, 232, 258, 279]. More promising results were obtained with biasing experiments. The basic idea behind these experiments is a transport

suppression by sheared flows [274]. Sheared flows are known to play a key role for transport barriers, which are responsible for the L-H transition in fusion devices [271, 298, 299]. Additionally, sheared flows are the central element of zonal flows [53], which attracted much interest due to their influence on turbulence and transport in fusion devices. Interesting results were reported in Refs. [225, 271, 303].

A completely different approach to reduce plasma fluctuations was triggered by the improved understanding of nonlinear dynamics. It was shown that many chaotic systems can be stabilized with chaos control techniques [135, 250]. A successful application of this concept to weak drift wave turbulence was demonstrated [75]. In contrast to the other methods, not all fluctuations were suppressed. Instead, a single mode was stabilized to suppress the other modes. Experiments in Kiel and Nancy showed that drift wave dynamics can be influenced with spatio-temporal driver signals [149, J-1]. This control method is capable to synchronize selected drift modes in a weakly turbulent plasma state and the synchronization process is well described by a driven Hasegawa Wakatani model [Fig. 2.2]. Recently, this control method was shown to work even for flute modes [35] and a detailed picture of the synchronization process [J-2, J-3] and related fluctuation-induced transport [J-3, J-4] was obtained. Interestingly, the latter are some of the very few investigations where transport processes were studied spatio-temporally.

To conclude, there is plenty of experimental progress related to linear and nonlinear drift waves but the advances in understanding drift wave turbulence and related structural formation are basically driven by theory and simulations. This dissatisfactory status is attributed to the fact that experiments are lacking diagnostics with a spatio-temporal resolution comparable with that of simulation codes. Hence, one of the experimental key issues today is the quest to image plasma turbulence.

2.1.2 Imaging Plasma Turbulence

The results of theory and computer simulations have taught us that high spatio-temporal resolution is mandatory for the investigation of structural formation in plasma turbulence. Typically, the temporal resolution should be of the order of the ion-gyrofrequency and a spatial resolution better than the drift scale parameter $\rho_s = c\sqrt{m_i T_e}/eB$ is desired for density and potential measurements. Technically this means sampling rates close to 1 MHz and a spatial resolution of a millimeter or less. Unfortunately, today this combination is beyond the specifications of any available diagnostic. Nevertheless, there are several attempts to construct diagnostics which fulfill these requirements at least partially.

Statistical Techniques

Conditional averaging (CA) is one of the most frequently used techniques to detect a coherent signal fraction (large-scale structures) in a broad-band and incoherent background. The method of CA to extract a coherent signal fraction was first used by TOWNSEND [286]. Later KAPLAN and LAUFER [122] as well as KOVASZNAY, KIBENS and BLACKWELDER [139] systematically used this method to investigate fluid turbulence. Its first application to plasmas was reported by HULD and coworkers [99]. Since then it has been used to investigate the role of large-scale structures in many experi-

ments. In most studies in linear magnetized machines [39, 78, 99, 100, 209, 267, 268], simple magnetized tori [71, 76, 204, 266, J-5], tokamaks [10, 27, 55, 64, 89, 115, 240], and stellerators [77, 151] special attention was paid to the cross-field transport related to the observed structures. Because of its experimental and computational simplicity, the main advantage of CA is the high spatial resolution that can be obtained by using just two probes and a scanning technique. On the one hand, this allows to achieve a spatial resolution of a few millimeter, but on the other hand one obtains only the average evolution of the coherent signal fraction, which might differ from the dynamics of individual structures [1]. Later studies concluded that the conditional average is a good representation of the coherent signal fraction if the trigger condition is selected carefully [19, 114].

Another common statistical method and a close relative of CA [1, 79, 208] is the analysis of cross-correlation functions (CCF). Compared to CA, this method has the benefit of producing an unbiased average. In addition, it can be performed on the same data set used for CA, i.e. CCF is a classical two probe technique which gains its spatial resolution from a scanning technique. It has been successfully used to compute spectral estimates of fluctuation induced transport [221] and wavenumber and frequency spectra [23]. Further, it served well for topological studies of drift waves [163, 226, 247]. However, CCF is a phase sensitive method and thus CCF-results do not allow to make statements on fluctuation amplitudes, which are essential for transport measurements. In many cases similar results are observed with CCF and CA. This similarity is frequently used to stress the validity of the results. However, the close relation between unconditional (CCF) and conditional statistics (CA) [1, 79, 208] does not support this conclusion, and the reliability of spatio-temporal CA- and CCF-results is still an open question.

Finally, it should be mentioned that other statistical techniques exist and have been used to characterize drift wave turbulence locally, e.g. crossphase analysis [198], scaling laws [143], and bispectral analysis [233, 234], which is believed to be helpful for the detection of zonal flows [109].

Diagnostic Arrays

Besides statistical techniques, a second branch of diagnostics has developed during the last 20 years. This type of diagnostic aims to image the plasma dynamics via a synchronous multichannel recording, e.g. electrostatic probe arrays [113, 150, 165, 192, 202, 226, 239, 249, 317] or spectroscopic arrays [206, 318]. Their spatial resolution is limited by probe size, plasma disturbance, and finally the technical efforts per channel. Typical spatial resolutions of down to $1\,\mathrm{cm}$ are achieved, and typical array sizes are about 10×10 channels, which is too poor for advanced turbulence investigations like energy cascades or transport barriers. However, the temporal resolution is in most cases by far sufficient. In many cases sample rates of some MHz are achieved which is almost one order of magnitude higher than necessary. Despite of their low spatial resolution many nice experimental results document the experimental and diagnostic progress in the field, e.g. on destabilization of drift waves[121, 241, 248], their transition to turbulence [38, 136], change of instability type [35], the influence of sheared flows on stability [121, 259], and on structures in turbulence and their transport properties [62, 192, 226, 269, 306, 319]. Some examples are reviewed in Fig. 2.3.

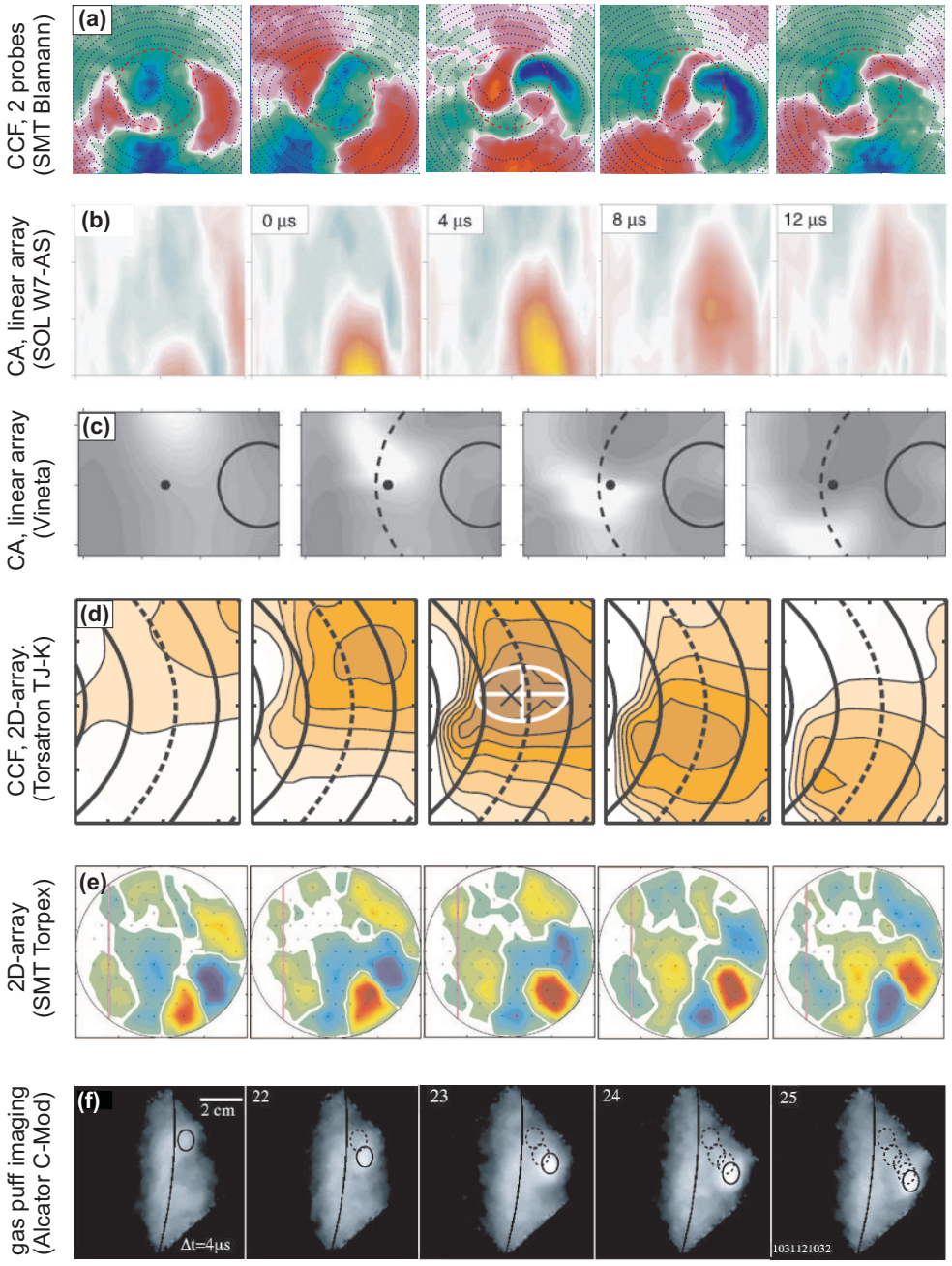

Fig. 2.3: Typical results of spatio-temporal diagnostics obtained with different techniques for various experimental configurations. (a) Cross correlation analysis of a helicon discharge in a simple magnetized torus [J-5], (b) conditional averaging result in the scrape-off layer of the stellerator W7-AS [77], (c) conditional averaging result in the linear device VINETA [306], (d) cross-correlation analysis of probe array data for a ECRH-plasma in the torsatron TJ-K [225], (e) probe array recording at the simple magnetized torus TORPEX [62], (f) images of the scrape-off layer of the tokamak Alcator C-Mod using the gas puff imaging technique [272]. Note, that in all measurements large-scale structures are clearly identified.

Recently TERRY and coworkers introduced an intensified high speed ($250\,$kHz) CCD camera with 64×64 pixel and a storage capacity of 300 frames. In combination with gas puffs they showed that short sequences of turbulence with high spatial and temporal resolution can be visualized in the edge of a fusion plasma [272]. Although this sophisticated system comes close to the desired specifications, the spatial resolution is still about a factor of $2-3$ too small, and the temporal resolution as well as the short recording times are not satisfying.

2.2 Spatio-Temporal Diagnostics

The general conclusion of Sect. 2.1 is that drift wave turbulence requires diagnostics with demanding spatio-temporal resolution to allow for an experimental investigation of structural formation. How this goal can be achieved is subject of this section. It reports on the prospects and limitations of spatio-temporal plasma diagnostics, introduces new developments, and discusses their applicability to plasma turbulence research.

2.2.1 Statistical Techniques

On the one hand, statistical techniques provide high spatial resolution on the expense that only the average evolution of the coherent signal fraction is accessible. On the other hand, the coherent signal fraction in a turbulent system might be small and contain a wealth of large-scale structures with different dynamical properties. This apparent contradiction raises a number of questions: How reliable are the results of statistical techniques like CA and CCF? What are their prospects and limitations? Are there possibilities to improve their performance? Answers to these questions are summarized in the following paragraphs.

Basics of Conditional Averaging

The common CA setup consists of two probes which simultaneously record a pair of time series, f_{RP} and f_{MP} [Fig. 2.4(a)]. One probe, called reference probe (RP), is located at a fixed position while the movable probe (MP) scans an area of interest. The typical procedure of CA requires that an event in the signal of the reference probe, $f_{RP}(t)$, lies within a prescribed amplitude interval and has a positive (negative) slope. Each time this trigger conditions is fulfilled, a short subseries (sequence) $f_{MP,k}(t^\star)$ with $t^\star \in [t_k - \Delta, t_k + \Delta]$ is selected from the time series, $f_{MP}(t)$ at the movable probe. Δ specifies the length of the subseries and is usually taken to be of the order of the correlation time of the signal. The subseries $f_{MP,k}(t^\star)$ are considered independent because they are not allowed to overlap. Finally, the CA-result is calculated by averaging over all subseries $f_{MP,k}(t^\star)$. Formally this reads

$$\langle f_{MP}(t^\star)\rangle_{ca} = \langle f_{MP,k}(t) \mid f_{c1} \le f_{RP}(t_k) \le f_{c2} \wedge \partial_t f_{RP}(t_k) \ge 0\rangle \tag{2.3}$$

with f_{c1} and f_{c2} denoting the lower and upper bound of the trigger window. The spatial resolution of CA results from a repetition of the above described procedure at all positions of the movable probe.

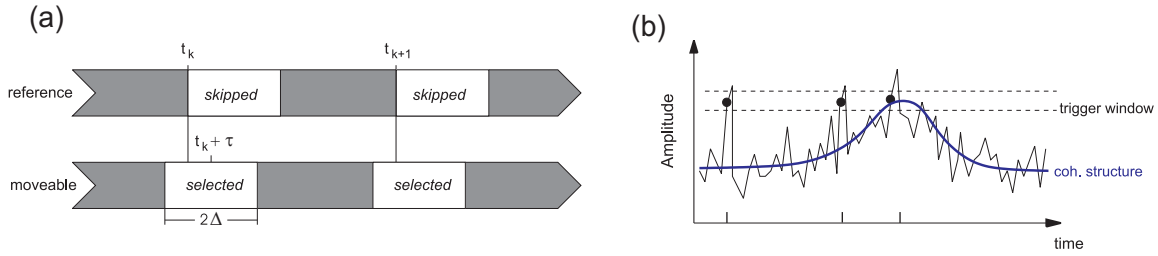

Fig. 2.4: (a) Data processing scheme for conditional averaging. A sequence of length 2Δ is taken from the movable probe signal at a time $t_k + \tau$ for each trigger event t_k found in the reference signal. Skipping a part of the reference signal after each detected trigger event avoids overlapping sequences. (b) Adding noise to a well-defined large-scale structure results in a finite probability for trigger events at wrong times. Those sampling steps which satisfy the trigger condition (window plus positive slope) are marked by circles. Two cases of wrong trigger events can be distinguished: (1) trigger errors are events without any coherent signal fraction being involved (left). (2) trigger jitter events are those with a slight deviation in t_k due to noise (center). From Ref. [J-6].

Theoretical Description of Conditional Averaging

To provide a better understanding of CA, it is worth to model the process. For this purpose the trigger condition is of central importance. Only a trigger condition which is specific for the coherent signal fraction assures a simple interpretation of the CA-result. Unfortunately, specific trigger conditions are difficult to define as they require a-priori knowledge of the structures, e.g. their shape. Therefore, it happens with a certain probability that the trigger condition is fulfilled by background fluctuations. In general, two typical scenarios can be distinguished [Fig. 2.4]:

1. trigger errors, i.e. a situation where noise causes a trigger event without any coherent structure being involved.

2. trigger jitter, i.e. a structure is recorded with a time shift due to noise.

To study their effect on CA and to provide a better understanding of CA an analytic model was derived [J-6]. Assuming large-scale structures being embedded in noise, it was shown that

$$\langle \tilde{f}(t^\star)\rangle_{ca} = \frac{\sum_{j=-\Delta}^{\Delta} p(t_k+j) f_{coh}(t_k+j)}{\sum_{j=-\Delta}^{\Delta} p(t_k+j)} \left[1 - M_{err}\right], \tag{2.4}$$

where M_{err} denotes the relative number of trigger errors and $p(t_k+j)$ is the probability for a trigger event at a time $t_k + j$. From the factor $[1 - M_{err}]$ in Eq. (2.4) it is directly seen, that the amplitude of the CA-result decreases with an increasing number of trigger errors. Whether the relative number of trigger errors is small or large is provided by the model as well:

$$M_{err} = \left(1 - \frac{M_{coh}}{M}\right) \sum_{j=0}^{2\Delta} p_{err}(t_k), \tag{2.5}$$

where M is the maximum number of sequences that can be placed within the recorded time series, M_{coh} is the number of coherent events, and p_{err} is the probability for a trigger event due to noise. This equation shows that M_{err} is small if the time series contains many coherent events, e.g. a wave embedded in noise. However, if the noise level is high or if coherent structures are rare, i.e. a typical situation in turbulence, M_{err} cannot be neglected. Thus our model shows that trigger errors have a severe influence on the amplitude of the CA-structure.

The influence of trigger jitter is not easily extracted from Eq. (2.4) and requires a detailed probabilistic treatment of the problem [J-6]. Essentially, the incoherent background introduces a finite probability for a shifted trigger positions [Fig. 2.4] and this probability becomes large if the coherent signal fraction is not significantly larger in amplitude than the incoherent part. Thus, the averaging process results in a broadening and damping of the CA-structure which is already substantial if the amplitudes of coherent and incoherent signal fraction are comparable [J-6].

Further, our model showed that CA is not scale sensitive if the common trigger condition [Eq. (2.3)] is used. Using a trigger window neither allows to detect only structures of a given amplitude nor does the temporal extent of a propagating structure reflect its spatial dimension in general. However, it was shown that CA recordings allow to measure the crossphase between density and potential fluctuations [J-5].

To benchmark our model, it was compared to CA of synthetic data. Figure 2.5 shows that both trigger effects cause a significant amplitude reduction of the detected coherent structures even for large structure amplitudes. Finally, the CA-results of synthetic data were found to agreed well with our model predictions [J-6]. Additional validation results from experimental data [J-5, J-7], where indeed a significant amplitude reduction was observed. Thus, it was demonstrated that our model contains all essential ingredients of CA and that the standard CA-method has severe limitations. Especially transport related to the coherent signal fraction is significantly underestimated. Moreover, if the CA-amplitudes are not reliable the closely related CCF method [1, 79, 208] would yield similar results, but for the same data set CCF would rely on a better statistical basis.

Improved Conditional Averaging

Once the problem of amplitude reduction is recognized, the question arises whether an improved trigger condition can avoid this and help to a retrieve reliable estimates of transport processes. In order to identify trigger errors and trigger jitter we introduced a correlation analysis of the CA-result [J-7]. The basic idea behind this is the following: If the CA-analysis allows to observe some structures, although their amplitude may be reduced, it is possible to use the CA-structures as a first estimate for the shape of the true structures, i.e. as a kind of *matched* filter. Computing the cross-correlation function (CCF) between CA-result and all selected subseries, it is possible to identify and select only those events which are neither trigger errors nor subject of trigger jitter. The results of this improved CA scheme were again tested with synthetic data. Figure 2.5(a) shows that the improved conditional averaging technique is able to recover the true structure amplitudes and the event statistic [Fig. 2.5(b)] reveals that this improvement is achieved by suppression of trigger errors and trigger jitter. We showed as well that this finding is reproduced with experimental data [J-7]. Therefore,

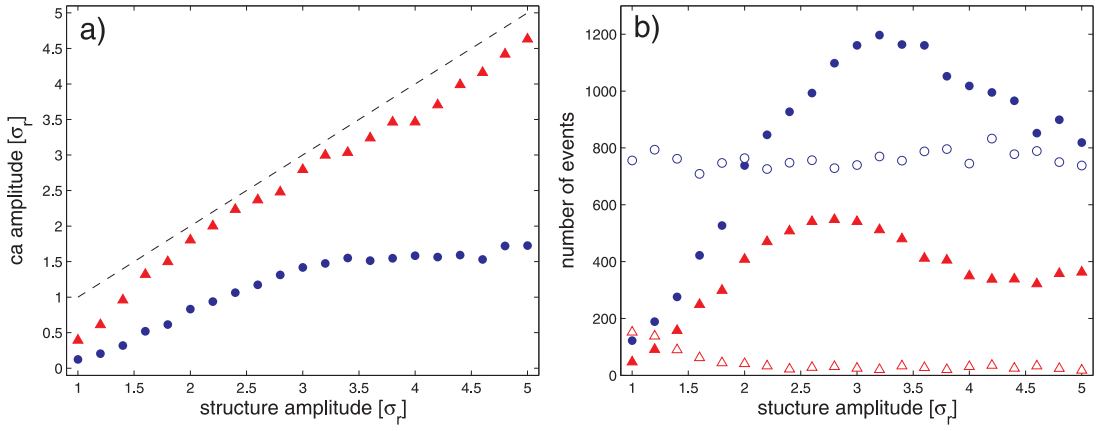

Fig. 2.5: Comparison of standard (circles) and improved CA-process (triangles) using synthetic data, i.e. randomly distributed Gaussian shaped structures. (a) Amplitude of CA-results as a function of structure amplitude. The dashed line indicates matching amplitudes. (b) shows the corresponding trigger event statistic for the amplitude scan shown in (a). The filled markers denote the number of correctly detected structures. The open markers give the number of trigger errors. Note that the number of trigger errors almost drops to zero for the improved CA-process (triangles) while the amplitudes are well recovered. From Ref. [J-7].

our improved conditional averaging scheme allows to obtain reliable information on structure amplitude. Consequently, the previous statement on the limitations of CA has to be extended: CA outperforms unconditional statistics if sophisticated trigger conditions are used. Further, this result stresses that the limitations of CA are closely linked with the trigger condition. Especially, spatial trigger conditions might improve CA even further.

2.2.2 Multiprobe Techniques

As discussed in Sect. 2.1, diagnostic arrays are lacking spatial resolution, but in many cases their temporal resolution is more than sufficient. This finding provokes the following questions: Does the low spatial resolution affect the measurement result? Are the observed structures reliable with respect to amplitude, shape and trajectory? If not, is it possible to identify the origin of the artifacts and can we remove them by data processing techniques? Finally, is it possible to enhance the resolution of diagnostic arrays?

Limitations of Diagnostic Arrays

Before discussing any measurement from probe arrays, it is essential to investigate the limitations of diagnostics arrays, especially to study the effects of a low spatial resolution on structure dynamics. From SHANNONs theorem, it is well known that a sampling frequency is required which is twice as high as the highest frequency to be measured. Transfered to spatial scales, this should not be violated for probe arrays. However, in many cases the structure size is close to the Nyquist limit. Hence, mea-

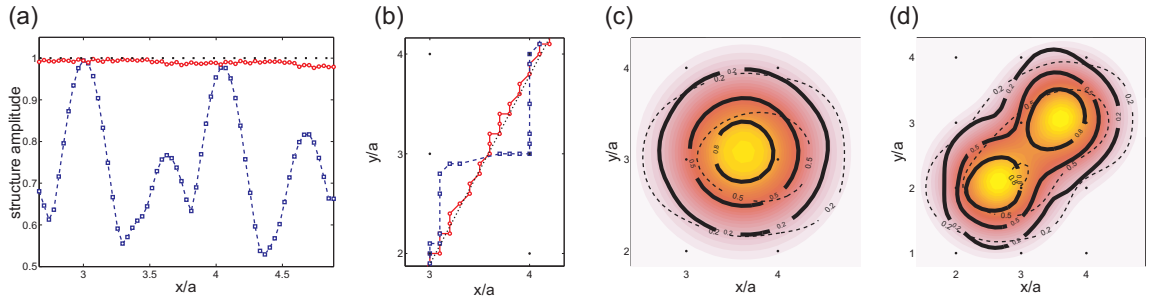

Fig. 2.6: Characterization of a Gaussian shaped structure of $\sigma = a/2$ measured with a probe grid with grid size a. The structure has a fixed amplitude and moves with constant velocity along a straight line. (a) Structure amplitude and (b) trajectory of the structure measured with (red) and without (blue) application of super-resolution. (c) shows the typical spatial distortion of the structure. The super-resolution result is shown as bold contour lines. The result without application of super-resolution (dashed contours) and a high-resolution image of the structure (color) as plotted for reference. (d) visualizes the achievable resolution with (bold contours) and without (dashed) application of super-resolution using the superposition of two Gaussian structures (color). After Ref. [J-8].

surements of structure amplitude, trajectory and shape should be studied carefully. For this purpose we used a virtual probe array consisting of 8×8 probes on a square grid. This array with grid size a was used to detect a Gaussian structure with $\sigma = a/2$ propagating with constant amplitude and velocity along a straight trajectory. Note, that this synthetic structure was studied with a virtual array and thus the results cannot be attributed to noise or probe displacements. The results are plotted in Fig. 2.6 [J-8]. In Fig. 2.6(a), the amplitude of the structure along its trajectory is plotted, which is an important quantity because it determines the lifetime and the transport properties of a structure. Strong amplitude fluctuations are observed, although the structure should have a constant amplitude (dotted line). Additionally, the trajectory does not follow the original path [Fig. 2.6(b)]. The trajectory basically consists of orthogonal parts which are aligned with the grid vectors of the probe array. Further, the maximum positions (squares) are not uniformly distributed along the trajectory, although they are measured with a fixed sample rate. They tend to focus close to probe positions, and hence the measured structure velocity shows strong modulation. Even the structure shape is strongly distorted [Fig. 2.6(c)]. Finally, the results show that even two structures in a distance a are not resolved [Fig. 2.6(d)]. Astonishingly, a systematic analysis revealed [J-8] that these distortions and errors are quite large even for structures with $\sigma = a$, i.e. structures which are significantly larger than the spatial Nyquist limit. Therefore, the low spatial resolution of diagnostic arrays is a severe limitation, especially as this is a general finding and not limited to Langmuir probe arrays. Additionally, the consequences are aggravated by the fact, that the spatial resolution of diagnostic arrays has technical and practical limitations [see Sect. 2.1.2].

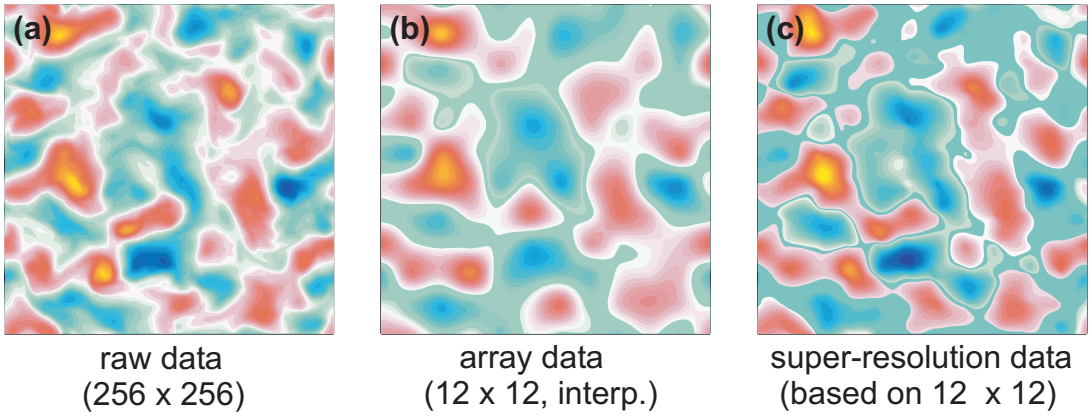

Fig. 2.7: (a) high-resolution image of turbulent density fluctuation obtained from a Hasegawa-Wakatani-drift wave model [196]. Red (blue) regions indicate positive (negative) amplitudes. The image is based on a data set of 256×256 data points. (b) Result of simple interpolation applied to a spatially down sampled data. The data basis is identical to (a) but uses only 12×12 data points to mimic the typical resolution of a probe array. (c) Result of super-resolution algorithm applied to the same down sampled data as used for (b). Normalization and color code are identical for all plots. From Ref. [J-8].

Super-Resolution Algorithm

A possible solution of the resolution dilemma are super-resolution algorithms, i.e. numerical schemes to enhance the resolution. The roots of super-resolution are in the field of computer vision, i.e. object recognition and tracking in satellite [203] or medical images [224, 211]. Here, typical applications of super-resolution techniques use several high-resolution images (~ 1 Mpixel) to produce a super-resolution image with even higher resolution. In general, super-resolution techniques require three basic steps to enhance the resolution of an image:

1. A series of low-resolution images is taken where all images are identical except for local or global subpixel shift due to object or camera motion.

2. The spatial shifts between images are estimated by computation of the optical flow field [20, 33, 94, 158, 167, 273].

3. The information of optical flow is used to register all images in a master frame which is resampled to produces a high-resolution image.

Although several super-resolution algorithms are described in literature, they are not applicable to spatio-temporal plasma diagnostics. While the first and third step do not cause severe problems, the second but most important step uses spatial derivatives which are subject of large errors for images consisting of just 10×10 pixels. Therefore, we developed a novel super-resolution algorithm which uses the high temporal resolution and a local correlation analysis to estimate the velocity field [J-8].

A basic performance test, using the same synthetic data as before, is plotted in Fig. 2.6. The results are encouraging. The structure amplitude is now fully recovered

[Fig. 2.6(a)], the trajectory follows the original path and the strong velocity modulation is significantly reduced [Fig. 2.6(b)]. Further, the structure shape is not distorted [Fig. 2.6(c)] and the increase of resolution is obvious [Fig. 2.6(d)]. These results show that the algorithm can handle the simple situation of an isolated structure without noise being involved.

In a next step we had to show that the algorithm can handle complex situations like turbulence, where many irregular shaped structures are involved, which obey complicated rules of motion. To demonstrate the applicability of super-resolution to turbulence data without lacking a well defined reference, simulations based on the Hasegawa-Wakatani drift wave model were performed. The simulations provided data with high spatial (256×256 pixel) and temporal resolution. A typical snapshot of density fluctuations with full spatial resolution is plotted in Fig. 2.7(a). To simulate a typical plasma diagnostic, the data was downsampled by a factor 23, i.e. the initial resolution of 256×256 was reduced to 12×12. The simple interpolated, low-resolution image is shown in Fig. 2.7(b). Clearly, the large-scale properties are similar, but the amplitudes are significantly lower and many small-scale structures have disappeared or merged to larger ones. Figure 2.7(c) bases on the same undersampled data, but this time the super-resolution algorithm was applied. The overall agreement with Fig. 2.7(a) has improved significantly. Now, the amplitude and shape of the structures are in good agreement. A more detailed study involving the temporal evolution showed that the super-resolution method at least doubles the resolution. Moreover, it removes all low-resolution artifacts, i.e. amplitude modulation, trajectory errors, and shape distortions [J-8]. Therefore, this novel super-resolution algorithm solves the resolution dilemma of diagnostic arrays and allows to retrieve reliable spatio-temporal recordings of a turbulent system.

2.2.3 Comparison of Statistical and Multiprobe Diagnostics

In Sect. 2.2.1 and 2.2.2 the prospects and limitations of both diagnostic branches have been discussed separately. Regarding the statistical methods CA and CCF, one question remained unanswered. It is still unclear whether the averaging process and the sequential recording introduce systematic errors. Fortunately, a direct comparison of both techniques is now feasible. The super-resolution algorithm allows to achieve a similar spatial resolution and its results were shown to be reliable. Hence, an application of both techniques to identical experimental conditions, should give a definite answer.

For this purpose, a Langmuir probe array consisting of 63 probes has been constructed and carefully calibrated [J-9]. This array and a 2D-scanning system were assembled in the linear, magnetized discharge arrangement KIWI [150]. Typical measurements of weak drift wave turbulence are plotted for both techniques in Fig. 2.8. The different columns depict the spatial fluctuation pattern for improved conditional averaging (left) and for four typical snapshots measured with the probe array [Fig. 2.8(a)-(d)]. The CA-result is a monopole-like structure, i.e. it reproduces the results of previous experiments using CA at this device [78] and at other devices [76, 77]. However, the probe array recording shows that the typical situation is not a monopole. In two thirds of the cases more than a single pronounced maximum is observed [Fig. 2.8(a)-(d) and Fig. 2.9(a)]. At first glance a surprising result because both

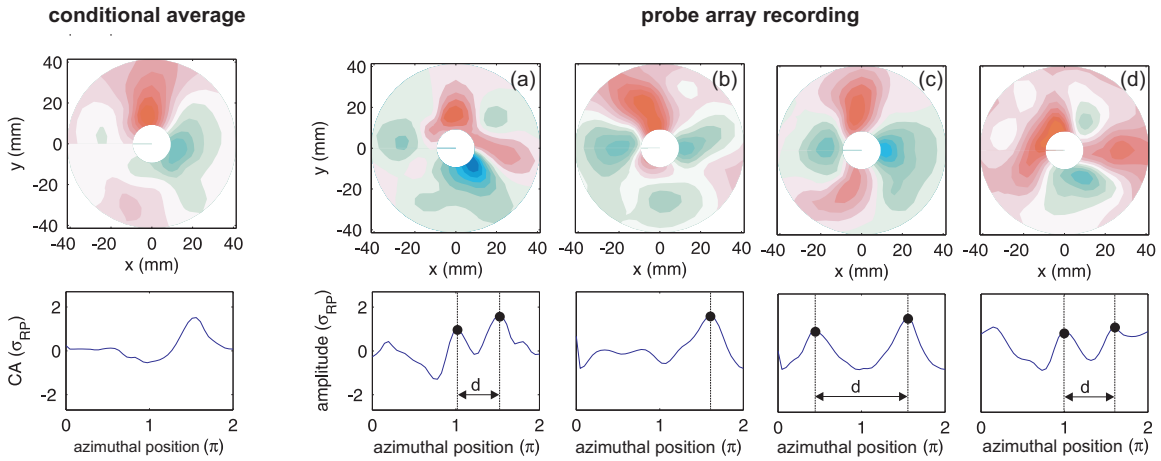

Fig. 2.8: Comparison of conditional averaging and a probe array recording. (a)-(d) typical spatial fluctuation pattern recorded with a 2D probe array for weak drift wave turbulence in the experiment KIWI. Density enhancements (reductions) are colored red (blue). The corresponding azimuthal fluctuation patterns at radial position $r = 2\,\mathrm{cm}$ are plotted below. The distance between local density enhancements is additionally marked. The conditional averaging result for the same data set is plotted on the left hand side. After Ref. [J-9].

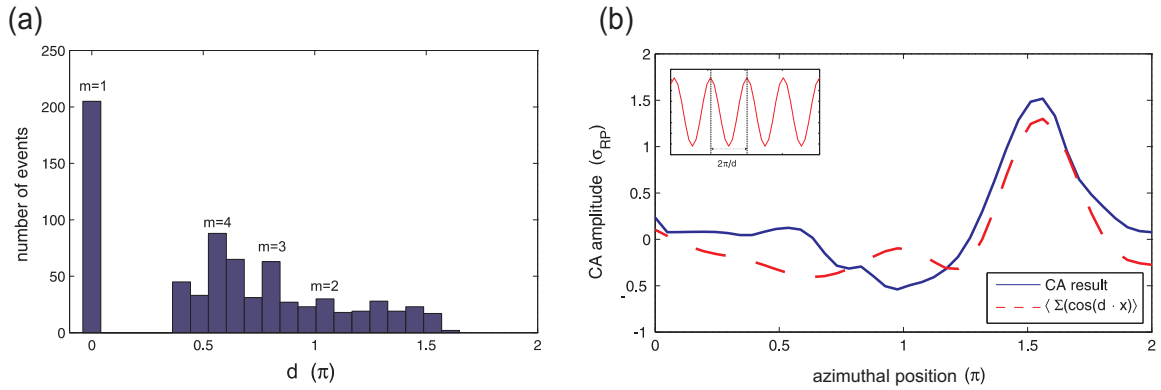

Fig. 2.9: (a) Distance distribution of two neighboring maxima as illustrated in Fig. 2.8. For subseries with a single maximum, the distance is set to 0. (b) The solid line is the CA-result as shown in Fig. 2.8. The dashed line is the sum of cosine functions with wavelength d, which is determined from each subseries used for the CA-process. The distribution of d is shown in plot (a). After Ref. [J-9].

techniques use the same data set. However, the wavelength distribution d measured with the probe array shows that the monopole simply consists of a superposition of monochromatic waves [Fig. 2.9(b)] [J-9]. Thus, the averaging process of statistical techniques can modify the result significantly. This is problematic, especially with respect to its physical implications. While large-scale monopoles are frequently taken as an indication of an inverse cascade in turbulent systems, a multi-mode situation does not support this interpretation.

To conclude, our measurement showed that even an improved conditional averaging technique reproduces structure size and amplitude only locally, i.e. close to the position of the reference probe. Globally, the fluctuation pattern of the CA-result differed significantly from a real spatio-temporal recording and this deviation is unambiguously related to the averaging process. Note, that this observation holds for unconditional statistical methods as well, because they involve a similar averaging process [J-9].

2.3 Synopsis

Motivated by the fact that the investigation of turbulence and related structural formation processes requires diagnostics with demanding spatio-temporal resolution and the circumstance that the available plasma diagnostics are not yet able to provide this, we have systematically investigated the prospects and limitations of current statistical and spatio-temporal diagnostics.

On the one hand, our results [J-6, J-7, J-9] showed that conditional and unconditional statistical approaches are well suited to obtain a local image of large-scale coherent fluctuations. If special attention is paid to the trigger condition, conditional averaging allows to retrieve absolute amplitude information and hence to estimate transport by means of cross-phase measurements of density and potential fluctuations [J-5]. Nevertheless, the results showed as well that the averaging process is an important limitation. It inhibits non-local imaging of the coherent signal fraction with just two probes. Only if a single structure type is buried by noise, the global average reflects the individual structure. Unfortunately, this does not apply to plasma turbulence and hence the prospects of statistical approaches are localized measurements only.

On the other hand, a systematic investigation of the properties of diagnostic arrays revealed limitations of similar importance [J-8]. It turned out that the low spatial resolution of diagnostic arrays causes strong distortions of amplitude, shape, velocity, and trajectory of a structure. However, these are essential quantities for the investigation of structural formation. This insight and the fact that the resolution of diagnostic arrays has reached technical limitations required a fundamentally different approach to enhance the spatial resolution of probe arrays. For this purpose we developed a super-resolution algorithm for plasma turbulence studies. Using super-resolution, it was demonstrated that it is possible to gain spatial resolution and to overcome the resolution dilemma.

To summarize, our investigations showed that diagnostics on the basis of arrays are capable to achieve the demanding spatio-temporal resolution requirements for plasma turbulence studies if novel data processing techniques are used. A combination of this

resolution enhancement with the technique of gas puff imaging [272] should allow to study zonal flow dynamics in detail and to contribute significantly to the understanding of transport processes in plasma turbulence. For many low β plasma experiments already the combination of super-resolution and probe arrays should yield a sufficient spatio-temporal resolution to investigate the details of structural formation experimentally.

Finally, it is important to note, that the future evaluation of spatio-temporal recordings will rely mostly on statistical techniques. Operations like detection, extraction and tracking of structures are indispensable parts of any spatio-temporal investigation of plasma turbulence. A first interesting concept has been introduced recently [192] and conditional averaging is certainly a promising candidate if spatio-temporal trigger conditions are used [J-6]. The presented results [J-6, J-7, J-9] provide a solid basis for this future development.

3. STRONGLY COUPLED PLASMAS

The classical way to enter the regime of strong coupling is a combination of low temperature and high density. Typical examples are high density plasmas, degenerated electron liquids [104] and laser-cooled ions [57]. However, a closer inspection of the coupling parameter

$$\Gamma = \frac{Q^2}{4\pi\epsilon_0 a_{ws}} \frac{1}{k_B T}. \tag{3.1}$$

(Q is the particle charge, a_{ws} denotes the Wigner-Seitz radius, and T is the temperature) reveals that highly charged particles will allow to observe strong coupling at moderate temperatures and low densities. These conditions are mostly achieved in complex (dusty) plasmas. Besides electrons and ions, a complex plasma contains a third comparably large and heavy species, namely dust particles. These micrometer sized particles typically attain several thousand elementary charges and play a role in astrophysical situations [295] and technical application [31]. In addition, complex plasmas are an ideal tool to study fundamental properties of strongly coupled matter experimentally. This chapter will briefly review the current status of research in the field of complex plasmas. Here, the focus is on the formation of three-dimensional (3D) dust clouds, their structure, and their dynamical properties.

3.1 Status of Research

The discovery that the dust particles in a complex plasmas can from crystalline structures [88, 178, 276] has opened a new field of research which allows to obtain a microphysical picture of strongly coupled matter. After 10 years, a broad spectrum of experiments, simulations, and theoretical approaches has achieved a considerable understanding of structural and dynamical processes in complex plasmas. A complete survey of the entire field of complex and dusty plasmas is beyond the scope of this thesis. For additional information the reader is referred to monographs [26, 31, 186, 262, 295, 296] and reviews on special topics in dusty and complex plasmas [69, 157, 180, 179, 187, 189, 213, 244, 260, 261, 291, 301, J-15]. Here, just a brief overview is given to introduce into the field and to formulate experimental objectives for this part of the thesis. A detailed description of previous research results is postponed to Sect. 3.2 to allow for a discussion in conjunction with own research activities.

3.1.1 Basics of Complex Plasmas

Compared with other strongly coupled systems, complex plasmas have a few advantages. First of all, they are stable at laboratory conditions. Second, typical densities of $1 \cdots 50$ particles per mm^3 and particle diameters of a few micrometers result in a high optical transparency and macroscopic dimensions of dust clouds. This transparency

can be used to illuminate particles at arbitrary position, i.e. even in the center of a cloud, and resolve the scattered light of individual particles with conventional CCD-cameras [63, 110] or to manipulate them [171]. Third, the charge-to-mass ratio of dust particles is small, and thus the dynamic response is slow. The dust plasma frequency ω_{pd} is in the order of several Hertz, and therefore the frame rate of CCD-cameras is sufficient to study dynamic processes in detail. Finally, the system is only subject of moderate damping due to friction with the neutral gas background, and thus many interesting dynamic phenomena, e.g. waves, can be investigated at a kinetic level. Especially for two-dimensional dust systems, the phase space evolution of all particles is experimentally accessible which provides a unique opportunity for a detailed comparison of experiment and theory. The latter is certainly the foundation of the success of complex plasma research.

One of the most important parameter in a complex plasma is the particle charge. Except for astrophysical situations [304], the particle charge is determined by the ambient plasma. For an isolated particle in a collisionless plasma the orbital motion limit (OML) model [6, 191] can be used to determine the floating potential at its surface. With help of a simple capacitance model [305] the particle charge is estimated. However, the validity of the OML model is questionable for many discharge conditions where different processes have to be taken into account, e.g. streaming ions [18, 102, 145, 199], collisions [36, 128, 193], and dense packing of dust particles [86, 309]. Measurements of the dust charge have been performed by means of resonance methods [178, 288], wave phenomena [92, 93, 231, 230] and particle collisions [138]. Unfortunately, none of them can easily be adapted to measure the particle charge in finite 3D dust clouds. Additionally, many plasma parameters cannot be measured with high precision in vicinity of dust so far. Thus, model-based calculations of the particle charge suffer from large uncertainties.

To understand dust confinement and dust dynamics, several forces are important. For large particles, the gravitational force exceeds all other forces because it scales with the volume of the particles. Due to the high particle charge, Coulomb forces are important for both, particle confinement and particle interaction. Furthermore, thermophoretic forces due to temperature gradients in the neutral gas [112, 238, 270] and friction with ions and neutral gas [61] cannot be neglected for dust particles. While gravitational, Coulomb, and thermophoretic forces as well as neutral gas friction are well understood, the ion drag force is still subject of intensive research activity. There are several models for the ion drag force [18, 101, 103, 123, 125, 126, 127, 130], but a complete self-consistent model is not yet available. On the one hand, the self-consistent treatment of the charging and shielding problem of particles is aggravated by the requirement to include streaming ions and collisions. On the other hand, a correct description of the contribution of scattered ions to the momentum transfer is not trivial. Although the recent models reflect considerable progress, the debate on the description of the ion drag force has not yet settled.

3.1.2 Confinement and Structure

To confine dust particles inside a plasma, the gravitational force has to be balanced. Thus, dust confinement is typically achieved in the plasma sheath region above an electrode where strong electric fields are present [152]. The trapping of the dust parti-

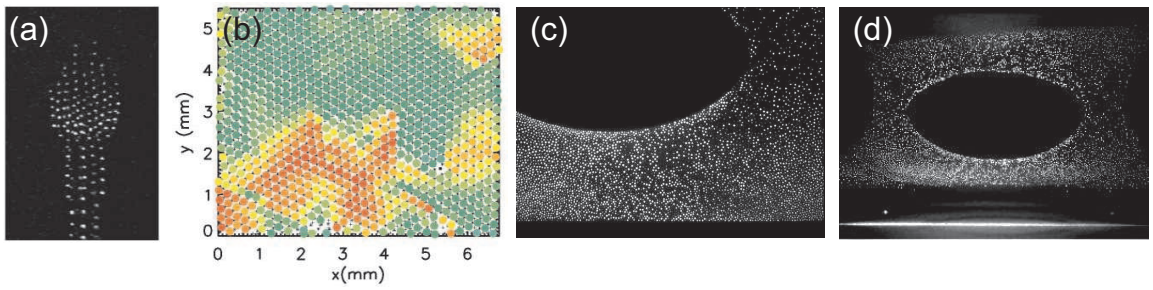

Fig. 3.1: Examples for experimental realizations of 3D dust clouds: (a) Dust cloud in an inductively coupled rf-discharge. Note that the dust grains form vertical chains due to a strong and directed ion flow. From Ref. [314]. (b) Structure of a multilayer crystal using small particles and high gas pressure to avoid chain formation. Coexistence of hcp (green) and fcc (red) lattices is observed. From Ref. [316]. (c) Typical dust cloud at microgravity conditions. A dust free zone (void) establishes in the center of the discharge due to ion drag forces. After Ref. [74, 188] (d) If gravity is compensated by thermophoresis, similar voids are observed. From Ref. [238].

cles in horizontal direction is established by depressions of the electrode surface [218] or flat metal rings on the electrode [288]. However, this results in a very anisotropic confinement potential. The confinement in vertical direction is much stronger and thus these dust clouds are mostly 2D systems which nevertheless can form highly ordered crystals with a hexagonal lattice structure [88, 178, 276]. Further, the supersonic ion flow towards the electrode is focused below each particle [169, 170, 177, 195, 253]. In multilayer systems, the resulting positive space-charge attracts particles in a lower layer. This process is responsible for chain formation observed in all dust clouds which are confined in regions of strong electric fields, i.e. regions with strong ion flows [see e.g. Figure 3.1(a)]. This alignment vanishes if small particles and high gas pressure are used [Fig. 3.1(b)] [87, 219, 316]. However, extended homogeneous 3D plasma crystals cannot be generated this way and investigations of dust dynamics are not feasible due to strong damping.

To produce extended 3D dust clouds, different approaches were followed. MERLINO and coworkers confined dust in a magnetized anodic plasma [16, 280] and investigated dust acoustic waves. Later, similar experiments on dust dynamics were performed in other discharges [68, 231, 230, 277]. To produce 3D plasma crystals, a number of experiments have been performed at microgravity conditions. These experiments have provided many interesting observations, e.g. of localized crystalline structures [197], of complex plasma boundaries [9, 37], of coalescence of complex plasma fluids [111], of transport properties [66, 67], and of low frequency waves and instabilities [129, 214, 243, 311]. However, the most striking observation was the formation of a dust free zone (void) in the center of the discharge [188, 197]. It was proposed that the ion drag force is responsible for the formation of voids [Fig. 3.1(c) and (d)] [74, 293, 292, 290]. The combination of simulations [3, 147, 146], experiments [134, 222, 238, 308], and recent ion drag models [101, 103, 123] were able to verify this. Although it was shown very recently that a void closure can be achieved [154], the formation of void-free crystalline dust clouds is still an important issue. Such dust clouds

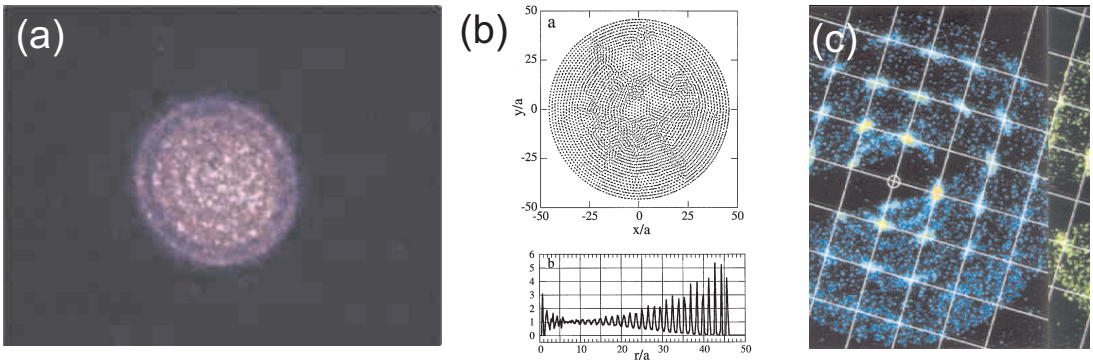

Fig. 3.2: Structure of ion crystals: (a) Image of a small, spherical ion cloud ($\sim$ 2000 ions) in a Paul trap. The ions arrange in distinct shells. After Ref. [190]. (b) MD-simulation of a cloud with 10^5 ions reveals bulk order close to the center and shell formation at the outside. From Ref. [283]. (c) Time-resolved Bragg diffraction pattern of a large ion cloud with a bcc lattice structure. From Ref. [107].

in a well defined confinement would allow to extend a large fraction of the successful research on 2D plasma crystals to 3D. Interesting observations were reported by ANNARATONE and coworkers [8, 11]. They observed spherical dust clouds with less than 50 particles in a secondary discharge in front of an adaptive electrode. Unfortunately, these clouds are rather in a liquid state and their confinement is not yet understood.

3.1.3 Dynamic Properties of Complex Plasmas

Most investigations on complex plasmas were focused on dynamic phenomena. New types of waves have been predicted and observed, e.g. dust acoustic waves [228], dust ion acoustic waves [50, 264], and dust lattice waves [168, 210]. Many nonlinear wave phenomena, e.g. shocks [161, 194, 243] and mach cones [56, 84, 175, 242] were studied and the role of compressional and shear waves in solids and fluids has been discussed [183, 215, 297, 300]. Certainly the detailed investigations of the solid-fluid phase transition are a highlight of complex plasma research [172, 254, 251, 275]. Recently, a growing interest on liquid complex plasmas can be noted. Several investigations aim at a deeper understanding of transport and diffusion processes in strongly coupled liquids [67, 66, 117, 156, 155, 201, 229, 294]. However, such dynamic properties were mostly studied in 2D complex plasmas.

3.1.4 Finite Systems

Systems consisting of just a few particles are of special interest, because their structural and dynamical properties strongly depend on the number of particles. Already THOMSON [282] investigated the structure of charged particle clusters in view of his atomic model. Although his results did not explain the structure of atoms, they mark the starting point for research on finite strongly coupled systems. In the field of non-neutral plasmas his ideas have been developed much further [57]. Using Penning and Paul traps [207] it was shown that the regime of strong coupling can be reached

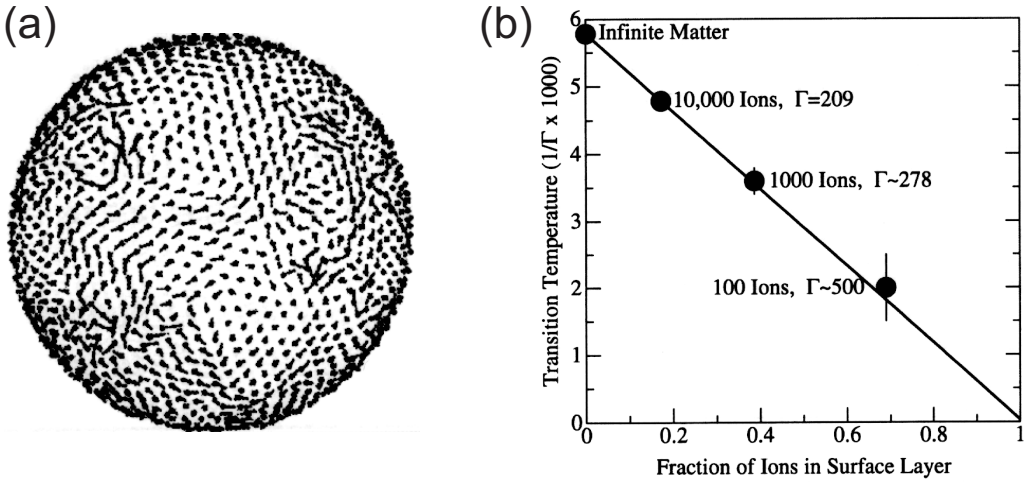

Fig. 3.3: Phase transition of finite Coulomb crystals: (a) MD-simulation of an ion cloud at a temperature near melting. The dots are the ions on the outer shell. From Ref. [245]. (b) Dependence of the transition temperature on cloud size. Note that smaller clouds tend to melt at lower temperatures. From Ref. [245].

for laser-cooled ions [54, 307]. With refined experimental techniques the ions were found to arrange on nested shells [72] and for large ion clouds *bcc* order was observed [Fig. 3.2] [30, 107]. The same results were obtained with molecular dynamics simulations [57, 83, 289] and it should be noted that the particle arrangement, especially those for closed shell configurations are very similar to those of noble gas [162] and metal clusters [13]. This finding is a hint that geometric constraints might determine the structure of small systems to a large extend. Nevertheless, approaching large clusters the shell formation should vanish and regular volume order should appear. This transition was predicted for ion clouds containing about 10^4 ions. However, recent experiments show that even small clouds ($N \sim 10^3$) can show *bcc* or *fcc* structure [190]. Further experiments investigated structural transitions due to resonant instabilities [131] and Coulomb bicrystals [95, 166]. In general it can be stated that many theoretical predictions [57] for these systems are not yet verified by experiments, e.g. the size dependence of the melting process [Fig. 3.3] [245]. The main reason for this is that the ion clouds are about 20 times smaller than complex plasma clouds with the same particle number and that the ion dynamic is too fast to track individual ions. Hence, these experiments are restricted to the analysis of the average structure of ion clouds. However, HUANG et al. [116] demonstrated that such experiments are generally possible in complex plasmas. KLINDWORTH et al. were able to show that the structural and dynamical properties of finite 2D cluster strongly depend on the particle number [133]. Further experiments and simulations treated normal modes [174], phase transitions [182], and structural properties of these systems [24, 252]. Nevertheless, for 3D systems experimental investigations are still missing, although they promise to answer many of the open questions.

3.1.5 Experimental Objectives

Although there are many open questions in complex plasmas, a striking challenge is the confinement and investigation of three-dimensional void-free dust clouds. Their structural and dynamical properties are mostly unexplored and the available predictions of theory and simulations lack an experimental verification. Especially, a detailed knowledge of finite strongly coupled dust clouds would certainly contribute to the general understanding of strongly coupled matter. Thus the experimental objectives of this part of the thesis are:

- Is it possible to produce compact dust clouds at laboratory conditions?
- Is it possible to reach the regime of crystallization?
- What are the structural properties of these clouds?
- How do they compare to other strongly coupled systems, e.g. laser-cooled ions?
- How can we measure the phase space evolution of such a 3D system?
- Is it possible to study the dynamical properties of strongly coupled dust clouds?
- Are liquid states or phase transitions experimentally accessible?
- Is it possible to generalize the obtained results?

3.2 3D Dust Clouds

To achieve these objectives, a number of dedicated experiments were performed. In a first step, the mutual interaction of dust particles and plasma was investigated (Sect. 3.2.1). This allowed us to address the confinement problem in a second step (Sect. 3.2.2), especially because we aimed at a quantitative understanding of the dust confinement. Once dust is trapped, new diagnostics are required to observe 3D dust clouds at a kinetic level. Recent progress in this field is described in Sect. 3.2.3. Finally, the Sect. 3.2.4 and 3.2.5 report on the current understanding of the structural and dynamical properties of 3D dust clouds.

3.2.1 Dust-Plasma Interaction

On the one hand, the presence of dust particles in a plasma might change characteristic plasma parameters, such as electron and ion densities, temperature, and plasma potential [4, 73, 85, 304]. On the other hand, plasma induced forces and especially the ion drag force are known to influence the structural properties of dust clouds [74, 253], but in both cases experimental verifications of theoretical predictions are rare [134, 176, 312, 313]. Nevertheless, the interpretation of many processes relies on an accurate knowledge of these quantities. In most cases plasma density, potential and temperature are obtained from Langmuir probe measurements [132], but how reliable are probe measurements in dusty plasmas? Further, how does dust affect the plasma? How important is the the Havnes effect [85] at moderate dust densities? How important are other effects like recombination on the dust particles? Is it possible to test

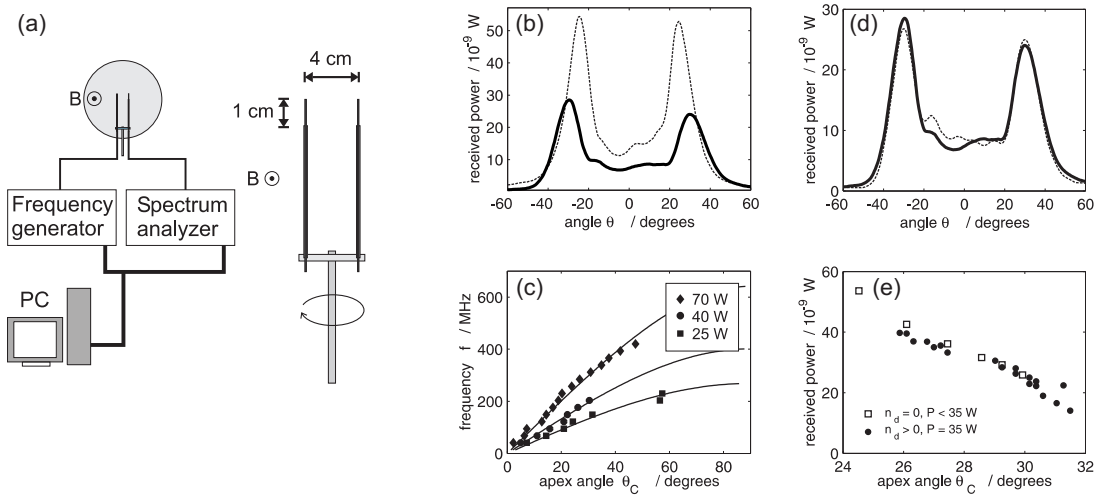

Fig. 3.4: Influence of dust on plasma density: (a) Schematic drawing of the set-up to measure resonance cones (left) and antenna arrangement (right). (b) Typical resonance cone measurement with (bold) and without dust for identical discharge power. The peaks indicate the apex angle of the resonance cone and allow to determine the electron density. (c) Observed apex angles for different plasma densities (discharge power P) and frequencies. The curves are the best fit values predicted by [65, 142]. (d) Two resonance cones for the same electron density. The measurement with dust is plotted bold. (e) Comparison of received power on the resonance cone for different discharge power and dust densities. From Ref. [J-10].

the theoretical predictions for the ion drag force experimentally, i.e. can we measure the ion drag force on a single isolated grain in the regime of low collisionality? The following paragraphs summarize recent activities to answer these questions.

Influence of Dust on Plasma Density

As mentioned above, measurements of the plasma density are usually performed with Langmuir probes [14, 160, 244, 278], which allow for high spatial resolution. Although Langmuir probes are generally regarded as a reliable instrument, their application bears some difficulties and limitations. First, an absolute measurement of densities demands for a good knowledge of the appropriate probe geometry [36, 132]. Second, in complex plasmas the active area of the probe surface can be reduced by deposition of dust grains [132]. Third, the probe can modify the dust density in its vicinity. Finally, an appropriate probe theory is mandatory. Especially, the presence of a magnetic field complicates the analysis of probe characteristics even further. In most cases the gyration of the electrons and ions has to be taken into account and demands for more sophisticated theories [144] than the classical OML [191] or ABR [7] theories.

To validate Langmuir probe measurements, independent and absolute measurements of densities, temperatures and potentials are required. In dust-free magnetized plasmas a suitable method for the measurement of the electron density is the resonance cone technique, which has been applied earlier in laboratory [25, 65, 105, 212, 216, 217] and ionospheric plasmas [236]. Although resonance cone measurements do not pro-

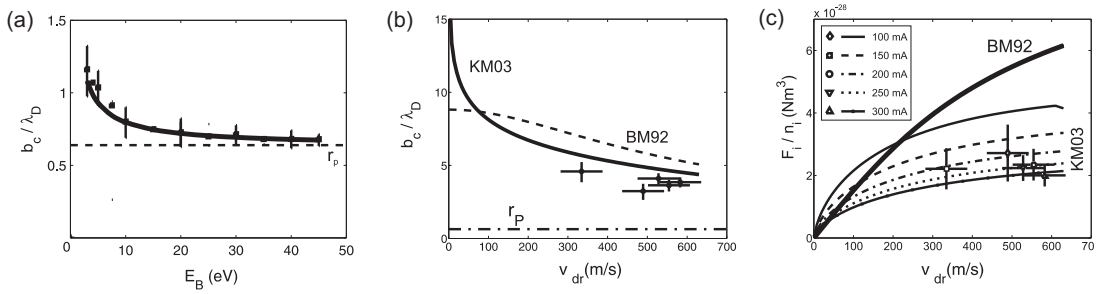

Fig. 3.5: Comparison of experiment and theory for the ion drag force in a collisionless plasma. KM03 refers to the ion drag model of Khrapak [125]. The model of Barnes [18] is labeled BM92. The particle radius r_p is plotted for reference. (a) Collection radius b_c for weak ion-dust interaction ($\beta < 1$). (b) Collection radius b_c for strong ion-dust interaction ($\beta \gg 1$). (c) Ion drag force for strong interaction.

vide the high spatial resolution of Langmuir probes, they allow for absolute density measurements without calibration and they are insensitive to contamination. To study the applicability of the resonance cone technique in dusty plasmas systematic measurements were performed with a standard resonance cone setup [Fig. 3.4(a)] [J-10]. For dust densities up to $n_d = 5 \times 10^8 \mathrm{m}^{-3}$ and large dust particles ($r_p \geq 10\mu$m) typical resonance cone curves were measured [Fig. 3.4(b)] and good agreement with a dust free description [65, 142] was found [Fig. 3.4(c)]. Additional measurements allowed to rule out that damping or scattering due to density inhomogeneities around the highly charged dust particles affect the resonance cone structure [Fig. 3.4(d) and (e)]. In summary, the resonance cone method was shown to be applicable to dusty plasmas.

This finding allowed to investigate the influence of dust on plasma density using both, Langmuir probe and resonance cone measurements. In our experiment, both techniques consistently found an electron density reduction of one third compared with the dust free situation [J-10], i.e. the resonance cone technique was successfully used to validate the Langmuir probe measurements. Further, a thorough evaluation of the Langmuir probe results [287] showed that the ion and electron density reductions were equal. For high dust densities, i.e. a situation where the Havnes parameter $P = 4\pi\lambda_{De}^2 r_p n_d$ [85] is larger than one, the electron density reduction is predicted to exceed those of the ions [73]. In our case the Havnes parameter was small ($P < 0.01$) and consistently an additional electron density reduction was not observed. However, the results showed that the dust had a notable influence on the plasma even at moderate dust densities because it basically acted as a loss surface. Especially for extended dust clouds, which are confined in a region of negligible plasma production, this finding has severe consequences. The dust charging and the shielding processes should differ in the bulk of the cloud and closer to its surface. Further dust-free discharge simulations are not suitable to estimate the plasma parameter of a dusty plasma. The importance of recombination processes was recently pointed out for the self-consistent modeling of dusty plasmas under microgravity conditions [2] and additional experimental evidence was reported by KLINDWORTH et al. [134]. Only for small clouds with just a few particles and hence a diameter of just a few interparticle distances, the density reduction due to recombination is certainly negligible.

Ion Drag Force

The force exerted on highly charged dust particles by streaming ions is an important aspect for the transport of dust particles [199, 256, 257] and the formation of voids [74, 188, 293] in radio frequency discharges. Although there are several models for the ion drag force in a collisionless regime [18, 123, 125, 130], only few experiments study the drag force quantitatively, e.g. Refs. [124, 310, 312, 313]. These experiments were performed in a parameter regime, where the influence of ion-neutral collisions during the scattering in the field of the dust particle cannot be neglected. Our experiments [J-11] were the first dedicated ion drag investigations in a collisionless situation. The ion drag force and the collection radius b_c were measured for weak ($\beta < 1$) and strong ($\beta \gg 1$) ion-dust interaction using monoenergetic ion beams and superthermal ion drifts to deflect free falling particles [Fig. 3.5]. For low values of beta ($\beta < 0.2$), i.e. high beam energy ($E_B < 3\,\mathrm{eV}$), already the model of BARNES [18] was found to give a suitable description, if the correct screening length is used. For large particle radii ($r_p \approx \lambda_D$), the ion drag force is mainly due to the collection of ions. Therefore, the collection radius b_c was directly calculated from the measured drag forces [Fig. 3.5(a)]. It was found that, at high ion energies, the collection of streaming ions was correctly described by the OML model [191]. For superthermal ion drifts ($\beta = 50 \cdots 122$), however, the OML model predicts collection radii $b_c > \lambda_D$. In this case, the collection radius was overestimated by the model of BARNES [Fig. 3.5(b)]. The critical parameter b_b from KHRAPAKs model [125] gave a better description of the capture of slowly streaming ions by highly charged particles and reproduced the measured ion drag forces [Fig. 3.5(c)]. Recently, NOSENKO et al. [200] repeated our experiments for $\beta = 16 \cdots 60$ and found good agreement with a slightly modified KHRAPAK model and thus they validated our results. Thus, our experiments have shown that the ion drag model of BARNES is not suitable for $\beta > 1$ and that a much better description is provided by the models of KHRAPAK.

3.2.2 Dust Confinement

Based on an improved understanding of the forces on dust particles, it is possible to tackle the confinement problem. In general, the recipe for dust confinement is simple: A sedimentation of particles in the plasma sheath can be avoided, if small particles, thermophoresis, or microgravity conditions are used. Further, if sufficient electric fields are provided to prevent a Coulomb explosion and if the ion drag force is small, it should be possible to observe stable void-free dust clouds. Unfortunately, this combination is difficult to achieve. Especially the experiments at microgravity conditions have taught us that typical discharge arrangements with plasma densities of $n > 10^{14}\mathrm{m}^{-3}$ always result in a strong ion drag force and related void formation. This section summarizes the recent experimental progress to produce void-free dust clouds. Two alternative discharge arrangements and their capability to confine dust were investigated. These investigations aimed at a detailed understanding of the dust confinement which is essential for any analysis of structural and dynamical properties of dust clouds.

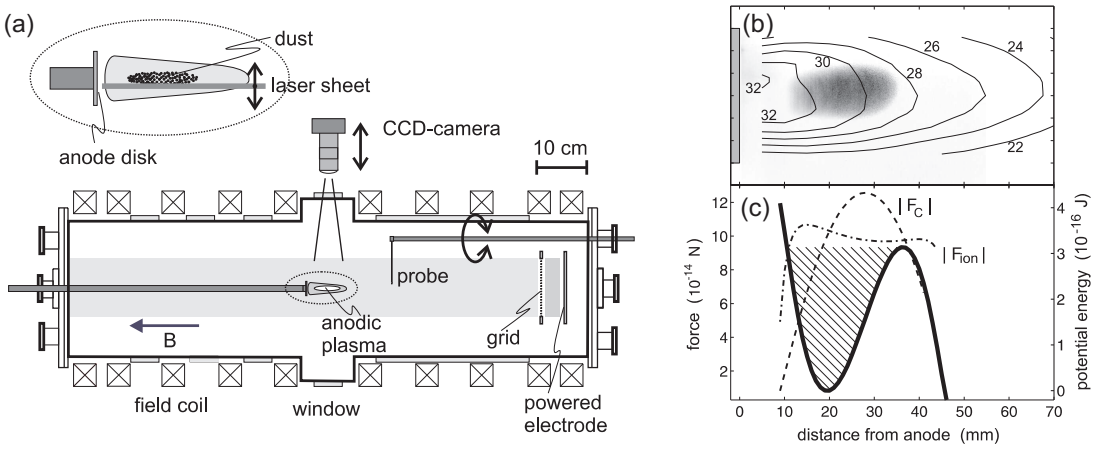

Fig. 3.6: Dust confinement in a magnetized anodic plasma: (a) Schematic side view of the setup. A laser sheet illuminates a horizontal slice of the particle cloud. A primary rf-plasma is produced at the right. The plasma expands through a grid and forms an extended plasma column. A positive voltage is applied to the anode and a secondary anodic plasma is formed in front of the disc electrode. (b) Potential contours at the midplane of the anodic plasma. The position of the confined dust cloud is indicated. (c) Effective potential well (solid line) and resulting confinement region (hatched) derived from Coulomb (dashed) and ion drag forces (dot-dashed). The forces are derived within a self-consistent discharge model using typical discharge parameter (B = 20 mT, p = 2 Pa, I_a = 6 mA) and spatially resolved probe measurements. From Ref. [J-12].

Confinement in Magnetized Anodic Plasmas

One approach to confine void-free dust clouds goes back to MERLINO and coworkers [17, 280]. They reported dust confinement close to a biased anode at the end of a Q-machine. Their observations provided first evidence that the coupling parameter of these dust clouds is large and might even be sufficient for the formation of a Coulomb crystal [17]. While the dust confinement close to the anode remained unclear, the confinement at the opposite side was assumed to be provided by a double layer. To analyze the confinement in detail, our experiments were performed with a similar experimental setup [Fig. 3.6(a)]. Our potential measurements clearly showed that the dust confinement is not related to the formation of double layers [Fig. 3.6(b)]. Instead, the axial confinement and the size of the dust cloud were quantitatively explained by an effective potential well formed by Coulomb and ion drag forces [Fig. 3.6(c)]. Additionally, a self-consistent model was formulated [J-12]. Based on probe measurements, it allowed to derive parameters which are not accessible by direct measurements, like ion temperature, ion drift velocity, and dust particle charge which are important for further investigations on structural formation and wave propagation. Our model revealed that the dust is highly charged ($Q = 3100e$), that the ion drift velocity is slightly superthermal and that the ion temperature ($k_b T_i = 0.1\,\mathrm{eV}$) is slightly higher than that of the neutral gas. First, these parameters show that the system is in a strongly coupled state and that indeed Coulomb crystallization could take place. It thus confirmed the observations and interpretations of BARKAN [17] and indeed PILCH et al.[220] re-

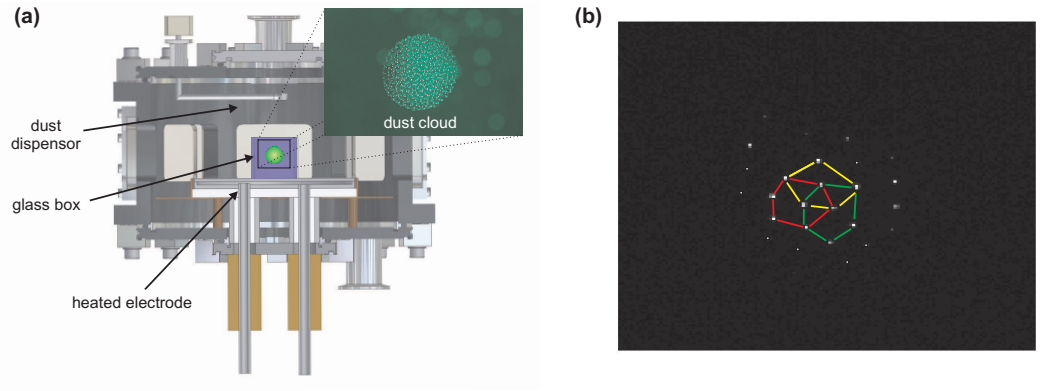

Fig. 3.7: (a) Side view of the discharge arrangement for Yukawa balls. The lower electrode is heated ($T < 90°$C). The vacuum vessel is grounded and keep at room temperature. The dust cloud is confined inside a glass cube where the upper and lower side are left open. The inset shows an image of a large dust cloud with 1 cm in diameter. (b) A thin slice at the front side of the cloud is illuminated. The particles basically arrange in a hexagonal lattice. After Ref. [J-13].

ally observed crystalline regions in these dust clouds very recently. Second, the E/p values, which denote the energy gain between two collisions, indicate that our experiments were not performed in a collisional regime. Although this is of minor importance for the confinement, it is important for the stability of the dust cloud with respect to dust density waves. So far dust acoustic instabilities were studied in the collisional regime only, e.g. Refs. [15, 280]. Our experimental setup allowed to investigate the kinetic regime of dust acoustic waves and to test related theories for the first time [see Sect. 3.2.5].

Confinement in RF-Discharges

A different approach to confine void-free dust clouds is motivated by experiments, simulations and theories on void formation [5, 74, 188, 238]. Those results showed that a void-free dust confinement at moderate plasma densities is hampered by the inherent ion flows towards the discharge boundaries. As a consequence, we have modified the usual setup of an asymmetric capacitively coupled rf-discharge [Fig. 3.7(a)]. To establish a vertical temperature gradient the rf-electrode was heated to $T = 60 \cdots 80°$C. The grounded vacuum vessel was kept at room temperature. The resulting thermophoretic force should balance gravity for particles with a radius $r_p < 3\,\mu$m, i.e. allow for dust levitation in the bulk plasma. In addition to the experimental setup used by ROTHERMEL [238], we proposed to place a glass box with squared cross section on the electrode. The glass box was left open at the top and at the bottom. For low discharge power ($P < 10$ W), we discovered that dust, which was dropped into the glass box, formed spherical void-free clouds [J-13]. A picture of a laser illuminated dust cloud (Yukawa ball) consisting of roughly 10000 dust particles is shown in the inset of Fig. 3.7(a). Already if only the front of such a dust cloud was illuminated with a laser sheet, interesting structural properties were observed [Fig. 3.7(b)]. The particle arrangement was static and particles on the surface of Yukawa balls seemed to have preferably 5 or 6

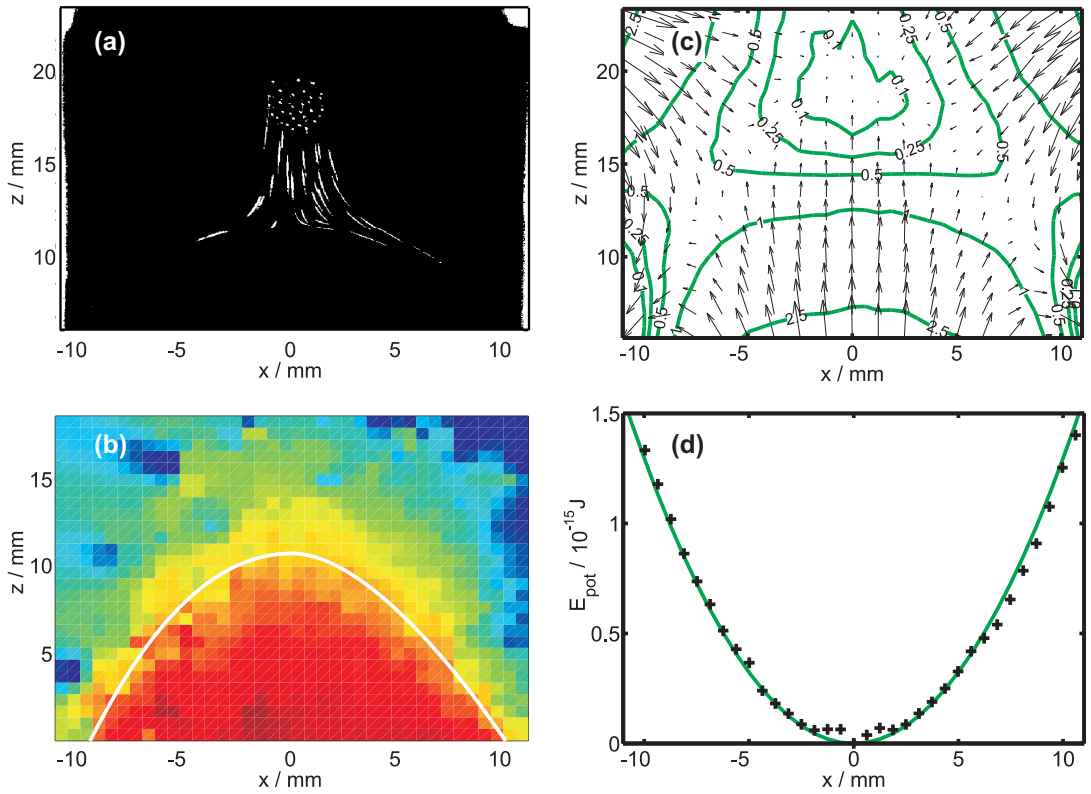

Fig. 3.8: Experiments on the confinement of Yukawa balls: (a) Superposition of multiple video frames. As soon as the discharge is switched off, the trapped particles fall down. Their motion is only affected by gravity and the thermophoretic force. (b) Vertical component of the experimentally determined thermophoretic force field. In 'red' regions the thermophoretic force exceeds gravity, in 'blue' regions gravity is dominant. The solid line shows where both forces balance. (c) Trap potential obtained from PIV measurements and fluid simulations. (d) A horizontal section through the trap center reveals an almost parabolic confinement. From Ref. [J-14].

nearest neighbors. Moreover, the particles did not form vertical chains, i.e. we found first evidence that the Yukawa balls were in a solid or even crystalline state.

To achieve a quantitative description of the dust confinement, fluid simulations with the SIGLO-2D code [28, 29, 265] in combination with additional experiments were performed [J-14]. The results are summarized in Fig. 3.8. It was found that thermophoresis alone was not sufficient to explain the confinement [Fig. 3.8(a)]. By means of particle imaging velocimetry (PIV) experiments the thermophoretic force field was measured [Fig. 3.8(b)]. It was found that thermophoresis contributed about 70 percent to the vertical confinement and that the radial confinement and the remaining 30 percent in vertical direction were provided by plasma induced forces, namely electrostatic fields due to surface charges on the glass [J-14]. Further, the fluid simulations showed that the Yukawa balls were confined in a region where the plasma production was negligible. Due to the low plasma density ($n \approx 10^{13}\mathrm{m}^{-3}$) and the weak electric fields the ion drifts were significantly below the ion sound speed. The resulting ion drag

force was about two orders of magnitude smaller than the electrostatic confinement force. Hence, it could be neglected and chain formation is not expected. The confinement provided by the combination of gravity, thermophoresis and electric fields is plotted in Fig. 3.8(c) and is in very good agreement with the experimental observations [Fig. 3.8(a)]. It yields the correct levitation height, its depth is sufficient to trap particles with a few thousand elementary charges and even its asymmetry was observable for huge clouds in the experiment [J-14]. For further structural analysis and especially for comparison with simulations and with other strongly coupled systems, it is important to note that the trapping potential is essentially isotropic and parabolic for dust clouds with a radius of less than $2\,\mathrm{mm}$, i.e. $N < 1000$ particles. Furthermore, for the trapping process an interaction of dust and plasma, as proposed by TOTSUJI [285, 284], is not required. The particle trap is provided by external forces only and thus our trap geometry is closely related to those of Penning and Paul traps [207]. This allows for a direct comparison of the structural properties of Yukawa balls and trapped laser-cooled ions.

3.2.3 3D-Diagnostic

The success of 2D plasma crystals and liquids is mostly attributed to the unique possibility to observe the system at a kinetic level. However, a conventional video microscope is not offhand applicable to 3D systems because it is not able to resolve the depth position along the optical axis and second the optical properties of macro lenses restrict the observable volume to a thin layer due to the necessity of a large aperture to collect enough light for particle detection. For the early experiments, only scanning video microscopes [219, 316, J-13] and a color-gradient based system [8] were developed and used for 3D diagnostic. The first consists of a standard video microscope which is mounted on a translation stage [Fig. 3.9(a)]. Scanning along the optical axis allows to illuminate and observe a sequence of slices of a trapped dust cloud. Using a laser sheet which is significantly thinner than the typical interparticle distance, the 3D coordinates of particles are determined from the variation of the particle brightness in subsequent frames. Although this diagnostic setup is simple and allows to cover volumes of the order of a few cubic centimeters, the sequential image recording limits its application to static particle configurations, i.e. liquid systems or dynamical processes cannot be studied. With a color-gradient based system these processes are accessible. Here, the particle cloud is illuminated with two overlapping laser sheets of different color and the depth information is deduced from the particle color. The trade off for the instantaneous measurement of the particle positions is a reduction of the observable volume to a few interparticle distances in depth because the aperture problem is not solved. Additionally, the sophisticated setup [8] requires a thorough calibration to achieve good spatial resolution and a conversion of the particle positions into absolute units. Finally, aligned particles are only separable if an additional camera with a different perspective is used.

To conclude, scanning video microscopy and color-gradient based diagnostics are first steps towards a versatile 3D diagnostic but their performance and/or usage are not satisfying. The following paragraphs will introduce two recent developments for 3D diagnostic, stereoscopic imaging [Fig. 3.9(b)] and digital holography [Fig. 3.9(c)].

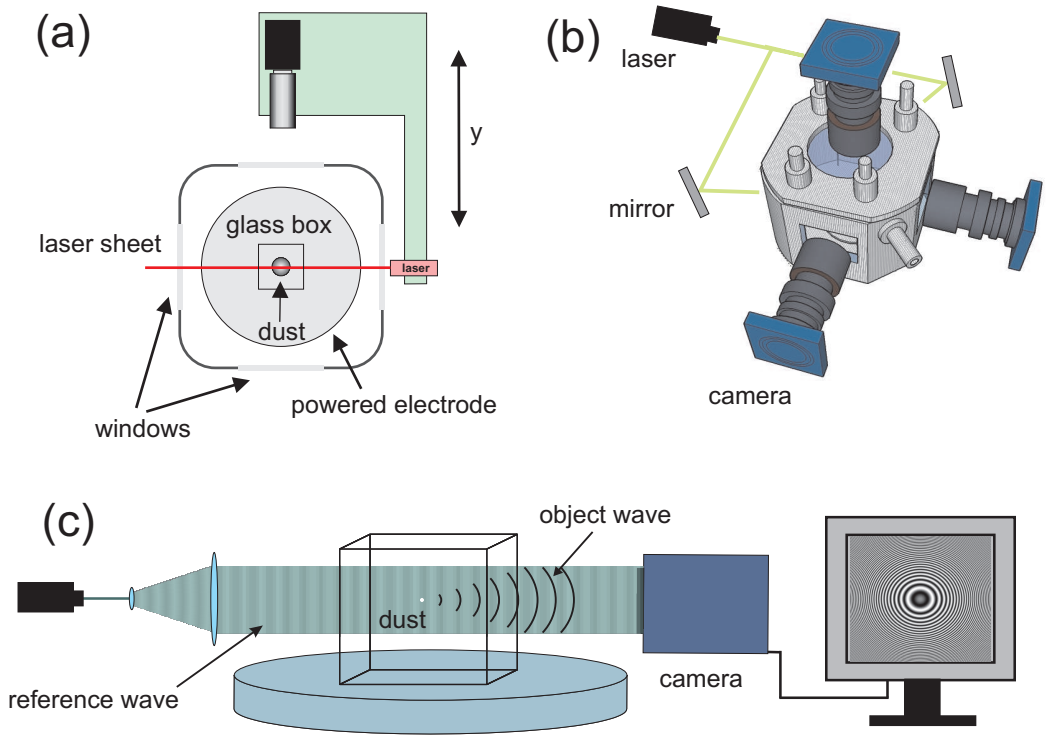

Fig. 3.9: Selected 3D diagnostics: (a) Top view of the scanning video microscopy setup. A vertical laser sheet illuminates a thin slice of the dust cloud. Images are taken at right angle by a CCD-camera with a macro lens. Camera and laser are mounted on a common translational stage to image all slices of the dust cloud during a scan. (b) The stereoscopic imaging setup consists of three cameras with perpendicular optical axes. The dust cloud is illuminated from two sides with an expanded laser beam. (c) Setup for digital inline holography. The expanded laser beam is the reference wave and interferes with the object wave at the CCD sensor. An interference pattern for a single particle is sketched on the monitor. From Ref. [J-15].

Stereoscopic Imaging System

A simultaneous determination of dust particle positions can be achieved if the particle cloud is observed with at least two cameras from different perspectives [120, C-3]. Such a stereoscopic imaging system (SIS) is sketched in Fig. 3.9(b). Three cameras with perpendicular optical axes are used to image the volume around the intersection of their optical axes. The particles are illuminated by two expanded laser beams and observed in forward scattering to maximize their brightness. The resolution of SIS is comparable to those of SVMs and the frame rate $f > 100$ fps allows to study fast dust dynamics, e.g. even the thermal fluctuations of the particles around their equilibrium position. Due to the aperture of the lens system the focal depth of each camera is limited to about $3\,\mathrm{mm}$, which implies that presently only small dust clouds with $N \leq 100$ particles are accessible with SIS. At first glance, three cameras should allow for an unambiguous determination of the 3D position of all particles even if the particle images overlap in one camera image. However, our results showed that the probability for shadowed parti-

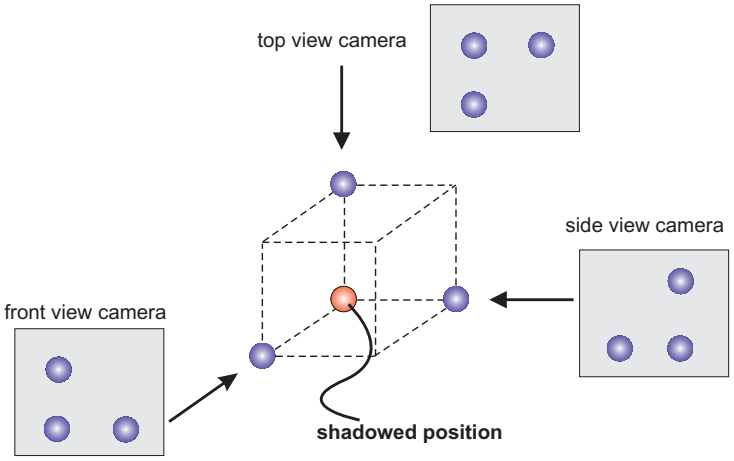

Fig. 3.10: Challenge of stereoscopic imaging: The sophisticated reconstruction of particle positions is additionally complicated by the finite particle size in each camera image. This results in a certain probability that a particle (red) is shadowed in all camera images.

cles [see Fig 3.10] has to be taken into account even for small dust clouds and especially for larger particle numbers an unambiguous position reconstruction becomes increasingly difficult. However, for small dust clouds, our reconstruction algorithm solves this problem and typical measurements with this system are presented in Sect. 3.2.4 and 3.2.5.

Digital Inline Holography

Since most problems discussed so far are caused by lenses, it stands to reason to use an imaging system without lenses. A well developed technique to encode 3D information in a single image is holography. In general, this method does not require any lens for the imaging process. Although it has never been used in the field of dusty plasmas, applications in other fields report promising results. In fluid dynamics [91], micrometer sized tracer particles immersed into a fluid were used to measure turbulent velocity fields. For biological applications, digital holographic microscopes are well developed [58, 106]. Further, it was demonstrated, that micrometer sized particles can even be resolved if a CCD-sensor is used instead of holographic photo plates [223]. It was shown that digital holography works for particle densities up to 10 per mm^3 and that the errors in particle position are just a few particle diameters if amplitude and phase information are used for particle detection [205]. Therefore, digital inline holography (DIH) should be applicable to dusty plasmas as well.

However, to apply holography to dusty plasmas additional problems have to be considered and solved. First, the particles are immersed in an incoherent light source, the plasma. Thus, it is questionable whether a sufficient signal to noise ratio can be achieved for a reliable hologram recording. Second, the particles are confined in a plasma reactor, i.e. in a vacuum chamber. This implies a number of technical challenges, i.e. to cancel out vibrations and to minimize the disturbance of the plasma chamber which separates the particles and the optical setup. Third, a very short exposure time ($\tau \ll 1\,\mathrm{ms}$) is required to avoid that the thermal motion of the particles

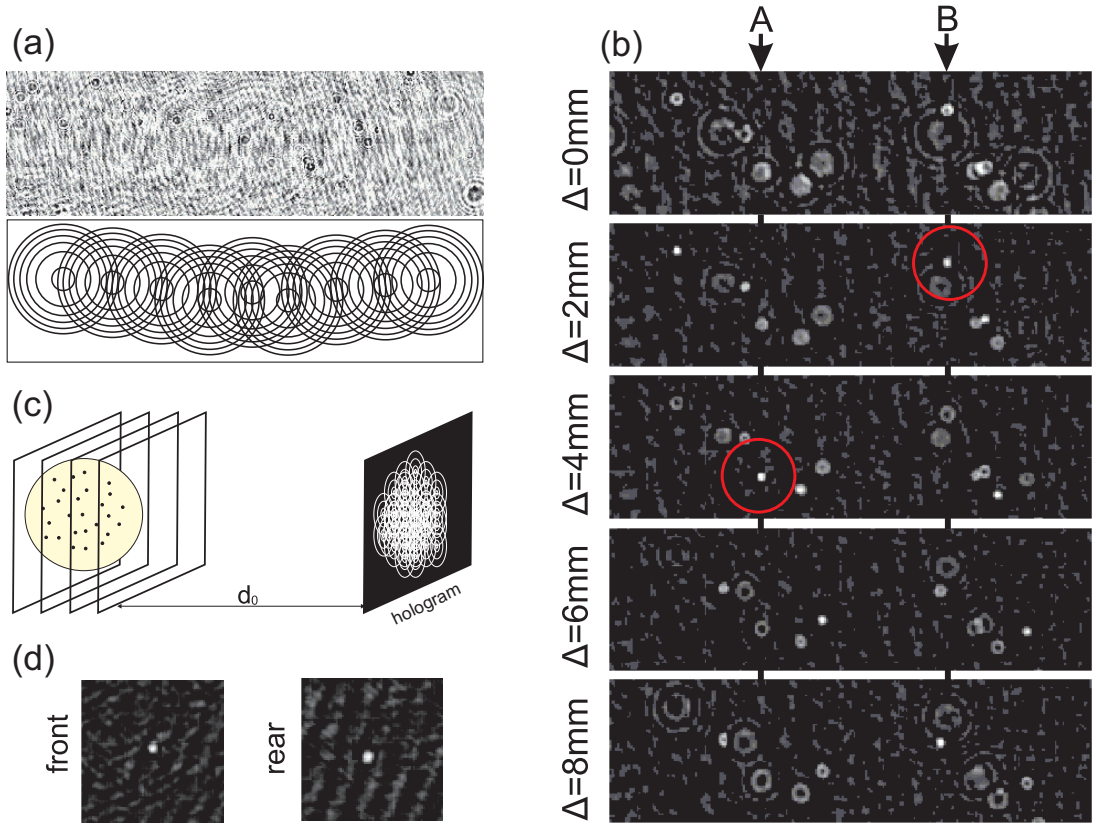

Fig. 3.11: Digital inline holography of dusty plasmas: (a) Contrast enhanced hologram of dust particles in a rf-discharge (top). A sketch of the hologram is plotted below. (b) Reconstruction of the hologram in a distance $d_0 + \Delta$. Two particles (A, B) are labeled and their focus planes are marked with red circles. (c) Illustration of the reconstruction geometry. The reconstruction planes shown in (b) are indicated by empty squares. The dust cloud is symbolized by the yellow sphere. (d) Focused particles with a distance $\Delta_{front} - \Delta_{rear} = 40\,\mathrm{mm}$, to illustrate that DIH overcomes the usual problem of a limited depth of focus.

destroys the interference pattern. Finally, it has to be demonstrated that its spatial resolution can compete with other 3D diagnostics.

Lately, we were able to demonstrate that the mentioned obstacles can be overcome. In our optical setup [Fig. 3.9(c)], the reference wave is a plane wave realized by an expanded laser beam. It illuminates the spherical particles. The small fraction of the scattered light is the object wave. Since both have a fixed phase relation, their interference pattern is detectable with the sensor of our CCD-camera. The typical hologram of a point-shaped object, which is a reasonable approximation for a spherical dust particle, is a Fresnel zone plate (FZP) plotted on the monitor in Fig. 3.9(c). It consists of concentric dark and bright rings. Figure 3.11(a) depicts a contrast enhanced hologram of dust spheres with radius $r_p = 10 \pm 2\,\mu\mathrm{m}$ inside a rf-discharge. The FZPs of individual dust particles are easily recognized with help of the schematic drawing below. To extract particle positions, it is necessary to reconstruct the particle cloud from the holographic recording. For a digital hologram the reconstruction is done numerically.

This enables us to use both, amplitude and phase information of the reconstructed image. Note, that the latter is inaccessible in a classical holographic setup. The numerical reconstruction bases on Huygens principle. Every point of the hologram is regarded as the origin of an elementary wave whose amplitude is defined by the intensity of the hologram at this point. The superposition of all these elementary waves forms the reconstructed object. The mathematical formulation of this principle is the Fresnel-Kirchhoff integral and numerical solutions are described in Ref. [246]. Numerical reconstructions of a part of our hologram in a distance $d_0 + \Delta$ [Fig. 3.11(c)] are shown in Fig. 3.11(b). Each image shows several particles which are located at different distances $d_0 + \Delta$. To demonstrate that the depth of focus of this setup covers several centimeters, Fig. 3.11(d) shows sharply focused particles at the front and rear side of the glass box. Using the PECA-method proposed by PAN et al. [205] our spatial accuracy is in the order of a few particle diameters [141]. Thus, our experimental results show that DIH is a suitable and powerful method to determine particle positions in 3D dust clouds.

3.2.4 Structural Properties of Yukawa Balls

To investigate the structural properties of Yukawa balls, we used the methods of scanning video microscopy and stereoscopy so far. These methods allow to obtain answers on a number of quite fundamental questions: First, are Yukawa balls liquid or solid? Is it possible to observe crystalline states? Second, are the structural properties affected by the finite size of the system? Third, are Yukawa balls similar to other strongly coupled systems like trapped laser-cooled ions? Does screening affect their structural properties? Finally, are the structural properties determined by geometric considerations or by the mutual interaction of the particles?

Global Properties

To answer the first question, it is instructive to look at the coupling parameter Γ. For an extended system the solid-liquid phase transition should occur around $\Gamma_c = 170$ [104]. If screening is included, this value almost increases exponentially with κ [80, 235]. Further, finite size effects increase the melting temperature [245] and thus for a system with $N = 100$ particles and $\kappa = 0.5 \cdots 1.0$, already values of $\Gamma_c > 800 \cdots 1360$ are required. For Yukawa balls, measurements of the particle density reveal a typical Wigner-Seitz radius $a_{ws} = 0.35 \pm 0.05\,\mathrm{mm}$. Thus, crystalline Yukawa balls require particle charges of $Q \geq 2000e$. Based on recent charging models [128] and plasma simulations, charge calculations show that this value is reasonable for Yukawa balls [J-14]. Unfortunately a direct charge measurement has not been feasible, but a test of the LINDEMANN citerion [153] allowed us to show that Yukawa balls are crystalline systems, which are close to the melting point [J-13].

Particle Arrangement

Once the particle arrangement is measured, the crystalline structure of Yukawa balls can be analyzed in detail. Fig. 3.12a visualizes the typical structure of an experimentally generated Yukawa ball. Using cylindrical coordinates z and $\rho = \sqrt{x^2 + y^2}$, a clear

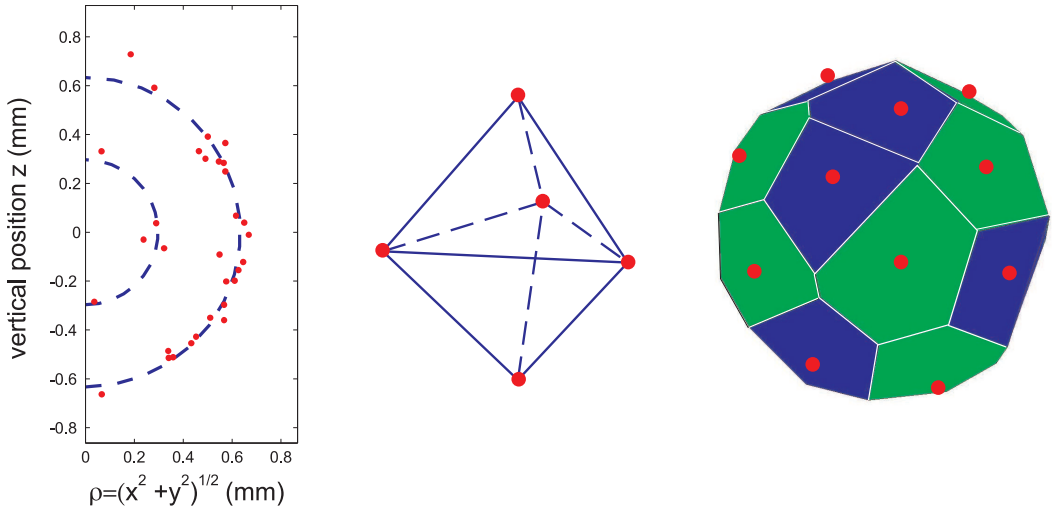

Fig. 3.12: Structure of a $N = 31$ cluster. (a) Particle positions in cylindrical coordinates in the ρ-z plane. The red dots are the average particle positions of a (5,26) configuration. The dashed lines indicate the shell radii. (b) Structure of the inner shell. (c) Voronoi analysis of the corresponding outer shell with $N_o = 26$. Pentagons are blue and hexagons are green. The particle positions are marked with dots. All plots show experimental results. From Ref. [J-15].

formation of shells is observed. The inner shell consists of 5 particles whereas 26 particles form the outer shell. While the inner shell is a symmetric double-tetrahedron [Fig. 3.12(b)] which represents a typical closed-packed structure, the Voronoi-analysis of the outer shell shows a pattern of hexagons and pentagons [Fig. 3.12(c)]. The same particle arrangement is expected for a 2D hexagonal lattice being bent to a sphere. Repeating this type of analysis for measurements of about 50 clusters consisting of 100 to 500 particles [C-4, J-16] revealed that the shell structure with its hexagonal lattice with pentagonal defects is the generic structure of Yukawa balls. Furthermore, the experimental data allowed us to compare the intershell distance d with the typical interparticle distance b. With $d = (0.86 \pm 0.06)\, b$ [C-2] an excellent agreement with local icosahedral ordering ($d_{ico} = \sqrt{3}b/2 = 0.866\, b$) was found [83]. Therefore, our experiments showed that Yukawa balls are crystals which have the same type of structure as laser-cooled ions [57, 83]. Moreover, the structural properties are fully reproduced in our molecular dynamics and Monte-Carlo simulations [22, 159, C-1, J-16]. Further, the so-called magic configurations, which are very stable clusters due to closed shell configurations, are similar to those arising from pure geometric considerations [159, 162, C-1].

Influence of Screening

Although the similarity of the structures of Yukawa balls and laser-cooled ions are striking, the latter are pure Coulomb systems, while the particle interaction in Yukawa balls is weakened by screening. This raises the question whether these systems are really identical or whether the screening substantially changes the structure. In Fig. 3.13(a) the experimentally determined cluster radii are compared with simulations for pure (dashed) and screened (solid) Coulomb systems. The experimental observations were found consistent with the simple picture that screening weakens the

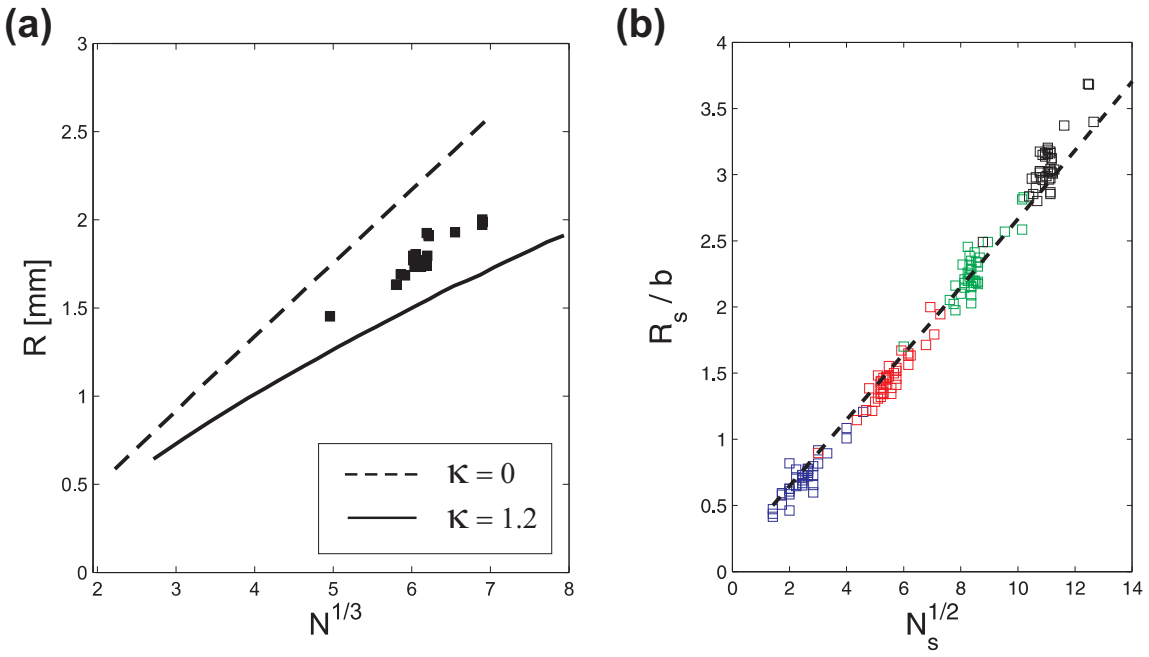

Fig. 3.13: Influence of screening: (a) Cluster radii as a function of cluster size (particle number). For comparison the cluster radii from MD-simulations are plotted. The dashed line marks the result for pure Coulomb interaction, while the solid line is computed for a screening length $\lambda = 0.5$ mm ($\kappa = 1.2$). (b) Shell radius as a function of shell occupation. The dashed line refers to unscreened Coulomb interaction [83, J-16]. From Ref. [C-4].

interparticle repulsion and that the same trapping force results in a higher density of the screened particle system. At first glance this interpretation even holds if the cluster radii are normalized with the interparticle distance [Fig. 3.13(b)]. The measured shell radii as a function of shell occupation agree well with the radii of a pure Coulomb system (dashed line). However, a close inspection hints at a systematic deviation. The inner shells are slightly smaller and the outer shells are slightly larger than predicted for a pure Coulomb system. Taking into account that the surface density (N_s/R_s^2) for an unscreened system is constant, the slight deviation in Fig. 3.13(b) would yield a parabolic density profile with higher density inside. To substantiate this finding, the shell occupation number was studied as a function of cluster size [Fig. 3.14(a)]. Compared to the Coulomb case, this comparison showed that Yukawa systems contain fewer particles in the outer shells while the population of the inner shells was enhanced. According to systematic MC- and MD-simulations this change of shell population can only be attributed to screening [21]. From MD-simulations best agreement with the experimental shell population was obtained for a screening parameter $\kappa \approx 0.65$ which agreed well with estimations based on experimental parameters [J-16].

Besides experiments and simulations, analytic calculations were performed [90, J-16, J-17]. Starting with a one-component plasma containing N particles with charge Q, a parabolic trapping potential $\Phi = \alpha r^2/2$, and a screened interaction potential $V \sim Q^2 e^{-\kappa r}/r$, a variational approach for the minimum energy configuration, with the restriction that the density n is positive and $\int n(\mathbf{r}) d^3r = N$, yields a radial density

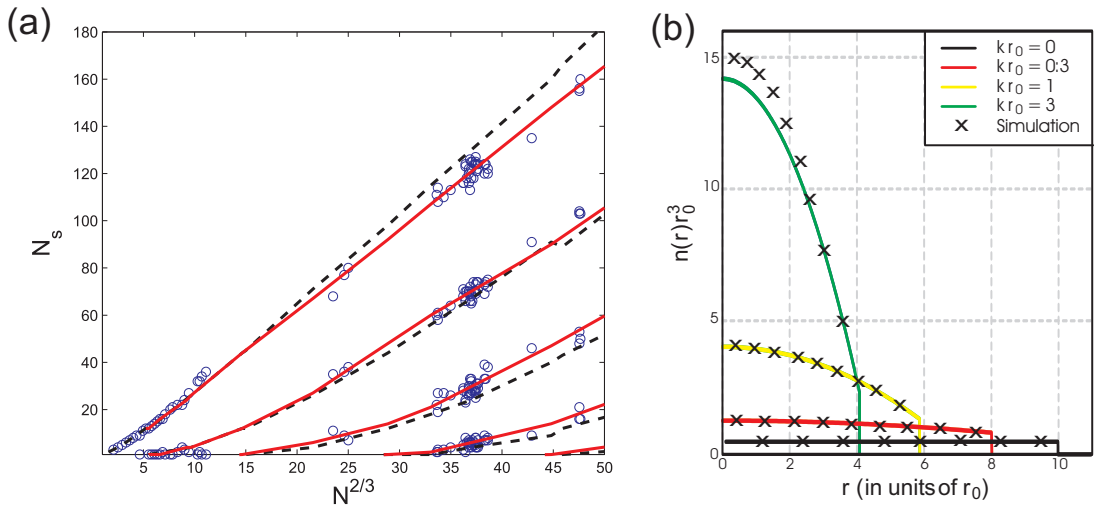

Fig. 3.14: Density profile of Yukawa balls: (a) Experiments (symbols) and simulations (lines) on the shell population of three-dimensional clusters. The dashed line marks the simulation results for unscreened Coulomb interaction of the particles. The solid line results from simulations with a screening parameter $\kappa r_0 = 0.6$ where r_0 is the stable distance of two particles in the absence of screening. (b) Radial density profiles obtained from a fluid model for different screening parameters. The results of MD-simulations are marked by symbols. Note that the density profile for an unscreened system is constant while screening introduces a radial density gradient. After Ref. [J-16, J-17].

profile

$$n(r) = \frac{\alpha N}{4\pi(N-1)Q^2}\left(c(\kappa,R) - \frac{\kappa^2 r^2}{2}\right)\Theta(R-r), \tag{3.2}$$

where $c(\kappa, R)$ is a constant depending on the cluster radius R and κ only. For $\kappa = 0$, Eq. 3.2 becomes independent of radius, i.e. a Coulomb system has a constant density profile. For increasing values of κ, $c(\kappa, R)$ increases and thus the average density increases. Further, the term $\kappa^2 r^2/2$ describes a parabolic decrease of density with radius. Thus, this fluid model fully reproduced the experimental findings of cluster compression and a parabolic density profile.

However, the fluid description was found to deviate from simulation results for small particle numbers and larger value of κ. Although the inclusion of correlation effects was shown to cure this [90], the fluid approach is not a valid approximation for systems containing just a very few particles. Especially for systems with $R \approx \lambda_D$, the question arises whether the structure is still affected by screening. For this purpose, we investigated the metastable states of Yukawa balls. Figure 3.15 shows the metastable configurations observed for a $N = 31$ cluster and the probability to observe a certain realization as function of κ. Analyzing the shells radii for the different metastable configurations revealed that the radial density profile steepens for increasing particle number on the inner shell [J-18]. Further, the simulations showed that the probability for configurations with higher particle number on the inner shell increases with increasing κ. Thus, it was shown that screening steepens the density profile even for small clusters. Moreover, these experiments showed that a radially inhomogeneous

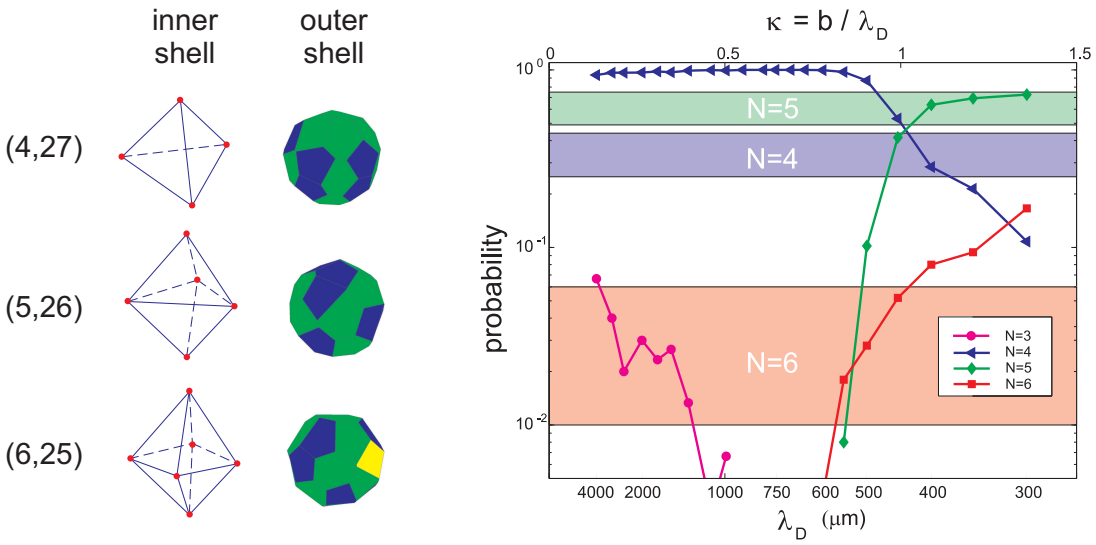

Fig. 3.15: Experiments on metastable configurations of Yukawa balls: (left) Average structure of the inner shell. The particle arrangement is shown for clusters with $N_\mathrm{i} = 4$, $N_\mathrm{i} = 5$, and $N_\mathrm{i} = 6$ particles. Additionally, the results of a Voronoi analysis (blue: pentagons, green: hexagons, yellow: defect) of the corresponding outer shells are plotted. All plots show experimental results. (right) Probability of realization of configurations with $N_\mathrm{i} = 3$, 4, 5 and 6 particles on the inner shell for a $N = 31$ cluster as a function of screening length λ_D. The experimental probabilities are indicated by the horizontal stripes. From Ref. [J-18].

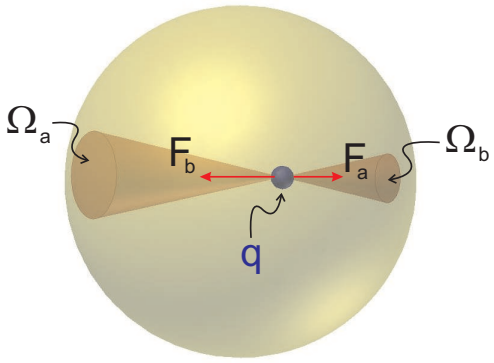

Fig. 3.16: Forces exerted on a test charge q inside a homogeneously charged spherical shell. Ω_a and Ω_b denote the surface fraction seen at opposite sides for a fixed solid angle.

density profile is characteristic for screened particle interaction regardless of the cluster size.

Basic Construction Principle

Guided by the fluid model [J-17], a quite simple explanation for the radially inhomogeneous density profile exists. Figure 3.16 illustrates the forces acting on a particle inside a homogeneously charged sphere. The force F_a depends on the distance and on the charge seen at a certain solid angle which is proportional to the shell surface fraction $\Omega_a \sim r^2$. In a pure Coulomb system, the net force on a particle inside a homogeneously charged shell is zero because the Coulomb force decreases proportional to r^{-2} and thus the contribution from opposite sides cancel. For a Coulomb crystal this means that inner shells in a Coulomb system do not experience a force from outer shells. However, for a screened Coulomb interaction this symmetry is broken. The nearest-neighbor interaction becomes dominant and a particle on an inner shell feels a radially inward-directed force. Therefore, a local force equilibrium for a shell configuration can only be reached if the radially inward-directed force is compensated by additional charges (i.e. particles) on inner shells. The result is a radial density gradient, as observed in experiment and simulation [J-16, J-18] as well as predicted by the fluid model [J-17].

3.2.5 Dynamic Properties

The previous section delivered a detailed insight to the structural properties of strongly coupled systems. This section focuses on dynamic processes in strongly coupled systems. While a number of investigations on wave propagation and related instabilities exist [17, 68, 70, 185, 230, 231, 277, 280, 315], phase transitions, normal modes, diffusion and viscosity have not been explored so far, because these investigations require true 3D diagnostics like SIS or DIH. The following paragraphs discuss recent progress in the field of dust acoustic instabilities and first experiments on dynamic processes in Yukawa balls.

Dust Acoustic Instability

So far the experiments on dust acoustic waves (DAW) were performed in the collisional regime [17, 68, 70, 185, 230, 231, 277, 280, 315]. Their dispersion relation has been measured and compared with fluid models [227]. In general, good agreement was observed if additional effects like streaming ions [230] or dust charge fluctuations [315] were taken into account. Our experiments were performed in the collisionless regime where quite different physical processes play a role [J-12]. In particular, the ion flow velocity becomes comparable with the ion thermal velocity and the excitation of the DAW is dominated by ion kinetic effects. In this regime fluid models fail and it is interesting to test the validity of kinetic models [237].

To measure the dispersion relation, self-excited and driven [281] DAWs were studied. Figure 3.17(a)-(c) show typical wave patterns. The typical saturation amplitudes were found to be $\tilde{n}_d/n_{d0} \approx 30\,\%$, which implies that nonlinear effects might play a role. Due to the finite size of the dust clouds, the classical spectral analysis and singular value decomposition were used to exclude systematic errors. The latter additionally

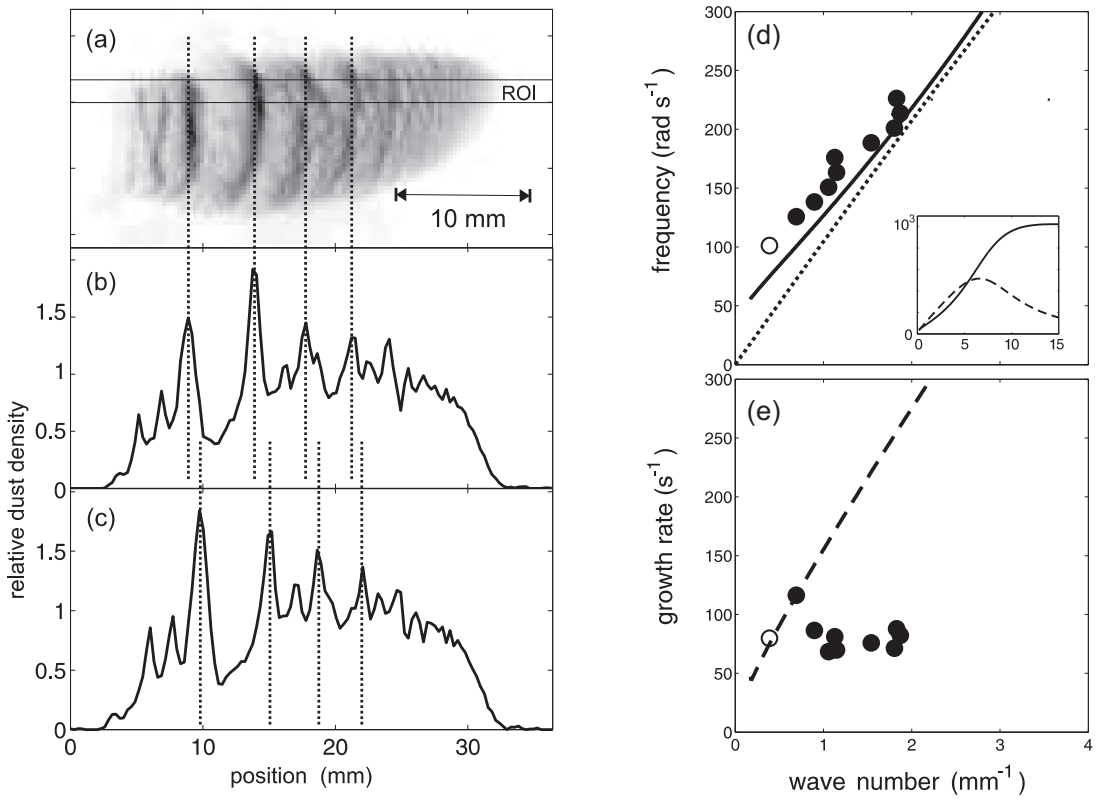

Fig. 3.17: Analysis of the wave pattern of a dust-acoustic instability. (a) Spatial dust density from a single frame of a movie. Dark regions indicate high dust densities. The horizontal lines mark the region of interest (ROI). (b,c) dust density in the ROI for two subsequent frames ($\Delta t = 8.3\,\mathrm{ms}$). The wave crests are marked with dotted lines for comparison. (c) Same as (b) for the subsequent frame. The displacement of the peaks shows the propagation. (d) Measured and theoretical wave dispersion. Open and closed circles are used for self-excited and synchronized waves, respectively. The kinetic theory [237] is shown as solid line. The inset shows the real part (solid) and imaginary part (dashed) of the kinetic theory over a wider range of wave numbers. (e) Comparison of the measured growth rate with kinetic theory. From Ref. [J-12].

allowed to determine local wave numbers and growth rates [J-12]. To compare experiment and theory, the parameters of our self-consistent discharge model were used [J-12], which involves no free parameter. Figure 3.17(d) shows that kinetic theory gives a close description of the real part of the measured dispersion. For the self-excited mode and at small wave numbers even the growth rates agree with the prediction of the kinetic theory while at large wave numbers the theory overestimates the growth rate [Fig. 3.17(e)]. The fact that the self-excited mode appears at small wave numbers, is a strong indication that this deviation is related to finite size, nonlinear, or strong coupling effects which are not included in the kinetic model of ROSENBERG [237]. From recent experiments PILCH et al. [220] concluded that the frequency cut-off hints at a finite size effect [263].

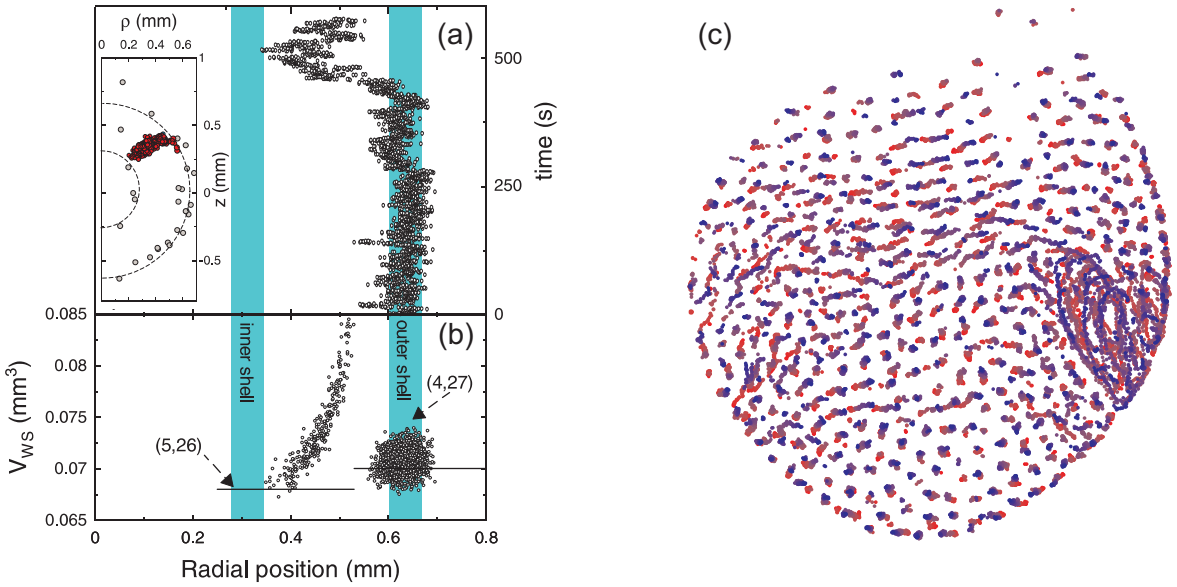

Fig. 3.18: (a) Radial component of the trajectory of the particle leaving the outer shell. The inset shows the particle trajectory in the ρ-z plane (black symbols). (b) Average Wigner-Seitz cell volume per particle for all particles belonging to the inner shell as a function of the radial position of the traveling particle. For $R < 0.55$ mm, the Wigner-Seitz cell of the traveling particle is included in the average. The solid lines are the average V_{WS} of the configurations (4,27) and (5,26). From Ref. [J-18]. (c) Vertical section through the center of a huge Coulomb ball with $N > 6000$ particles. The motion of all individual particles is traced by superimposing the particle positions in 1 s intervals for a total of 120 seconds. The system shows frozen domains as well as slow and fast fluid motion. From [J-13].

Dynamic Processes in Yukawa Balls

In Sect. 3.2.4 it was shown that Yukawa balls are solids. However, the coupling parameter was close to the predicted value for a phase transition to a liquid state. Therefore, it is tempting to investigate whether liquid Yukawa balls are observable in a slightly different parameter regime. For 2D plasma crystals the neutral gas pressure and the discharge power were identified to allow for a continuous variation of the coupling parameter and hence to study the melting process in its very details [173, 172, 253]. An important experimental detail for these measurements is that the confinement of the 2D crystal changes only marginal. For Yukawa balls the situation is different. As shown in Sect. 3.2.2, the trapping is realized by a combination of thermophoresis, gravity and plasma induced forces [J-14]. Additionally, the trap is very sensitive to variations of neutral gas pressure and discharge power, which has impeded a detailed investigation of phase transitions so far. Nevertheless, first promising observations were made [Fig. 3.18]. With the stereoscopic imaging system we were able to record a shell transition in a small cluster ($N = 31$) [J-15, J-18]. Without external stimulus a particle from the outer shell started to move radially inwards and approached the inner shell. [Fig. 3.18(a)]. The radial positions of the other 30 particles stayed nearly constant. This transition was a very slow, gradual process. It is different from the hopping motion

observed in 2D crystals occurring on the time scale of the Einstein frequency of nearest neighbor oscillations, which is of the order of a few Hertz [40]. Taking into account that the motion of the particles was dominated by friction with the neutral gas the energy dissipated by the particle motion can be estimated to 45 meV which is of the order of the thermal energy of particles at 300 K. Even more important, this is slightly higher than the energy barrier of $\Delta E = 34$ meV between ground and metastable states found in simulation. Hence, this measurements consistently showed that metastable configurations are thermally accessible in experiments at room temperature.

Further, these observations allowed to study the variation of the density profile. The particle density is defined as the reciprocal volume of the Wigner-Seitz (WS) cell V_{WS} per particle. Figure 3.18(b) shows the average WS volume V_{WS} for all particles on the inner shell as a function of the radial position of the traveling particle. For $r > 0.55$ mm, the cell volume V_{WS} was computed only for the four particles belonging to the inner shell. For $r < 0.55$ mm, the traveling particle was included. For comparison, the WS cell volumes for the (4,27) and (5,26) configurations are indicated by the short solid lines. Figure 3.18(b) reveals that a slight but significant decrease of V_{WS} was observed, i.e. the particle density on the inner shell increases for a (metastable) configuration with higher N_{i}. Thus, different metastable configurations have different radial density profiles and the density gradient steepens with increasing N_{i}. This nicely verified our results on the structural properties of metastable states discussed in Sect. 3.2.4 and shows how close structural properties and dynamic processes are linked in these systems.

Shell transitions are of enormous importance in melting processes, because transitions among metastable states mark the onset of melting. Since smaller systems should melt at lower temperatures than larger systems [245] our experiments on small Yukawa balls promise to gain insight into the microscopic processes of phase transitions in finite strongly coupled systems. Even for large Yukawa balls ($N > 6000$), we have first observations of liquid and solid regimes [J-13], which indicate grain boundary melting [48].

3.3 Synopsis

In the previous sections various experiments have been described. To stress their relation and to link the obtained results, this section provides a brief summary. Guided by the experimental objectives [see Sect. 3.1.5], four subtopics were investigated experimentally to extend the current understanding of strongly coupled 3D systems.

The first set of experiments aimed at a better understanding of the dust-plasma interaction. For this purpose a new diagnostic method for magnetized dusty plasmas, the excitation of lower hybrid resonance cones, was introduced [J-10]. It was shown that the resonance cone method provides absolute measurements of the free electron density in a dusty plasma. Thus, it was used to validate Langmuir probe results and the combination of Langmuir probe and resonance cone diagnostic enabled us to prove that the plasma is influenced even at moderate dust densities. The Havnes effect was found negligible, but the plasma losses at the dust particle surface were significant and caused a notable reduction of plasma density [J-10]. The importance of recombination processes for extended dust clouds was pointed out and it was concluded that only for

small clouds the reduction of plasma density due to recombination processes is negligible. In addition, our fundamental experiments on the ion drag force in a collisionless regime and the detailed comparison with competing theoretical models [J-11] allowed to conclude that the generation of dust crystals without chain or void formation demands for very low plasma densities.

The second set of experiments was performed to produce small void-free dust clouds. They further aimed at a detailed understanding of the dust confinement to provide the basis for a meaningful discussion of the structural and dynamical properties of the confined dust clouds. In our first experiment dust was confined in a magnetized anodic plasma [J-12]. Our measurements unambiguously showed that the dust confinement is not provided by a double layer. Electric fields and ion drag forces were shown to generate a stable confinement region, which agrees very well with the experimental observations. Further important plasma parameters have been derived from a self-consistent discharge model [J-12]. Thus, we could conclude that the dust particles are certainly in a liquid state and that crystallization might occur. However, due to the low collisionality of the plasma and the strong ion drifts, the particles are expected to form chains. Moreover, the dust cloud was found to be unstable with respect to dust acoustic waves. Thus, this discharge arrangement was used to investigate the dynamics of finite dust clouds, but it is not favorable to produce 3D plasma crystals. Using a different experimental setup, we discovered that spherical 3D plasma crystals (Yukawa balls) can be generated at laboratory conditions [J-13]. Detailed experiments showed that the dust is confined in a low density plasma [J-14]. These measurements showed further that the confinement potential is essentially parabolic and that only external forces, i.e. electric fields, themophoresis, and gravity are required to explain the observations. A dust-plasma interaction is not needed to trap the particles. Thus, this trap has strong similarities with Penning and Paul traps used for the generation of ion-crystals.

To investigate the structural and dynamical properties of 3D dust clouds, established (SVM) and novel (SIS, DIH) diagnostics were used [J-15]. While the scanning video microscopy (SVM) allowed to study the structural properties of Yukawa balls, a stereoscopic imaging system was developed to observe Yukawa balls at the kinetic level [C-3, 120, J-18]. The temporal and spatial resolution were shown to be sufficient to access the dynamics of Yukawa balls in detail [J-18]. However, the application of SIS is limited to small dust clouds. To measure the dynamics of large dust clouds a setup for digital inline holography (DIH) was developed and tested. We were able to demonstrate that DIH is applicable to dusty plasmas. The obtained spatial resolution is competitive with other 3D diagnostics, but in addition we showed that DIH does not suffer from a limited depth of focus [see Sect. 3.2.3]. Hence, with SIS and DIH two powerful methods exist to study the phase space evolution of 3D dust clouds.

These diagnostics enabled us to investigate the structural properties of finite crystalline dust clouds for the first time. Besides the proof that Yukawa balls are crystals [J-13], we showed that the generic structure of Yukawa balls is the formation of nested shells with a hexagonal lattice structure on each shell. To adapt this hcp-lattice pentagonal defects are required and observed in the experiment. Thus, concerning the shell formation and the structure on the shell, Yukawa balls are close relatives of ion-crystals [57]. However, a detailed structural analysis revealed that the screened Coulomb interaction

in Yukawa balls requires a radially inhomogeneous density profile to establish a force equilibrium [C-2, J-16, J-17]. The selective generation of metastable configurations of small Yukawa balls allowed us to show that this basic construction principle even hold for systems where the screening length and system dimensions are comparable [J-18]. In general, our results stress previous findings that the shell formation reflects geometric constraints and that the boundary (trapping) condition determines the structure of finite systems to a large extent. However, our results unambiguously show that the mutual interaction of the particles and especially its range determines the detailed shell arrangement and shell population. Therefore, the differences of Yukawa balls and ion-crystals permitted to investigate the influence of the interparticle interaction on structural formation in finite strongly coupled particle clouds.

Beyond the structural properties, we performed first investigations on the dynamics of these 3D dust clouds. The experiments in magnetized anodic plasmas allowed to measure the dispersion relation of dust acoustic waves in a kinetic regime [J-12]. A detailed comparison of experiment and kinetic theory revealed a good agreement. Nevertheless, deviations of the measured from the predicted growth rates as well as an observed frequency cut-off were interpreted as indications for nonlinear and finite size effects. For Yukawa balls, we were able to show that the regime of a solid-liquid phase transition is experimentally accessible. We observed shell transitions in small Yukawa balls as well as solid and liquid regions in large Yukawa balls. Both observations show that detailed investigations are generally feasible.

To conclude, our experiments and simulations on the structure and dynamics of 3D dust clouds provided many interesting results, which shed light on the structural and dynamical processes in finite strongly coupled systems. Especially the discovery of Yukawa balls, their close relation to ion-crystals, and the development of true 3D diagnostics promise a deeper understanding of 3D dust clouds in near future.

4. CONCLUDING REMARKS

Within the last century a substantial understanding of plasma physics has been achieved. Nevertheless, in nearly all fields of plasma physics several phenomena are only partly understood, certain parameter regimes are almost unexplored and still new fields emerge. This thesis has focused on recent progress in two of these fields, the rather old but vivid field of drift wave turbulence as well as the still young research field of complex plasmas. Especially the demand for new experimental techniques to access the spatio-temporal evolution in both fields was addressed. In this thesis novel techniques have been introduced, developed and tested. In the field of drift wave turbulence, a super-resolution method for very low resolution data was introduced and benchmarked. It was verified that this method is a solution to the resolution dilemma of diagnostic arrays and that statistical techniques are in general not competitive. Further, the diagnostic advances which are achievable with super-resolution indicate that a number of experimental investigations on transport processes in turbulent plasmas are now feasible, which so far were just accessible with numerical and theoretical techniques.

In the field of complex plasmas, our discovery of Yukawa balls allowed to study the dynamical and structural properties of finite crystalline particle arrangements in its very details for the first time. The combination of novel experimental techniques and simulations matching the experimental conditions provided the unique opportunity to identify the basic physical processes which determine the observed structural and dynamical properties of Yukawa balls. In addition, our experiments have proven the close relation between Yukawa balls and trapped laser-cooled ions. Thus, the results on Yukawa balls might stimulate research in other fields where finite strongly coupled systems are of interest. So far, Yukawa balls seem to be a typical strongly coupled systems, which however offers unique experimental possibilities. The near future will show whether they can trigger a similar research activity as the 2D plasma crystals and contribute to a more fundamental understanding of strongly coupled matter.

Acknowledgments

Prof. Dr. A. Piel is gratefully acknowledged for his continuous interest and support of this work. Special thanks belongs to all members of the atomic and plasma physics group. Their enthusiasm to tackle physical and technical problems provided the stimulating climate necessary for interesting and successful research. Especially O. Arp, B. Brede, F. Greiner, S. Harms, M. Hirt, M. Kroll, I. Teliban, and T. Trottenberg contributed considerably to results presented here. Their steady support and the many fruitful discussion require a special acknowledgment. Further, I would like to express my gratitude to my coworkers from other institutes: G. Bonhomme (Nancy, France), T. Klinger and coworkers (IPP Greifswald), A. Melzer and coworkers (Univ. Greifswald),

V. Naulin (Riso, Denmark), and M. Bonitz and coworkers (Univ. Kiel). Furthermore, financial support from the Deutsche Forschungsgemeinschaft is gratefully acknowledged.

Most of all, I am deeply indebted to my family Anja, Moritz, and Annika. Their love gave me strength and thus supported this work in a unique and indispensable manner.

BIBLIOGRAPHY

[1] R.J. Adrian. Conditional eddies in isotropic turbulence. *Phys. Fluids*, 22(11):2065–2070, 1979.

[2] M. R. Akdim. *Modelling of complex plasmas*. PhD thesis, Instituut voor Plasmafysica Rijnhuizen, 2003.

[3] M. R. Akdim and W. J. Goedheer. Modelling of voids in colloidal plasmas. *Phys. Rev. E*, 65:015401, 2002.

[4] M. R. Akdim and W. J. Goedheer. Modeling of dust in a silane/hydrogen plasma. *J. Appl. Phys.*, 94:104–109, 2003.

[5] M. R. Akdim and W. J. Goedheer. Modeling of dust voids in electronegative discharges under microgravity. *IEEE Trans. Plasma Sci.*, 32:680–690, 2004.

[6] J.E. Allen. Probe theory - the orbital motion approach. *Plasma Sources Sci. Technol.*, 45:497–503, 1992.

[7] J.E. Allen, R.L.F. Boyd, and P. Reynolds. The collection of positive ions by a probe immersed in a plasma. *Proc. Roy. Soc. (London)*, 70:297–304, 1957.

[8] B. M. Annaratone, T. Antonova, D. D. Goldbeck, H. M. Thomas, and G. E. Morfill. Complex-plasma manipulation by radiofrequency biasing. *Plasma Phys. Control. Fusion*, 46(12B):495–509, 2004.

[9] B. M. Annaratone, M. Glier, T. Stuffler, M. Raif, H. M. Thomas, and G. E. Morfill. The plasma-sheath boundary near the adaptive electrode as traced by particles. *New J. Phys.*, 5:92, 2003.

[10] G. Y. Antar, P. Devynck, X. Garbet, and S. C. Luckhardt. Turbulence intermittency and burst properties in tokamak scrape-off layer. *Phys. Plasmas*, 8:1612, 2001.

[11] T. Antonova, B.M. Annaratone, D.D. Goldbeck, V. Yaroshenko, H.M. Thomas, and G.E. Morfill. Measurement of the interaction force among particles in three-dimensional plasma clusters. *Phys. Rev. Lett.*, 96:115001, 2006.

[12] V.V. Arsenin and V.A. Chuyanov. Suppression of plasma instabilities by feedback method. *Sov. Phys. Usp.*, 20(9):736–762, 1977.

[13] F. Baletto and R. Ferrando. Structural properties of nanoclusters. *Rev. Mod. Phys.*, 77:371–423, 2005.

[14] A. Barkan, N. D'Angelo, and R.L. Merlino. Charging of dust grains in a plasma. *Phys. Rev. Lett.*, 73:3093–3096, 1994.

[15] A. Barkan, N. D'Angelo, and R.L. Merlino. Laboratory experiments on electrostatic ion cyclotron waves in a dusty plasma. *Planet. Space Sci.*, 43:905–908, 1995.

[16] A. Barkan and R.L. Merlino. Confinement of dust particles in a double layer. *Phys. Plasmas*, 2:3261, 1995.

[17] A. Barkan, R.L. Merlino, and N. D'Angelo. Laboratory observation of the dust-acoustic wave mode. *Phys. Plasmas*, 2:3563–3565, 1995.

[18] M.S. Barnes, J.H. Keller, J.C. Forster, J.A. O'Neill, and D.K. Coultas. Transport of dust particles in glow–discharge plasmas. *Phys. Rev. Lett.*, 68:313–316, 1992.

[19] R. Barni, C. Riccardi, Th. Pierre, G. Leclert, A. Escarguel, D. Guyomarc'h, and K. Quotb. Formation of spiral structures and radial convection in the edge region of a magnetized rotating plasma. *New J. Phys.*, 7(225), 2005.

[20] J. L. Barron, D. J. Fleet, and S. S. Breauchemin. Performance of optical flow techniques. *Int. J. Comp. Vis.*, 12(1):43–77, 1994.

[21] H. Baumgartner. Monte–carlo Simulation von Coulomb balls. Master's thesis, Christian–Albrechts–Universität zu Kiel, Januar 2006.

[22] H. Baumgartner, H. Kählert, V. Golubnychiy, S. Käding, C. Henning, A. Melzer, and M. Bonitz. Shell structure of Yukawa balls. *Contrib. Plasma Phys.*, 47:281–290, 2007.

[23] J.M. Beall, Y.C. Kim, and E.J. Powers. Estimation of wavenumber and frequency spectra using fixed probe pairs. *J. Appl. Phys.*, 53:3933–3940, 1982.

[24] V.M. Bedanov and F. Peeters. Ordering and phase transitions of charged particles in a classical finite two-dimensional system. *Phys. Rev. B*, 49:2667–2676, 1994.

[25] P. M. Bellan and K. L. Wong. Effect of density fluctuations on lower hybrid resonance cone propagation. *Phys. Fluids*, 21:592, 1978.

[26] P.V. Bliokh, V. Sinitsin, and V. Yaroshenko. *Dusty and self-gravitational plasma in space*. Kluwer Academic Publ., Dordrecht, 1995.

[27] J. A. Boedo, D. L. Rudakov, R.A. Moyer, G. R. McKee, R. J. Colchin, M. J. Schaffer, P. G. Stangeby, W. P. West, S. L. Allen, T. E. Evans, R. J. Fonck, E. M. Hollmann, S. Krasheninnikov, A. W. Leonard, W. Nevins, M. A. Mahdavi, G. D. Porter, G. R. Tynan, D. G. Whyte, and X. Xu. Transport by intermittency in the boundary of the diii-d tokamak. *Phys. Plasmas*, 10:1670, 2003.

[28] J. P. Boeuf and L. C. Pitchford. Two-dimensional model of a capacitively coupled rf discharge and comparisons with experiments in the gaseous electronics conference reference reactor. *Phys. Rev. E*, 51:1376–1390, 1995.

[29] J.P. Boeuf, Ph. Belenguer, and T. Hbid. Plasma particle interacctions. *Plasma Sources Sci. Technol.*, 3:407–417, 1994.

[30] J.J. Bollinger, T.B. Mitchell, X.P. Huang, W.M. Itano, J.N. Tan, B.M. Jelenkovic, and D.J. Wineland. Crystalline order in laser-cooled, non-neutral ion plasmas. *Phys. Plasmas*, 7:7, 2000.

[31] A. Bouchoule. *Dusty plasmas: physics, chemistry, and technological impacts in plasma processing*. John Wiley & Sons Ltd, New York, 1999.

[32] L. Boufendi, M. Mikikian, and P. K. Shukla, editors. *Fourth international conference on the physics of dusty plasmas*, Orléans, France 2005, 2005. AIP Conference Proceedings.

[33] S. S. Breauchemin and J. L. Barron. The computation of optical flow. *ACM Computing Surveys*, 27(3):433–467, 1996.

[34] A. J. Brizard and T. S. Hahm. Foundations of nonlinear gyrokinetic theory. *Rev. Mod. Phys.*, 79(421), 2007.

[35] F. Brochard, G. Bonhomme, E. Gravier, S. Oldenbürger, and M. Philipp. Spatiotemporal control and synchronization of flute modes and drift waves in a magnetized plasma column. *Phys. Plasmas*, 13(5):052509, 2006.

[36] P. Bryant. Floating potential of spherical probes and dust grains in collisional plasmas. *J. Phys. D: Appl. Phys.*, 36:2859–2868, 2003.

[37] P. Bryant. The structure of the complex plasma boundary. *New J. Phys.*, 6:1–15, 2004.

[38] M. J. Burin, G. R. Tynan, G. Y. Antar, N. A. Crocker, and C. Holland. On the transition to drift turbulence in a magnetized plasma column. *Phys. Plasmas*, 12:052320, 2005.

[39] T. A. Carter. Intermittent turbulence and turbulent structures in a linear magnetized plasma. *Phys. Plasmas*, 13:010701, 2006.

[40] C.L. Chan, W.Y. Woon, and L. I. Shear banding on mesoscopic dusty plasma liquids. *Phys. Rev. Lett.*, 93:220602, 2004.

[41] F.F. Chen. Normal modes for electrostatic ion waves in an inhomogeneous plasma. *Phys. Fluids*, 7:949–955, 1964.

[42] F.F. Chen. Effect of sheaths on drift instabilities in thermionic plasmas. *Phys. Fluids*, 8:752–754, 1965.

[43] F.F. Chen. Resistive overstabilities and anomalous "diffusion". *Phys. Fluids*, 8:912–919, 1965.

[44] F.F. Chen. "Universal" overstability of a resistive, inhomogeneous plasma. *Phys. Fluids*, 8:1323–1333, 1965.

[45] F.F. Chen. Nonlocal drift modes in cylindrical geometry. *Phys. Fluids*, 10:1647–1651, 1967.

[46] F.F. Chen. *Introduction to Plasma Physics and Controlled Fusion*. Plenum Press, New York, 2 edition, 1984.

[47] T.K. Chu, B. Coppi, H.W. Hendel, and F.W. Perkins. Drift instabilities in a uniformly rotating plasma cylinder. *Phys. Fluids*, 12(1):203–208, 1969.

[48] S.T. Chui. Grain-boundary theory of melting in two dimensions. *Phys. Rev. B*, 28:178–194, 1983.

[49] N. D'Angelo. Low-frequency oscillations in cesium thermionic converters. *Phys. Fluids*, 4:1054–1055, 1961.

[50] N. D'Angelo. Low-frequency electrostatic waves in dusty plasmas. *Planet. Space Sci.*, 38:1143–1146, 1990.

[51] N. D'Angelo and N. Rynn. Diffusion and recombination of a highly ionized cold plasma in a magnetic field. *Phys. Fluids*, 4:1303–1306, 1961.

[52] N. D'Angelo and N. Rynn. Diffusion of a cold cesium plasma across a magnetic field. *Phys. Fluids*, 4:275–276, 1961.

[53] P. H. Diamond, S.-I. Itoh, K. Itoh, and T. S. Hahm. Zonal flows in plasmas - a review. *Plasma Phys. Control. Fusion*, 47:35–161, 2005.

[54] F. Diederich, E. Peik, J. M. Chen, W. Quint, and H. Walther. Observatuion of a phase transition of stored laser-cooled ions. *Phys. Rev. Lett.*, 59(26):2931–2934, 1987.

[55] L. F. Dong, Q. L. Zhang, and L. Wang. Conditional analysis and biorthogonal decomposition of plasma turbulence in the ct-6b tokamak. *Chin. Phys. Lett.*, 19(12):1838, 2002.

[56] D.H.E. Dubin. The phonon wake behind a charge moving relative to a 2d plasma crystal. *Phys. Plasmas*, 7:3895–3903, 2000.

[57] D.H.E. Dubin and T.M. O'Neil. Trapped nonneutral plasmas, liquids and crystals (the thermal equilibrium states). *Rev. Mod. Phys.*, 71:87–172, 1999.

[58] F. Dubois, L. Joannes, and J. Legros. Improved three-dimensional imaging with a digital holography microscope with a source of partial spatial coherence. *Appl. Opt.*, 38:7085, 1999.

[59] R.F. Ellis and E. Marden-Marshall. Comparison of local and nonlocal theories of the collisional drift instability. *Phys. Fluids*, 22:2137–2139, 1979.

[60] R.F. Ellis, E. Marden-Marshall, and R. Majeski. Collisional drift instability of a weakly ionized argon plasma. *Plasma Phys.*, 22:113–132, 1980.

[61] P.S. Epstein. On the resistance experienced by spheres in their motion through gases. *Phys. Rev.*, 23:710–733, 1924.

[62] A. Fasoli, B. Labit, M. McGrath, S. H. Müller, G. Plyushchev, M. Podesta , and F. M. Poli. Electrostatic turbulence and transport in a simple magnetized plasma. *Phys. Plasmas*, 13:055902, 2006.

[63] Y. Feng, J. Goree, and B. Liu. Accurate particle position measurement from images. *Rev. Sci. Instrum.*, 78:053704, 2007.

[64] A.V. Filippas, R.D. Bengston, G.X. Li, M.A. Meier, C.P. Ritz, and E.J. Powers. Conditional analysis of floating potential fluctuations at the edge of the texas experimental tokamak upgrade (TEXT-U). *Plasma Phys.*, 2(3):839–845, 1995.

[65] R.K. Fisher and R.W. Gould. Resonance cones in the field pattern of a short antenna in an anisotropic plasma. *Phys. Rev. Lett.*, 22(21):1093–1095, 1969.

[66] V. E. Fortov, O. S. Vaulina, O. F. Petrov, V. I. Molotkov, A. M. Lipaev, G. E. Morfill, H. Thomas, S. A. Khrapak, Y. P. Semenov, and A. I. Ivanov. Dynamics and structural properties of dusty plasma liquid in microgravity: experiments onboard the international space station. *Plasma Phys. Control. Fusion*, 46(12B):359–366, 2004.

[67] V. E. Fortov, O. S. Vaulina, O. F. Petrov, V. I. Molotkov, A. M. Lipaev, V. M. Torchinsky, H. M. Thomas, G. E. Morfill, S. A. Khrapak, Y. P. Semenov, A. I. Ivanov, S. K. Krikalev, A. Y. Kalery, S. V. Zaletin, and Y. P. Gidzenko. Transport of microparticles in weakly ionized gas-discharge plasmas under microgravity conditions. *Phys. Rev. Lett.*, 90:245005, 2003.

[68] V.E. Fortov, A.G. Khrapak, S.A. Khrapak, V.I. Molotkov, A.P. Nefedov, O.F. Petrov, and V.M. Torchinsky. Mechanism of dust acoustic instability in a direct current glow discharge plasma. *Phys. Plasmas*, 7:1374–1380, 2000.

[69] V.E. Fortov, V.I. Molotkov, A.P. Nefedov, and O.F. Petrov. Liquid and crystallike structures in strongly coupled dusty plasmas. *Phys. Plasmas*, 6:1759–1768, 1999.

[70] V.E. Fortov, A.D. Usachev, A.V. Zobnin, V.I. Molotkov, and O.F. Petrov. Dust-acoustic wave instability at the diffuse edge of radio frequency inductive low-pressure gas discharge plasma. *Phys. Plasmas*, 10:1199–1208, 2003.

[71] Å. Fredriksen, C. Riccardi, L. Cartegni, and H. Pécseli. Coherent structures, transport and intermittency in a magnetized plasma. *Plasma Phys. Control. Fusion*, 45(5):721–733, 2003.

[72] S. L. Gilbert, J. J. Bollinger, and D. J. Wineland. Shell-structure phase of magnetically confined strongly coupled plasmas. *Phys. Rev. Lett.*, 60(20):2022–2025, 1988.

[73] C.K. Goertz. Dusty plasmas in the solar system. *Rev. Geophys.*, 27:271–292, 1989.

[74] J. Goree, G.E. Morfill, V.N. Tsytovich, and S.V. Vladimirov. Theory of dust voids in plasmas. *Phys. Rev. E*, 59:7055–7067, 1999.

[75] E. Gravier, X. Caron, G. Bonhomme, and T. Pierre. Control of the chaotic regimes of nonlinear drift waves in a magnetized laboratory plasma. *Phys. Plasmas*, 6(5):1670–1673, 1999.

[76] O. Grulke, F. Greiner, T. Klinger, and A. Piel. Comparative experimental study of coherent structures in a simple magnetized torus. *Plasma Phys. Control. Fusion*, 43(4):525–542, 2001.

[77] O. Grulke, T. Klinger, M. Endler, A. Piel, and W7-AS Team. Analysis of large-scale fluctuation structures in the scrape-off layer of the wendelstein 7-as stellarator. *Phys. Plasmas*, 8:5171, 2001.

[78] O. Grulke, T. Klinger, and A. Piel. Experimental study of the dynamics of conditionally averaged structures in weakly developed electrostatic turbulence. *Phys. Plasmas*, 6(3):788–796, 1999.

[79] Y. G. Guezennec. Stochastic estimation of coherent structures in turbulent boundary layers. *Phys. Fluids A*, 1:1054, 1989.

[80] S. Hamaguchi, R.T. Farouki, and D.H.E. Dubin. Triple point of yukawa systems. *Phys. Rev. E*, 56:4671–4682, 1997.

[81] A. Hasegawa and K. Mima. Pseudo-three-dimensional turbulence in magnetized nonuniform plasma. *Phys. Fluids*, 21(1):87–92, 1978.

[82] A. Hasegawa and M. Wakatani. Plasma edge turbulence. *Phys. Rev. Lett.*, 50:682–686, 1983.

[83] R. W. Hasse and V. V. Avilov. Structure and madelung enery of spherical coulomb crystals. *Phys. Rev. A*, 44(7):4506–4515, 1991.

[84] O. Havnes, T.K. Aslaksen, T.W. Hartquist, F. Li, F. Melandsø, G.E. Morfill, and T. Nitter. Probing the properties of planetary ring dust by the observation of mach cones. *J. Geophys. Res.*, 100:1731–1734, 1995.

[85] O. Havnes, C.K. Goertz, G.E. Morfill, E. Grün, and W.H. Ip. Dust charges, cloud potential, and instabilities in a dust cloud embedded in a plasma. *J. Geophys. Res.*, 92 A3:2281–2287, 1987.

[86] O. Havnes, G.E. Morfill, and C.K. Goertz. Plasma potential and grain charge in a dust cloud embedded in a plasma. *J. Geophys. Res.*, 89:10999–11003, 1984.

[87] Y. Hayashi. Structure of a three-dimensional coulomb crystal in a fine-particle plasma. *Phys. Rev. Lett.*, 83:4764–4767, 1999.

[88] Y. Hayashi and K. Tachibana. Observation of coulomb crystal formation from carbon particles grown in a methane plasma. *Jpn. J. Appl. Phys.*, 33:L804–L806, 1994.

[89] M. V. A. P. Heller, Z. A. Brasilio, I. L. Caldas, J. Stöckel, and J. Petrzilka. Scrape-off layer intermittency in the castor tokamak. *Phys. Plasmas*, 6(3):846–853, 1999.

[90] C. Henning, P. Ludwig, A. Filinov, A. Piel, and M. Bonitz. Ground state of a confined yukawa plasma including correlation effects. *Phys. Rev. E*, 76:036404, 2007.

[91] K. D. Hinsch. Holographic particle image velocimetry. *Meas. Sci. Technol.*, 13:R61–R72, 2002.

[92] A. Homann, A. Melzer, S. Peters, R. Madani, and A. Piel. Determination of the dust screening length by laser-excited lattice waves. *Phys. Rev. E*, 56:7138–7141, 1997.

[93] A. Homann, A. Melzer, S. Peters, R. Madani, and A. Piel. Laser-excited dust lattice waves in plasma crystals. *Phys. Lett. A*, 242:173–180, 1998.

[94] B. K. P. Horn and B. G. Schunck. Determining optical flow. *Artificial Intelligence*, 17:185–204, 1988.

[95] L. Hornekaer, N. Kjaergaard, A. M. Thommesen, and M. Drewsen. Structural properties of two-component coulomb crystals in a linear paul trap. *Phys. Rev. Lett.*, 86(10):1994–1997, 2001.

[96] W. Horton. Nonlinear drift waves and transport in magnetized plasmas. *Phys. Rep.*, 192(1-3):1–177, 1990.

[97] W. Horton. Drift waves and transport. *Rev. Mod. Phys.*, 71(3):735–778, 1999.

[98] G. Hu, J.A. Krommes, and J.C. Bowman. Statistical theory of resistive drift-wave turbulence and transport. *Phys. Plasmas*, 4(6):2116–2133, 1997.

[99] T. Huld, A.H. Nielsen, H.L. Pecseli, and J.J. Rasmussen. Plasma vortices and their relation to cross-field diffusion: A laboratory study. *Phys. Rev. Lett.*, 64(25):3023–3026, 1990.

[100] T. Huld, A.H. Nielsen, H.L. Pecseli, and J.J. Rasmussen. Coherent structures in two-dimensional plasma turbulence. *Phys. Fluids B*, 3(7):1609–1625, 1991.

[101] I.H. Hutchinson. Ion collection by a sphere in a flowing plasma: 3. floating potential and drag force. *Plasma Phys. Control. Fusion*, 47:71–87, 2005.

[102] I.H. Hutchinson. Spherical particle interaction with flowing plasma: computational discoveries. In Boufendi et al. [32].

[103] I.H. Hutchinson. Collisionless ion drag force on a spherical grain. *Plasma Phys. Control. Fusion*, 48:185–202, 2006.

[104] S. Ichimaru. Strongly coupled plasmas: high density classical plasmas and degenerate electron liquids. *Rev. Mod. Phys.*, 54:1017–1059, 1982.

[105] J. Ickovic, R. L. Stenzel, and W. Gekelman. Direct density. display with a resonance cone rf probe. *Rev. Sci. Instr.*, 48:485, 1977.

[106] G. Indebetouw and W. Zhong. Scanning holographic microscopy of three-dimensional fluorescent specimens. *J. Opt. Soc. Am. A*, 23:1699, 2006.

[107] W. M. Itano, J. J. Bollinger, J. N. Tan, B. Jelenkovic, X.-P. Huang, and D. J. Wineland. Bragg diffraction from crystallized ion plasmas. *Nature*, 279:686–689, 1998.

[108] K. Itoh, S.-I. Itoh, and A. Fukuyama. *Transport and structural formation in plasmas*. IOP Series on Plasma Physics, 1999.

[109] K. Itoh, Y. Nagashima, S.-I. Itoh, P. H. Diamond, A. Fujisawa, M. Yagi, and A. Fukuyama. On the bicoherence analysis of plasma turbulence. *Phys. Plasmas*, 12:102301, 2005.

[110] Y. Ivanov and A. Melzer. Particle positioning techniques for dusty plasma experiments. *Rev. Sci. Instr.*, 78:033506, 2007.

[111] A.V. Ivlev, H.M. Thomas, G.E. Morfill, V. Molotkov, A.M. Lipaev, V.E. Fortov, T. Hagl, H. Rothermel, and S. Krialev. Coalescence of complex plasma clouds. *New J. Phys.*, 8:25, 2006.

[112] G.M. Jellum, J.E. Daugherty, and D.B. Graves. Particle thermophoresis in low pressure glow discharges. *J. Appl. Phys.*, 69:6923–6934, 1991.

[113] S. J. Jeon, G. S. Eom, J. H. Kim, and W. Choe. Multichannel rf-compensated langmuir probe array driven by a single bias supply. *Rev. Sci. Instr.*, 73:277, 2002.

[114] H. Johnson, H. L. Pecseli, and J. Trulsen. Conditional eddies in plasma turbulence. *Phys. Fluids*, 30(7):2239–2254, 1987.

[115] B.K. Joseph, R. Jha, P.K. Kaw, S.K. Mattoo, C.V.S. Rao, Y.C. Saxena, and ADITYA Team. Observation of vortex-like coherent structures in the edge plasma of the aditya tokamak. *Phys. Plasmas*, 4(12):4292–4300, 1997.

[116] W.-T. Juan, Z.-H. Huang, J.-W. Hsu, Y.-J. Lai, and L. I. Observation of dust coulomb clusters in a plasmatrap. *Phys. Rev. E*, 58(6):R6947–R6950, 1998.

[117] W.-T. Juan and Lin I. Anomalous diffusion in strongly coupled quasi-2d dusty plasmas. *Phys. Rev. Lett.*, 80:3073, 1998.

[118] J.D. Jukes. Micro-instabilities in magnetically confined, inhomogeneous plasma. *Phys. Fluids*, 7:1468–1474, 1964.

[119] S.-I. Itoh K. Itoh, P. H. Diamond, T. S. Hahm, A. Fujisawa, G. R. Tynan, M. Yagi, and Y. Nagashima. Physics of zonal flows. *Phys. Plasmas*, 13:055502, 2006.

[120] S. Käding and A. Melzer. Three-dimensional stereoscopy of yukawa (coulomb) balls in dusty plasmas. *Phys. Plasmas*, 13:090701, 2006.

[121] T. Kaneko, E. W. Reynolds, R. Hatakeyama, and M. E. Koepke. Velocity-shear-driven drift waves with simultaneous azimuthal modes in a barium-ion q-machine plasma. *Phys. Plasmas*, 12:102106, 2005.

[122] R. E. Kaplan and J. Laufer. In *Proc. 12th Int. Cong. Appl. Mech.*, page 236, Stanford Univ., 1969.

[123] S. A. Khrapak, A. V. Ivlev, G. E. Morfill, and H. M. Thomas. Ion drag force in complex plasmas. *Phys. Rev. E*, 66:046414, 2002.

[124] S.A. Khrapak, A.V. Ivlev, G.E. Morfill, H.M. Thomas, S.K. Zhdanov, U. Konopka, M.H. Thoma, and R.A. Quinn. Comment on "measurement of the ion drag force on falling dust particles and its relation to the void formation in complex (dusty) plasmas. *Phys. Plasmas*, 10:4579–4581, 2003.

[125] S.A. Khrapak, A.V. Ivlev, G.E. Morfill, and S.K. Zhdanov. Scattering in the attractive yukawa potential in the limit of strong interaction. *Phys. Rev. Lett.*, 90:225002–1–2, 2003.

[126] S.A. Khrapak, A.V. Ivlev, G.E. Morfill, S.K. Zhdanov, and H.M. Thomas. Scattering in the attractive yukawa potential: application to the ion-drag force in complex plasmas. *IEEE Trans. Plasma Sci.*, 32:555–560, 2004.

[127] S.A. Khrapak, A.V. Ivlev, S.K. Zhdanov, and G.E. Morfill. Hybrid approach to the ion drag force. *Phys. Plasmas*, 12:042308, 2005.

[128] S.A. Khrapak, S.V. Ratynskaia, A.V. Zobnin, A.D. Usachev, V.V. Yaroshenko, M.H. Thoma, M. Kretschmer, H. Höfner, G.E. Morfill, O.F. Petrov, and V.E. Fortov. Particle charge in the bulk of gas discharges. *Phys. Rev. E*, 72:015406, 2005.

[129] S.A. Khrapak, D. Samsonov, G.E. Morfill, H. Thomas, V. Yaroshenko, H. Rothermel, V. Fortov, A. Nefedov, V. Molotkov, O. Petrov, A. Lipaev, A. Ivanov, and Yu.M. Baturin. Compressional waves in complex (dusty) plasmas under microgravity conditions. *Phys. Plasmas*, 10:1–4, 2003.

[130] M.D. Kilgore, J.E. Daugherty, R.K. Porteous, and D.B. Graves. Ion drag on an isolated particulate in a low pressure discharge. *J. Appl. Phys.*, 73:7195–7202, 1993.

[131] N. Kjaergaard and M. Drewsen. Observation of a structural transition for coulomb crystals in a linear paul trap. *Phys. Rev. Lett*, 91(9):095002, 2003.

[132] M. Klindworth, O. Arp, and A. Piel. Langmuir probe system for dusty plasmas under microgravity. *Rev. Sci. Instrum.*, 78:033502, 2007.

[133] M. Klindworth, A. Melzer, A. Piel, and V.A. Schweigert. Laser-excited intershell rotation of finite coulomb clusters in a dusty plasma. *Phys. Rev. B*, 61:8404–8410, 2000.

[134] M. Klindworth, A. Piel, and A. Melzer. Dust free regions around langmuir probes in complex plasmas under microgravity. *Phys. Rev. Lett.*, 93:195002, 2004.

[135] T. Klinger. Control of plasma instabilities, 1998. Habilitationsschrift.

[136] T. Klinger, A. Latten, A. Piel, G. Bonhomme, T. Pierre, and T.D. de Wit. The route to drift wave chaos and turbulence in a bounded low-β plasma experiment. *Phys. Rev. Lett.*, 79:3913–3916, 1997.

[137] A.E. Koniges, J.A. Crotinger, and P.H. Diamond. Structure formation and transport in dissipative drift-wave turbulence. *Plasma Phys. Control. Fusion*, 4(9):2785–2793, 1992.

[138] U. Konopka, L. Ratke, and H.M. Thomas. Central collisions of charged dust particles in a plasma. *Phys. Rev. Lett.*, 79:1269–1272, 1997.

[139] L. S. G. Kovasznay, V. Kibens, and R. F. Blackwelder. Large-scale motion in the intermittent region of a turbulent boundary layer. *J. Fluid. Mech.*, 41:283, 1970.

[140] N.A. Krall and A.W. Trivelpiece. *Principles of Plasma Physics*. McGraw-Hill, Maidenhead (UK), 1973.

[141] M. Kroll. private communications.

[142] H.H. Kuehl. Interference structure near the resonance cone. *phf*, 16(8):1311–1320, 1973.

[143] B. Labit, I. Furno, A. Fasoli, A. Diallo, S. H. Müller, G. Plyushchev, M. Podestà, and F. M. Poli. Universal statistical properties of drift-interchange turbulence in torpex plasmas. *Phys. Rev. Lett.*, 98:255002, 2007.

[144] J.G. Laframboise and L.J. Sonmor. Current collection by probes and electrodes in space magnetoplasmas: a review. *J. Geophys. Res.*, 98:337–357, 1993.

[145] M. Lampe. Limits of validity for orbital-motion-limited theory for a small floating collector. *J. Plasma Phys.*, 65:171–180, 2001.

[146] V. Land and W.J. Goedheer. Effect of large-angle scattering, ion flow speed and ion-neutral collisions on dust transport under microgravity conditions. *New J. Phys.*, 8:8, 2006.

[147] V. Land, W.J. Goedheer, and M.R. Akdim. Dust transport in a magnetized radio-frequency discharge under microgravity conditions. *Phys. Rev. E*, 72:046403, 2005.

[148] H. Lashinsky. Universal instability in a fully ionized inhomogeneous plasma. *Phys. Rev. Lett.*, 12:121–123, 1964.

[149] A. Latten. *Multisondendiagnostik von Driftwellenturbulenz und anomalem Radialtransport in Laborplasmen*. PhD thesis, Christian-Albrechts-Universität Kiel, 1997.

[150] A. Latten, T. Klinger, A. Piel, and Th. Pierre. A probe array for the investigation of spatio-temporal structures in drift wave turbulence. *Rev. Sci. Instr.*, 66(5):3254–3262, 1995.

[151] C. Lechte, S. Niedner, and U. Stroth. Comparison of turbulence measurements and simulations of the low-temperature plasma in the torsatron tj-k. *New J. Phys.*, 4:34, 2002.

[152] M.A. Liebermann and A.J. Lichtenberg. *Principles of plasma discharges and material processing*. John Wiley & Sons Inc., New York, 1994.

[153] F. Lindemann. über die Berechnung molekularer Eigenfrequenzen. *Z. Phys.*, 11:609, 1910.

[154] A. M. Lipaev, S. A. Khrapak, V. I. Molotkov, G. E. Morfill, V. E. Fortov, A. V. Ivlev, H. M. Thomas, A. G. Khrapak, V. N. Naumkin, A. I. Ivanov, S. E. Tretschev, and G. I. Padalka. Void closure in complex plasmas under microgravity conditions. *Phys. Rev. Lett.*, 98:265006, 2007.

[155] B. Liu and J. Goree. Superdiffusion in two-dimensional yukawa liquids. *Phys. Rev. E*, 75:016405, 2007.

[156] B. Liu, J. Goree, and O. S. Vaulina. Test of the stokes-einstein relation in a two-dimensional yukawa liquid. *Phys. Rev. Lett.*, 96:015005, 2006.

[157] J.M. Liu, W.T. Juan, J.-W. Hsu, Z.-H. Huang, and L. I. Strongly coupled dusty plasmas: crystals, liquids, clusters and waves. *Plasma Phys. Control. Fusion*, 41:A47–A60, 1999.

[158] B. D. Lucas and T. Kanade. An iterative technique of image registration and its application to stereo. *Proc. 7th International Joint Conference on Artificial Intelligence*, pages 674–679, 1981.

[159] P. Ludwig, S. Kosse, and M. Bonitz. Structure of spherical three dimensional coulomb crystals. *Phys. Rev. E*, 71:046403, 2005.

[160] Q.Z. Luo and N. D'Angelo. Observation of dusty plasmas with magnetized dust grains. *J. Phys. D: Appl. Phys.*, 33:2754–2758, 2000.

[161] Q.Z. Luo, N. D'Angelo, and R.L. Merlino. Experimental study of shock formation in a dusty plasma. *Phys. Plasmas*, 6:3455–3458, 1999.

[162] A. L. Mackay. A dense non-crystallographic packing of equal spheres. *Acta Cryst.*, 15(9):916–918, 1962.

[163] N. Mahdizadeh, F. Greiner, T. Happel, A. Kendl, M. Ramisch, B. D. Scott, and U. Stroth. Investigation of the parallel dynamics of drift-wave turbulence in toroidal plasmas. *Plasma Phys. Control. Fusion*, 49(7):1005–1017, 2007.

[164] E. Marden-Marshall, R.F. Ellis, and J.E. Walsh. Collisional drift instability in a variable radial electric field. *Plasma Phys. Control. Fusion*, 28(9B):1461–1482, 1986.

[165] E. Martines, M. Hron, and J. Stöckel. Coherent structures in the edge turbulence of the castor tokamak. *Plasma Phys. Control. Fusion*, 44:351–359, 2002.

[166] T. Matthey, J. P. Hansen, and M. Drewsen. Coulomb bicrystals of species with identical charge-to-mass ratios. *Phys. Rev. Lett.*, 91(16):165001, 2003.

[167] G. R. McKee, R. J. Fonck, D. K. Gupta, D. J. Schlossberg, and M. W. Shafer. Turbulence velocimetry of density fluctuation imaging data. *Rev. Sci. Instr.*, 75(10):3490–3492, 2004.

[168] F. Melandsø. Lattice waves in dust plasma crystals. *Phys. Plasmas*, 3:3890–3901, 1996.

[169] F. Melandsø and J. Goree. Polarized supersonic plasma flow simulation for charged bodies such as dust particles and spacecraft. *Phys. Rev. E*, 52:5312–5326, 1995.

[170] F. Melandsø and J. Goree. Particle simulation of two dimensional dust crystal formation in a mesothermal plasma flow. *J. Vac. Sci. Technol. A*, 14:511–518, 1996.

[171] A. Melzer. Laser manipulation of particles in dusty plasmas. *Plasma Sources Sci. Technol.*, 10:303–310, 2001.

[172] A. Melzer, A. Homann, and A. Piel. Experimental investigation of the melting transition of the plasma crystal. *Phys. Rev. E*, 53:2757–2766, 1996.

[173] A. Melzer, A. Homann, and A. Piel. Experimental investigation of the melting transition of the plasma crystal. *Phys. Rev. E*, 53:2757, 1996.

[174] A. Melzer, M. Klindworth, and A. Piel. Normal modes of 2d finite clusters in complex plasmas. *Phys. Rev. Lett.*, 87:115002, 2001.

[175] A. Melzer, S. Nunomura, D. Samsonov, and J. Goree. Laser-excited mach cones in a dusty plasma crystal. *Phys. Rev. E*, 62:4162–4176, 2000.

[176] A. Melzer, V.A. Schweigert, and A. Piel. Transition from attractive to repulsive forces between dust molecules in a plasma sheath. *Phys. Rev. Lett.*, 83:3194–3197, 1999.

[177] A. Melzer, V.A. Schweigert, I.V. Schweigert, A. Homann, S. Peters, and A. Piel. Structure and stability of the plasma crystal. *Phys. Rev. E*, 54:R46–R49, 1996.

[178] A. Melzer, T. Trottenberg, and A. Piel. Experimental determination of the charge on dust particles forming coulomb lattices. *Phys. Lett. A*, 191:301–308, 1994.

[179] R. L. Merlino. Experimental investigations of dusty plasmas. In *New Vistas in Dusty Plasmas*, volume 799 of *AIP Conf. Proc.*, page 3, 2005.

[180] R.L. Merlino, A. Barkan, C. Thompson, and N. D'Angelo. Laboratory studies of waves and instabilities in dusty plasmas. *Phys. Plasmas*, 5:1607–1614, 1998.

[181] A.B. Mikhailovskii. *Theory of Plasma Instabilities*. vol 1. Consultans Bureau, New York, 1974.

[182] T. Miksch and A. Melzer. Fluorescent microspheres as tracer particles in dusty plasmas. *Phys. Rev. E*, 75:016404, 2007.

[183] T. Misawa, N. Ohno, K. Asano, M. Sawai, S. Takamura, and P.K. Kaw. Experimental observation of vertically polarized transverse dust-lattice wave propagating in a one-dimensional strongly coupled dust chain. *Phys. Rev. Lett.*, 86:1219–1222, 2001.

[184] S.S. Moiseev and R.Z. Sagdeev. On the bohm diffusion coefficient. *JETP*, 17:515–517, 1963.

[185] V.I. Molotkov, A.P. Nefedov, V.M. Torchinsky, V.E. Fortov, and A.G. Khrapak. Dust acoustic waves in a dc glow-discharge plasma. *JETP*, 89:477–480, 1999.

[186] G. E. Morfill, V. N. Tsytovich, and H. Thomas. *Elementary Physics of Complex Plasmas (Lecture Notes in Physics)*. Springer, Berlin, 2007.

[187] G.E. Morfill, B.M. Annaratone, P. Bryant, A.V. Ivlev, H.M. Thomas, M. Zuzic, and V.E. Fortov. A review of liquid and crystalline plasmas - new physical states of matter? *Plasma Phys. Control. Fusion*, 44:263–277, 2002.

[188] G.E. Morfill, H.M. Thomas, U. Konopka, H. Rothermel, M. Zuzic, A. Ivlev, and J. Goree. Condensed plasmas under microgravity. *Phys. Rev. Lett.*, 83:1598–1601, 1999.

[189] G.E. Morfill, H.M. Thomas, U. Konopka, and M. Zuzic. The plasma condensation: liquid and crystalline plasmas. *Phys. Plasmas*, 6:1769–1780, 1999.

[190] A. Mortensen, E. Nielsen, T. Matthey, and M. Drewsen. Obervation of three-dimensional long-range order in small ion coulomb crystals in an rf trap. *Phys. Rev. Lett.*, 96:103001, 2006.

[191] H.M. Mott-Smith and I. Langmuir. The theory of collectors in gaseous discharges. *Phys. Rev.*, 28:727–763, 1926.

[192] S. H. Müller, A. Diallo, A. Fasoli, I. Furno, B. Labit, G. Plyushchev, M. Podestà, and F. M. Poli. Probabilistic analysis of turbulent structures from two-dimensional plasma imaging. *Phys. Plasmas*, 13:100701, 2006.

[193] C.M.C. Nairn, B.M. Annaratone, and J.E. Allen. On the theory of spherical probes and dust grains. *Plasma Sources Sci. Technol.*, 7:478–490, 1998.

[194] Y. Nakamura, H. Bailung, and P.K. Shukla. Observation of ion-acoustic shocks in a dusty plasma. *Phys. Rev. Lett.*, 83:1602–1605, 1999.

[195] M. Nambu, S.V. Vladimirov, and P.K. Shukla. Attractive forces between charged particulates in plasmas. *Phys. Lett. A*, 203:40–42, 1995.

[196] V. Naulin. *Nichtlinearer Transport in ebenen Driftwellenmodellen*. PhD thesis, Heinrich-Heine-Universtiät Düsseldorf, 1995.

[197] A. P. Nefedov, G. E. Morfill, V. E. Fortov, H. M. Thomas, H. Rothermel, T. Hagl, A. V. Ivlev, M. Zuzic, B. A. Klumov, A. M. Lipaev, V. I. Molotkov, O. F. Petrov, Y. P. Gidzenko, S. K. Krikalev, W. Shepherd, A. I. Ivanov, M. Roth, H. Binnenbruck, J. A. Goree, and Y. P. Semenov. Pke?nefedov: plasma crystal experiments on the international space station. *New J. Phys.*, 5:33, 2003.

[198] S. Niedner, B. D. Scott, and U. Stroth. Statistical properties of drift wave turbulence in low-temperature plasmas. *Plasma Phys. Control. Fusion*, 44(4):397–408, 2002.

[199] T. Nitter. Levitation of dust in rf and dc glow discharges. *Plasma Sources Sci. Technol.*, 5:93–111, 1996.

[200] V. Nosenko, R. Fisher, R. Merlino, S. Khrapak, G. Morfill, and K. Avinash. Measurement of the ion drag force in a collisionless plasma with strong ion-grain coupling. *Phys. Plasmas*, 14:103702, 2007.

[201] S. Nunomura, D. Samsonov, S. Zhdanov, and G. E. Morfill. Self-diffusion in a liquid complex plasma. *Phys. Rev. Lett.*, 96:015003, 2006.

[202] K. Ohkuni, K. Toi, S. Ohdachi, and S. Takagi. Langmuir probe array for edge plasma study on the compact helical system heliotron/torsatron. *Rev. Sci. Instr.*, 70:419, 1999.

[203] N. Omrane and P. L. Palmer. Superresolution for translated satellite images using the walsh functions. *Proceedings of SPIE*, 5238:62–71, 2004.

[204] F.J. Oynes, O.-M. Olsen, H.L. Pecseli, A. Fredriksen, and K. Rypdal. Experimental study of low-frequency electrostatic fluctuations in a magnetized toroidal plasma. *Phys. Rev. E*, 57(2):2242–2255, 1998.

[205] G. Pan and H. Meng. Digital holography of particle fields: reconstruction by use of complex amplitude. *Appl. Opt.*, 42:827, 2003.

[206] H. Park, C. C. Chang, B. H. Deng, C. W. Domier, A. J. H. Donné, K. Kawahata, C. Liang, X. P. Liang, H. J. Lu, N. C. Luhmann Jr., A. Mase, H. Matsuura, E. Mazzucato, A. Miura, K. Mizuno, T. Munsat, Y. Nagayama, M. J. van de Pol, J. Wang, Z. G. Xia, and W-K. Zhang. Recent advancements in microwave imaging plasma diagnostics. *Rev. Sci. Instr.*, 74:4239, 2003.

[207] W. Paul. Electromagnetic traps for charged and neutral particles. *Rev. Mod. Phys.*, 62:531–540, 1990.

[208] H. L. Pecseli and J. Trulsen. Analytical expressions for conditional averages: A numerical test. *Phys. Scripta*, 43:503, 1991.

[209] H.L. Pecseli, E.A. Coutsias, T. Huld, J.P. Lynov, A.H. Nielsen, and J.J. Rasmussen. Coherent vortical structures in two-dimensional plasma turbulence. *Plasma Phys. Control. Fusion*, 34(13):2065–2070, 1992.

[210] F.M. Peeters and X. Wu. Wigner crystal of a screened-coulomb-interaction colloidal sdystem in two dimensions. *Phys. Rev. A*, 35:3109–3114, 1987.

[211] S. Peled and Y. Yeshurun. Superresolution in mri: Application to human white matter fiber tract visualization by diffusion tensor imaging. *Magnetic Resonance in Medicine*, 45:29–35, 2001.

[212] A. Piel. Die Resonanzkegelmethode zur Diagnostik magnetisierter Plasmen, 1986. Habilitationsschrift.

[213] A. Piel, A. Homann, and A. Melzer. Laser-excited waves in a plasma crystal. *Plasma Phys. Control. Fusion*, 41:A453–A461, 1999.

[214] A. Piel, M. Klindworth, O. Arp, A. Melzer, and M. Wolter. Obliquely propagating dust density waves in the presence of an ion beam. *Phys. Rev. Lett.*, 97:205009, 2006.

[215] A. Piel, V. Nosenko, and J. Goree. Laser-excited shear waves in solid and liquid two-dimensional dusty plasmas. *Phys. Plasmas*, 13:042104, 2006.

[216] A. Piel and G. Oelerich. Experimental study of kinetic effects on. resonance cones. *Phys. Fluids*, 27:273–284, 1984.

[217] A. Piel and G. Oelerich. Thermal structures on resonance cones in a weakly collisional plasma. *Phys. Fluids*, 28:1366, 1985.

[218] J.B. Pieper and J. Goree. Dispersion of plasma dust acoustic waves in the strong coupling regime. *Phys. Rev. Lett.*, 77:3137–3140, 1996.

[219] J.B. Pieper, J. Goree, and R.A. Quinn. Three-dimensional structure in a crystallized dusty plasma. *Phys. Rev. E*, 54:5636–5640, 1996.

[220] I. Pilch, A. Piel, T. Trottenberg, and M. E. Koepke. Dynamics of small dust clouds trapped in a magnetized anodic plasma. *Phys. Plasmas*, 2007. submitted.

[221] E.J. Powers. Spectral techniques for experimental investigation of plasma diffusion due to polychromatic fluctuations. *Nuclear Fusion*, 14:749, 1974.

[222] G. Praburam and J. Goree. Cosmic dust synthesis by accretion and coagulation. *Astrophys. J.*, 441:830–838, 1996.

[223] Y. Pu and H. Meng. Four-dimensional dynamic flow measurement by holographic particle image velocimetry. *Appl. Opt.*, 44:7697, 2005.

[224] R. Peeters *et al.* The use of superresolution techniques to reduce slice thickness in functional mri. *International Journal of Imaging Systems and Technology (IJIST), Special issue on High Resolution Image Reconstruction*, 14(3):131–138, 2004.

[225] M. Ramisch, F. Greiner, N. Mahdizadeh, K. Rahbarnia, and U. Stroth. Observation of large-scale coherent structures under strong e x b shear in the torsatron tj-k. *Plasma Phys. Control. Fusion*, 49(6):777–789, 2007.

[226] M. Ramisch, N. Mahdizadeh, U. Stroth, F. Greiner, C. Lechte, and K. Rahbarnia. ρ_s scaling of characteristic turbulent structures in the torsatron tj-k. *Phys. Plasmas*, 12:032504, 2005.

[227] N.N. Rao. Dust-coulomb and dust-acoustic wave propagation in dense dusty plasmas with high fugacity. *Phys. Plasmas*, 7:795–807, 2000.

[228] N.N. Rao, P.K. Shukla, and M.Y. Yu. Dust-acoustic waves in dusty plasmas. *Planet. Space Sci.*, 38:543–546, 1990.

[229] S. Ratynskaia, K. Rypdal, C. Knapek, S. Khrapak, A. V. Milovanov, A. Ivlev, J. J. Rasmussen, and G. E. Morfill. Superdiffusion and viscoelastic vortex flows in a two-dimensional complex plasma. *Phys. Rev. Lett.*, 96:105010, 2006.

[230] S.V. Ratynskaia, S.A. Khrapak, A.V. Zobnin, M.H. Thoma, M. Kretschmer, A.D. Usachev, V. Yaroshenko, R.A. Quinn, G.E. Morfill, O. Petrov, and V.E. Fortov. Experimental determination of dust particle charge in a discharge at elevated pressures. *Phys. Rev. Lett.*, 93:085001, 2004.

[231] S.V. Ratynskaia, M. Kretschmer, S.A. Khrapak, R.A. Quinn, G.E. Morfill, M.H. Thoma, A.V. Zobnin, A.D. Usachev, O. Petrov, and V.E. Fortov. Dust mode in collisionally dominated complex plasmas with particle drift. *IEEE Trans. Plasma Sci.*, 32:613–616, 2004.

[232] B. Richards, T. Uckan, A.J. Wootton, B. Carreras, R.D. Bengston, P. Hurwitz, G.X. Li, A.K. Sen, and J. Uglum. Modification of tokamak edge turbulence using feedback. *Phys. Plasmas*, 1(5):1606–1611, 1994.

[233] C.P. Ritz, E.J. Powers, and R.D. Bengtson. Experimental measurement of three-wave coupling and energy cascading. *Phys. Fluids B*, 1:153–163, 1989.

[234] C.P. Ritz, E.J. Powers, T.L. Rhodes, R.D. Bengtson, K.W. Gentle, H. Lin, P.E. Phillips, A.J. Wootton, D.L. Brower, N.C. Luhmann Jr., W.A. Peebles, P.M. Schoch, and R.L. Hickok. Advanced plasma fluctuation analysis techniques and their impact on fusion research. *Rev. Sci. Instrum.*, 59:1739–1744, 1988.

[235] M.O. Robbins, K. Kremer, and G.S. Grest. Phase diagram and dynamics of yukawa systems. *J. Chem. Phys.*, 88:3286–3312, 1988.

[236] V. Rohde, A. Piel, H. Thiemann, and K. I. Oyama. In situ diagnostics of ionospheric plasma with the resonance cone technique. *J. Geophys. Res.*, 98:19163, 1993.

[237] M. Rosenberg. A note on ion-dust streaming instability in a collisional dusty plasma. *J. Plasma Phys.*, 67:235–242, 2002.

[238] H. Rothermel, T. Hagl, G.E. Morfill, M.H. Thoma, and H.M. Thomas. Gravity compensation in complex plasmas by application of a temperature gradient. *Phys. Rev. Lett.*, 89:175001–1–1, 2002.

[239] D. L. Rudakov, M. G. Shats, R. W. Boswell, C. Charles, and J. Howa. Overview of probe diagnostics on the h-1 heliac. *Rev. Sci. Instr.*, 70:476, 1999.

[240] S. K. Saha and S. Chowdhury. Intermittent transport in the scrape-off layer of the sinp tokamak. *Phys. Plasmas*, 13:092512, 2006.

[241] Y. Saitou, A. Yonesu, S. Shinohara, M. V. Ignatenko, N. Kasuya, M. Kawaguchi, K. Terasaka, T. Nishijima, Y. Nagashima, Y. Kawai, M. Yagi, S.-I. Itoh, M. Azumi, and K. Itoh. Reduction effect of neutral density on the excitation of turbulent drift waves in a linear magnetized plasma with flow. *Phys. Plasmas*, 14:072301, 2007.

[242] D. Samsonov, J. Goree, Z.W. Ma, A. Bhattacharjee, H.M. Thomas, and G.E. Morfill. Mach cones in a coulomb lattice and a dusty plasma. *Phys. Rev. Lett.*, 83:3649–3652, 1999.

[243] D. Samsonov, G.E. Morfill, H. Thomas, T. Hagl, and H. Rothermel. Kinetic measurements of shock wave propagation in a three-dimensional complex dusty plasma. *Phys. Rev. E*, 67:036404, 2003.

[244] N. Sato, G. Uchida, T. Kaneko, S. Shimizu, and S. Iizuka. Dynamics of fine particles in magnetized plasmas. *Phys. Plasmas*, 8:1786–1790, 2001.

[245] J.P. Schiffer. Melting of crystalline confined plasma. *Phys. Rev. Lett.*, 88:205003, 2002.

[246] Schnars and Jüptner. *Digital Holography*. Springer Berlin, 2004.

[247] Ch. Schröder, O. Grulke, T. Klinger, and V. Naulin. Spatial mode structures of electrostatic drift waves in a collisional cylindrical helicon plasma. *Phys. Plasmas*, 11(9):4249–4253, 2004.

[248] Ch. Schröder, O. Grulke, T. Klinger, and V. Naulin. Drift waves in a high-density cylindrical helicon discharge. *Phys. Plasmas*, 12(4):042103, 2005.

[249] M. Schubert, M. Endler, and H. Thomsen. Spatiotemporal temperature fluctuation measurements by means of a fast swept langmuir probe array. *Rev. Sci. Instr.*, 78(5):053505, 2007.

[250] H.G. Schuster. *Handbook of Chaos Control*. VCH Verlagsgesellschaft, Weinheim, 1 edition, 1998.

[251] I.V. Schweigert, V.A. Schweigert, A. Melzer, and A. Piel. Melting of a dust crystal with defects. *JETP Lett.*, 71:58–61, 2000.

[252] V.A. Schweigert and F. Peeters. Spectral properties of classical two-dimensional clusters. *Phys. Rev. B*, 51:7700, 1995.

[253] V.A. Schweigert, I.V. Schweigert, A. Melzer, A. Homann, and A. Piel. Alignment and instability of 'dust' crystals in plasmas. *Phys. Rev. E*, 54:4155–4166, 1996.

[254] V.A. Schweigert, I.V. Schweigert, A. Melzer, A. Homann, and A. Piel. Plasma crystal melting: a nonequilibrium phase transition. *Phys. Rev. Lett.*, 80:5345, 1998.

[255] B. D. Scott. Low frequency fluid drift turbulence in magnetised plasmas, 2000. Habilitationsschrift.

[256] G.S. Selwyn, J.S. McKillop, K.L. Haller, and J.J. Wu. In situ plasma contamination measurements by hene laser light scattering: A case study. *J. Vac. Sci. Technol. A*, 8:1726–1731, 1990.

[257] G.S. Selwyn, J. Singh, and R.S. Bennett. In situ laser diagnostic studies of plasma–generated particulate contamination. *J. Vac. Sci. Technol. A*, 7:2758–2765, 1989.

[258] A.K. Sen. Control and diagnostic uses of feedback. *Phys. Plasmas*, 7(5):1759–1766, 2000.

[259] S. Shinohara, N. Matsuoka, and S. Matsuyama. Establishment of strong velocity shear and plasma density profile modification with associated low frequency fluctuations. *Phys. Plasmas*, 8(4):1154–1158, 2001.

[260] P.K. Shukla. New collective processes in dusty plasmas: application to space and laboratories. *Plasma Phys. Control. Fusion*, 42:B213–B221, 2000.

[261] P.K. Shukla. A survey of dusty plasma physics. *Phys. Plasmas*, 8:1791–1803, 2001.

[262] P.K. Shukla and M.M. Mamun. *Introduction to dusty plasma physics*. IOP, 2002.

[263] P.K. Shukla and M. Rosenberg. Boundary effects on dust-ion-acoustic and dust-acoustic waves in collisonal dusty plasmas. *Phys. Plasmas*, 6:1038–1040, 1999.

[264] P.K. Shukla and V.P. Silin. Dust ion–acoustic wave. *Physica Scripta*, 45:508, 1992.

[265] Siglo-2D. Version 1.1, kinema software.

[266] A. K. Singh and Y. C. Saxena. Observation of intermittent structures associated with the low-frequency turbulence in toroidal magnetized plasma. *Phys. Plasmas*, 1:2926, 1994.

[267] R. L. Stenzel and J. M. Urrutia. Electron magnetohydrodynamic turbulence in a high-beta plasma. iii. conditionally averaged multipoint fluctuation measurements. *Phys. Plasmas*, 7:4466, 2000.

[268] R.L. Stenzel. A new probe for measuring small electric fields in plasmas. *Rev. Sci. Instr.*, 62(1):130–139, 1991.

[269] U. Stroth, F. Greiner, C. Lechte, N. Mahdizadeh, K. Rahbarnia, and M. Ramisch. Study of edge turbulence in dimensionally similar laboratory plasmas. *Phys. Plasmas*, 11(5):2558–2564, 2004.

[270] L. Talbot, R. K. Cheng, R. W. Scheffer, and D. R. Willis. Thermophoresis of particles in a heated boundary layer. *J. Fluid Mech.*, 101(4):737–758, 1980.

[271] R.J. Taylor, M.L. Brown, B.D. Fried, H. Grote, J.R. Liberati, G.J. Morales, P. Pribyl, D. Darrow, and M. Ono. H-Mode behavior induced by cross–field currents in a tokamak. *Phys. Rev. Lett.*, 63(21):2365–2368, 1989.

[272] J. L. Terry, S. J. Zweben, B. Bose, O. Grulke, E. S. Marmar, J. Lowrance, V. Mastrocola, and G. Renda. High speed movies of turbulence in alcator c-mod. *Rev. Sci. Instr.*, 75:4196–4199, 2004.

[273] J. L. Terry, S. J. Zweben, O. Grulke, M. J. Greenwald, and B. LaBombard. Velocity fields of edge/scrape-off-layer turbulence in alcator c-mod. *J. Nucl. Mat.*, 337-339:322–326, 2005.

[274] P.W. Terry. Suppression of turbulence and transport by sheared flow. *Rev. Mod. Phys.*, 72(1):109–165, 2000.

[275] H. Thomas and G.E. Morfill. Melting dynamics of a plasma crystal. *Nature*, 379:806–809, 1996.

[276] H. Thomas, G.E. Morfill, V. Demmel, J. Goree, B. Feuerbacher, and D. Möhlmann. Plasma crystal: Coulomb crystallization in a dusty plasma. *Phys. Rev. Lett.*, 73:652–655, 1994.

[277] E. Thomas Jr. and R.L. Merlino. Dust particle motion in the vicinity of dust acoustic waves. *IEEE Trans. Plasma Sci.*, 29:152–157, 2001.

[278] E. Thomas Jr. and M. Watson. Charging of silica particles in an argon dusty plasma. *Phys. Plasmas*, 7:3194–3197, 2000.

[279] K.I. Thomassen. Feedback stabilization in plasmas. *Nuclear Fusion*, 11:175–186, 1971.

[280] C. Thompson, A. Barkan, N. D'Angelo, and R. L. Merlino. Dust acoustic waves in a direct current glow discharge. *Phys. Plasmas*, 4:2331–2335, 1997.

[281] C. Thompson, A. Barkan, N. D'Angelo, and R.L. Merlino. Dust acoustic waves in a direct current glow discharge. *Phys. Plasmas*, 4:2331–2335, 1997.

[282] J. J. Thomson. On the structure of the atom. *Philos. Mag.*, 39(7):237–265, 1904.

[283] H. Totsuji, T. Kishimoto, C. Totsuji, and K. Tsuruta. Competition between two forms of ordering in finite coulomb clusters. *Phys. Rev. Lett.*, 88:125002, 2002.

[284] H. Totsuji, T. Ogawa, C. Totsuji, and K. Tsuruta. Structure of spherical yukawa clusters: A model for dust particles in dusty plasmas in an isotropic environment. *Phys. Rev. E*, 72:036406, 2005.

[285] H. Totsuji, C. Totsuji, T. Ogawa, and K. Tsuruta. Ordering of dust particles in dusty plasmas under microgravity. *Phys. Rev. E*, 71:045401–1–0, 2005.

[286] A. A. Townsend. *Australien J. Sci. Res.*, 2:451, 1949.

[287] T. Trottenberg. *Diagnostik mit Resonanzkegeln, Partikeleinschluss und staubakustische Wellen in magnetisierten komplexen Plasmen*. PhD thesis, Christian–Albrechts–Universität zu Kiel, 2006.

[288] T. Trottenberg, A. Melzer, and A. Piel. Measurement of the electric charge on particulates forming coulomb crystals in the sheath of an rf plasma. *Plasma Sources Sci. Technol.*, 4:450–458, 1995.

[289] K. Tsuruta and S. Ichimaru. Binding energy, microstructure and shell model of coulomb clusters. *Phys. Rev. A*, 48:1339–1344, 1993.

[290] V. Tsytovich. Evolution of voids in dusty plasmas. *Physica Scripta*, 89:89–94, 2001.

[291] V.N. Tsytovich, G.E. Morfill, and H. Thomas. Complex plasmas: I. complex plasmas as unusual state of matter. *Plasma Physics Reports*, 28:623–651, 2002.

[292] V.N. Tsytovich, S.V. Vladimirov, G.E. Morfill, and J. Goree. Erratum: Theory of collision-dominated dust voids in plasmas. *Phys. Rev. E*, 64:029902(E), 2001.

[293] V.N. Tsytovich, S.V. Vladimirov, G.E. Morfill, and J. Goree. Theory of collision-dominated dust voids in plasmas. *Phys. Rev. E*, 63:056609, 2001.

[294] O. S. Vaulina and S. V. Vladimirov. Diffusion and dynamics of macro-particles in a complex plasma. *Phys. Plasmas*, 9:835, 2002.

[295] F. Verheest. *Waves in dusty space plasmas*. Kluwer Academic Publ., Dordrecht, 2000.

[296] S. V. Vladimirov, K. Ostrikov, and A. A. Samarian. *Physics and Applications of Complex Plasmas*. Imperial College Press, 2005.

[297] S.V. Vladimirov, P.V. Shevchenko, and N.F. Cramer. Vibrational modes in the dust-plasma crystal. *Phys. Rev. E*, 56:R74–R76, 1997.

[298] F. Wagner, G. Becker, K. Behringer, D. Campbell, A. Eberhagen, W. Engelhardt, G. Fussmann, O. Gehre, J. Gernhardt, G. v. Gierke, G. Haas, M. Huang, F. Karger, M. Keilhacker, O. Klüber, M. Kornherr, K. Lackner, G. Lisitano, G.G. Lister, H.M. Mayer, D. Meisel, E.R. Müller, H. Murmann, H. Niedermeyer, W. Poschenrieder, H. Rapp, H. Röhr, F. Schneider, G. Siller, E. Speth, A. Stäbler, K.-H. Steuer, G. Venus, O. Vollmer, and Z. Yü. Regime of improved confinement and high beta in neutral-beam-heated divertor discharges of the ASDEX tokamak. *Phys. Rev. Lett.*, 49(19):1408–1412, 1982.

[299] F. Wagner, G. Fussmann, T. Grave, M. Keilhacker, M. Kornherr, K. Lackner, K. McCormick, E.R. Müller, A. Stäbler, G. Becker, K. Bernhardi, U. Ditte, A. Eberhagen, O. Gehre, J. Gernhardt, G. v. Gierke, E. Clock, O. Gruber, G. Haas, M. Heese, G. Janeschitz, F. Karger, S. Kissel, O. Klüber, G. Lisitano, H.M. Mayer, D. Meisel, V. Mertens, H. Murmann, W. Poschenrieder, H. Rapp, H. Röhr, F. Ryter, F. Schneider, G. Siller, P. Smeulders, F. Söldner, E. Speth, K.-H. Steuer, Z. Szymanski, and O. Vollmer. Development of an edge transport barrier at the H-mode transition of ASDEX. *Phys. Rev. Lett.*, 53(15):1453–1456, 1984.

[300] X. Wang, A. Bhattacharjee, and S. Hu. Longitudinal and transverse waves in yukawa crystals. *Phys. Rev. Lett.*, 86:2569–2572, 2001.

[301] Y. Watanabe. Dust phenomena in processing plasmas. *Plasma Phys. Control. Fusion*, 39:A59–A72, 1997.

[302] J. Weiland. *Collective Modes in Inhomogeneous Plasmas: Kinetic and Advanced Fluid Theory*. IOP Series on Plasma Physics, 1999.

[303] R.R. Weynants and G. Van Oost. Edge biasing in tokamaks. *Plasma Phys. Control. Fusion*, 35:B177–B189, 1993.

[304] E.C. Whipple. Potentials of surfaces in space. *Rep. Prog. Phys.*, 44:1197–1250, 1981.

[305] E.C. Whipple, T.G. Northrop, and D.A. Mendis. The electrostatics of a dusty plasma. *J. Geophys. Res.*, 90 A8:7405–7413, 1985.

[306] T. Windisch, O. Grulke, and T. Klinger. Radial propagation of structures in drift wave turbulence. *Phys. Plasmas*, 13:122303, 2006.

[307] D.J. Wineland, J.C. Bergquist, W.M. Itano, J.J. Bollinger, and C.H. Manney. Atomic-ion coulomb clusters in an ion-trap. *Phys. Rev. Lett.*, 59:2935–2938, 1987.

[308] M. Wolter, A. Melzer, O. Arp, M. Klindworth, and A. Piel. Force measurement in dusty plasmas under microgravity by means of laser manipulation. *Phys. Plasmas*, 2007. submitted.

[309] H. Yamaguchi and Y.-N. Nejoh. Temporal evolution of dust grain-charge in a plasma. *Phys. Plasmas*, 6:1048–1051, 1999.

[310] V. Yaroshenko, S. Ratynskaia, S.A. Khrapak, M.H. Thoma, M. Kretschmer, H. Höfner, G.E. Morfill, A. Zobnin, A. Usachev, O. Petrov, and V. Fortov. Experimental determination of the ion drag force in a complex plasma. In Boufendi et al. [32].

[311] V.V. Yaroshenko, B.M. Annaratone, S.A. Khrapak, H.M. Thomas, G.E. Morfill, V.E. Fortov, A.M. Lipaev, V.I. Molotkov, O.F. Petrov, A.I. Ivanov, and M.V. Turin. Electrostatic modes in collisional complex plasmas under microgravity conditions. *Phys. Rev. E*, 69:066401, 2004.

[312] C. Zafiu, A. Melzer, and A. Piel. Ion drag and thermophoretic forces acting on free falling charged particles in an rf-driven complex plasma. *Phys. Plasmas*, 9:4794, 2002.

[313] C. Zafiu, A. Melzer, and A. Piel. Measurement of the ion drag force on falling dust particles and its relation to the void formation in complex dusty plasmas. *Phys. Plasmas*, 10:1278–1282, 2003.

[314] A.V. Zobnin, A.P. Nefedov, V.A. Sinel'shchikov, O.A. Sinkevich, A.D. Usachev, V.S. Filippov, and V.E. Fortov. Ordered dusty structures in the plasma of an rf electrodeless gas discharge. *Plasma Physics Reports*, 26:415–423, 2000.

[315] A.V. Zobnin, A.D. Usachev, O.F. Petrov, and V.E. Fortov. Dust-acoustic instability in and inductive gas-discharge plasma. *JETP*, 95:429–439, 2002.

[316] M. Zuzic, A.V. Ivlev, J. Goree, G.E. Morfill, H.M. Thomas, H. Rothermel, U. Konopka, R. Sütterlin, and D.D. Goldbeck. Three-dimensional strongly coupled plasma crystal under gravity conditions. *Phys. Rev. Lett.*, 85:4064–4067, 2000.

[317] J. Zweben. Search for coherent structure within tokamak plasma turbulence. *Phys. Fluids*, 28(3):974–982, 1985.

[318] S. J. Zweben, J. Caird, W. Davis, D. W. Johnson, and B. P. Le Blanc. Plasma turbulence imaging using high-power laser thomson scattering. *Rev. Sci. Instr.*, 72(1):1151–1154, 2001.

[319] S. J. Zweben, R. J. Maqueda, J. L. Terry, T. Munsat, J. R. Myra D. D'Ippolito, D. A. Russell, J. A. Krommes, B. LeBlanc, T. Stoltzfus-Dueck, D. P. Stotler, K. M. Williams, C. E. Bush, R. Maingi, O. Grulke, S. A. Sabbagh, and A. E. White. Structure and motion of edge turbulence in the national spherical torus experiment and alcator c-mod. *Phys. Plasmas*, 13(5):056114, 2006.

[320] Z. Zzz. Experiments on meta-stable configurations of trapped particle cluster. submitted.

[321] Z. Zzz. Mode selective control of drift wave turbulence. *Phys. Rev. Lett.*, 86(25):5711–5714, 2001.

[322] Z. Zzz. Synchronization of drift waves. *Phys. Rev. E*, 63(5), 2001.

[323] Z. Zzz. Observation of mode like coherent structures in curved magnetic fields of a simple magnetized torus. *Contrib. Plasma Phys.*, 44(4):335–346, 2003.

[324] Z. Zzz. Resonance cones in dusty magnetized plasmas. *Phys. Plasmas*, 10(12):4627–4632, 2003.

[325] Z. Zzz. Transport studies of driven drift waves i: monochromatic waves. *Plasma Phys. Control. Fusion*, 45(4):413–425, 2003.

[326] Z. Zzz. Transport studies of driven drift waves ii: weak turbulence. *Plasma Phys. Control. Fusion*, 45(4):427–437, 2003.

[327] Z. Zzz. Dust coulomb balls: Three-dimensional plasma crystals. *Phys. Rev. Lett.*, 93:165004, 2004.

[328] Z. Zzz. Measurement of the ion drag force on free falling microspheres in a plasma. *Phys. Plasmas*, 11(12):5690–5696, 2004.

[329] Z. Zzz. 3d coulomb balls: Experiment and simulation. *J. Phys. Conf. Ser.*, 11:234–247, 2005.

[330] Z. Zzz. Confinement of coulomb balls. *Phys. Plasmas*, 12:122102, 2005.

[331] Z. Zzz. Coulomb balls in experiment and simulation. In *New Vistas in Dusty Plasmas*, volume 799 of *AIP Conf. Proc.*, page 454, 2005.

[332] Z. Zzz. Stereoscopic investigations of 3d coulomb balls. In *New Vistas in Dusty Plasmas*, volume 799 of *AIP Conf. Proc.*, page 335, 2005.

[333] Z. Zzz. Dust confinement and dust-acoustic waves in weakly magnetized anodic plasmas. *Phys. Plasmas*, 13:042105, 2006.

[334] Z. Zzz. Experiments on structure and trapping of coulomb balls. In *Non-Neutral Plasma Physics VI*, volume 862 of *AIP Conf. Proc.*, page 203, 2006.

[335] Z. Zzz. Ground state of a confined yukawa plasma. *Phys. Rev. E*, 74:056403, 2006.

[336] Z. Zzz. Prospects and limitations of conditional averaging. *Phys. Scripta*, T122:25–33, 2006.

[337] Z. Zzz. Structural properties of screened coulomb balls. *Phys. Rev. Lett.*, 96:075001, 2006.

[338] Z. Zzz. Super-resolution method for spatio-temporal plasma diagnostics. *Plasma Phys. Control. Fusion*, 48:419–431, 2006.

[339] Z. Zzz. Experimental comparison of statistical and spatio-temporal probe diagnostics. *Plasma Phys. Control. Fusion*, 49:1707–1718, 2007.

[340] Z. Zzz. Improved conditional averaging technique for plasma fluctuation diagnostic. *Plasma Phys. Control. Fusion*, 49:485–497, 2007.

[341] Z. Zzz. Structural and dynamical properties of 3d dust clouds. *Plasma Phys. Control. Fusion*, 2007. in press.

LIST OF PUBLICATIONS

Publications in Peer-Reviewed Journals

[J-1] Ch. Schröder, T. Klinger, D. Block, A. Piel, G. Bonhomme, and V. Naulin.
Mode selective control of drift wave turbulence.
Phys. Rev. Lett. 86(25), 5711-5714 (2001).

[J-2] D. Block, A. Piel, Ch. Schröder, and T. Klinger.
Synchronization of drift waves.
Phys. Rev. E 63(5), 056401 (2001).

[J-3] D. Block and A. Piel.
Transport studies of driven drift waves: I. monochromatic waves.
Plasma Phys. Controlled Fusion 45(4):413–425 (2003).

[J-4] D. Block and A. Piel.
Transport studies of driven drift waves: II. weak turbulence.
Plasma Phys. Controlled Fusion 45(4):427–437 (2003).

[J-5] F. Greiner, D. Block, and A. Piel.
Observation of mode like coherent structures in curved magnetic fields of a simple magnetized torus.
Contrib. Plasma Phys. 44(4):335–346 (2003).

[J-6] D. Block, I. Teliban, F. Greiner, and A. Piel
Prospects and limitations of conditional averaging
Physica Scripta T122, 25-33 (2006).

[J-7] I. Teliban, D. Block, A. Piel, and F. Greiner
Improved conditional averaging technique for plasma fluctuation diagnostic
Plasma Phys. Control. Fusion 49, 485-497 (2007).

[J-8] I. Teliban, D. Block, A. Piel, and V. Naulin
A super-resolution method for spatio-temporal plasma diagnostics
Plasma Phys. Control. Fusion 48, 419-431 (2006).

[J-9] D. Block, I. Teliban, and A. Piel
Experimental comparison of statistical and spatio-temporal probe diagnostics
Plasma Phys. Control. Fusion 49, 1707-1718 (2007).

[J-10] T. Trottenberg, B. Brede, D. Block, and A. Piel
Resonance cones in dusty magnetized plasmas
Phys. of . Plasmas. 10(12), 4627–4632 (2003).

[J-11] M. Hirt, D. Block and A. Piel.
Measurement of the ion drag force on free falling microspheres in a plasma.
Phys. Plasmas 11(12), 5690-5696 (2004).

[J-12] T. Trottenberg, D. Block, and A. Piel,
Dust confinement and dust-acoustic waves in weakly magnetized anodic plasmas
Phys. Plasmas 13, 042105 (2006).

[J-13] O. Arp, D. Block, A. Piel, and A. Melzer.
Dust Coulomb balls: Three-dimensional plasma crystals
Phys. Rev. Lett. 93, 165004 (2004). *Phys. News Update* 705, 20 Oct., 2004 and *Phys. Today* Dec. 2004.

[J-14] O. Arp, D. Block, M. Klindworth, and A. Piel
Confinement of Coulomb balls
Phys. Plasmas 12, 122102 (2005).

[J-15] D. Block, M. Kroll, O. Arp, A. Piel, S. Käding, Y. Ivanov, A. Melzer, H. Baumgartner, C. Henning, and M . Bonitz
Structural and dynamical properties of 3D dust clouds
Plasma Phys. Control. Fusion, in press (2007).

[J-16] M. Bonitz, D. Block, O. Arp, V. Golubnychiy, H. Baumgartner, P. Ludwig, A. Piel, and V. Filinov
Structural properties of screened Coulomb balls
Phys. Rev. Lett. 96, 075001 (2006).

[J-17] C. Henning, H. Baumgartner, A. Piel, P. Ludwig, V. Golubnichiy, M. Bonitz, D. Block Ground state of a confined Yukawa plasma *Phys. Rev. E* , 74, 056403 (2006).

[J-18] D. Block, S. Käding, A. Melzer, A. Piel, H. Baumgartner, and M. Bonitz
Experiments on meta-stable configurations of trapped particle cluster
submitted.

Selected Contributions to International Conferences

[C-1] O. Arp, D. Block, M. Bonitz, H. Fehske, V. Golubnychiy, S. Kosse, P. Ludwig, A. Melzer, and A. Piel. 3D Coulomb balls: Experiment and simulation *J. Phys.*, Conf. Ser. 11, 234-247 (2005).

[C-2] D. Block, O. Arp, A. Piel, and A. Melzer Coulomb balls in experiment and simulation AIP Conf. Proc. 799, 454 (2005).

[C-3] S. Käding, A. Melzer, O. Arp, D. Block, and A. Piel Stereoscopic investigations of 3D Coulomb balls AIP Conf. Proc. 799, 335 (2005)

[C-4] D. Block, O. Arp, A. Piel, and A. Melzer Experiments on structure and trapping of Coulomb balls AIP Conf. Proc. 862, 203 (2006).